Functional Immunogenetics of Two GWAS Genes in Autoimmunity

Functional Immunogenetics of Two GWAS Genes in Autoimmunity

A dissertation presented

by

Janice Marie Nieves-Bonilla

to

The Division of Medical Sciences

in partial fulfillment of the requirements

for the degree of

Doctor of Philosophy

in the subject of

Biological and Biomedical Sciences

Harvard University

Cambridge, Massachusetts

April 2020

Dissertation Advisor: Stephan Kissler Janice Marie Nieves-Bonilla

Functional Immunogenetics of Two GWAS Genes in Autoimmunity

Abstract

Type I diabetes (T1D) is a chronic T cell-mediated autoimmune disease that results in the destruction of insulin producing pancreatic β cells. More than 50 genomic regions have been implicated by genome-wide association studies (GWAS) in the modulation of T1D risk. One such region located within chromosome 16p13.13 (Ch16p13.13) includes the candidate genes *DEXI* & *CLEC16A*. While our lab previously reported that *Clec16a* deficiency protected against autoimmunity by the modification of immune reactivity using the T1D nonobese diabetic (NOD) mouse model, conclusive evidence for the causality of Ch16p13.13 in disease association is missing. Due to T1D-associated SNPs within *CLEC16A* also impacting *DEXI* expression others have argued that *DEXI* is the causal gene in Ch16p13.13. Since functional data for *DEXI*'s role in T1D was lacking, we generated a *Dexi* knockout (KO) NOD mouse to resolve *DEXI*'s involvement in disease. The frequency of diabetes was not affected in *Dexi*-deficient NOD mice when compared to wild type (WT) NOD. Moreover, intercrossing *Dexi*-deficient NOD and *Clec16a* knockdown (KD) NOD mice allowed testing for possible interactions between *Clec16a* and *Dexi* and their potential effects on disease. We found that *Dexi* KO did not modify the previously observed protection in *Clec16a* KD NOD mice. This led to the conclusion that Dexi alone does not play a role in the autoimmune diabetes modeled by NOD mice. The data presented in this thesis work clarifies the previous dichotomy in the field by providing strongly suggestive evidence that *CLEC16A*, as opposed to *DEXI*, is causal for the T1D association of disease variants within Ch16p13.13.

Table of Contents

Acknowledgements

When it comes to giving thanks, words never seem to be enough for me to express a deep sense of gratitude. Finding the right words is even more difficult when appreciating people that have been instrumental in reaching the end of an arduous and lengthy journey. Nevertheless, my doctoral degree journey has been made possible only by the support of a community of people that truly deserve to be mentioned and thanked for their support throughout my pursuit of becoming a scientist.

My deepest gratitude goes to my thesis advisor Stephan Kissler who has served not only as such, but as a career mentor since before I joined his lab. Stephan: I know that I wasn't the easiest graduate student to mentor, I made many mistakes and probably caused you a few headaches in the process. I am grateful that amongst the many failures, you always supported, encouraged, and were patient and helped me become a better scientist and a better person. Thank you for giving me the opportunity to join your lab, for believing in me when I felt discouraged, for pushing me to reach higher and do better, and for providing such a rich and positive learning environment. I am constantly inspired by your generosity, intellect, sense of humor, and excitement for science. I am so immensely grateful that you didn't give up on me and that you encouraged my curiosity, it is a true honor to call you my thesis mentor and to have embarked on this journey with you and your group.

I must also express deep gratitude to all past and current members of the Kissler lab. Each and every one of you has contributed uniquely to my development as a scientist, and as a human being. Thank you especially for taking the time to reach out, teach, listen, challenge, and help me in every step of this crazy journey. There are many

of you and unfortunately, I don't have the time or space to address every single one but know that I am incredibly grateful and that you will remain in my thoughts and prayers for the rest of my life. That being said, I do want to briefly mention a handful of people that have closely worked with me. To Conny, thank you for always being available when I had questions, and for teaching me so much about so much. It is thanks to your hard work and dedication that I was able to not only have a project to work on, but to also learn most of the techniques I used in this dissertation, you are an inspiration! Yuki, I also want to thank you for all of the advice you gave me on experiments, even amid your very busy schedule you always made time for me when I had questions. I will forever be inspired by your work ethic and intellect; they are a true gift to all of us. To Anna, you did so much for me in the little time you were in the lab and I will be eternally grateful for that. Thank you for lending an extra set of hands for many of the experiments described here, for lending your ear to listen to my frustrations, for believing in me, and for making the lab a fun place to work at. Badr, thank you for letting me participate and help you on the CD5 project. I have learned so much from you in the little time that we have shared together. I am grateful for the support, advice and help you have provided for me. I will take with me all I have learned from our conversations, which truly enriched my life as a scientist and otherwise. I want to also thank our "genome editing guru" Taylor, whose charisma continuously encourages me and everyone in the lab to smile more and grow as a lab community. Thank you Taylor for all the times you listened to my frustrations and encouraged me to not despair, for the times you made me laugh, for all the times you gathered us for lunch, and for all the times you cheered me on or celebrated me… it all meant a great deal! A brief thank you

also to John Stockton for his help with the embryo microinjections necessary to generate *Dexi* KO mice and the staff at the Joslin Diabetes Center core facilities for their training and help using different complex lab equipment.

Being part of the BBS program has been such an amazing journey, and that is thanks to the great community of peers and friends that are part of it. I am constantly inspired by you all, and I am glad that I had the opportunity to both share this journey with so many of you as well as to watch your progress through your own thesis projects. I want to offer a brief gratitude to Kayla Davis for her efforts in the administration of the mental health surveys and in advocating for the mental health of PhD students. I myself struggle with maintaining good mental health and am often hesitant to reach out for help in this area. Kayla, the efforts of you and your team made me feel like it was safe and courageous to ask my peers for help, thank you! A very special thanks must go to Renee Geck for not only being an amazing roommate, supporter and friend, but for also being a dedicated and passionate teacher. Thank you for teaching me how to master the art that is western blotting, for the countless times you tutored me and/or helped me edit assignments, proposals, statements, job applications, etc., for the times you listened to me vent about my frustrations, for having fun with me and encouraging me to leave the house once in a while, and for traveling to Puerto Rico for my wedding. Your friendship has been incredibly instrumental in my success as a PhD student, and I owe you a deep gratitude that is truly greater than words can express. It is a blessing to know you and have had shared this PhD journey with you. Huge thanks are also owed to the BBS program administrators (present and past): Daniel Gonzalez, Anne O'Shea, Kate Hodgins and Maria Bollinger who helped with the many tasks that entail being a

graduate student. I especially thank Danny for his support during both the PQE and defense process, and Anne for her support during all of my DAC meetings. I would also like to express deep gratitude to all of the members of my dissertation advisory committee: Dr. Judy Lieberman, Dr. Francisco Quintana and Dr. Isaac Chiu for their great advice, support and encouragement. I especially thank you all for your patience and consideration at each of our meetings and when reading all of my progress reports.

I want to also thank my peers and friends of the Leder Human Biology & Translational Medicine program. It has been a blessing to be part of the Leder program and have had that added layer of support, advising and growth opportunity. I am especially grateful to Connie and Thomas for their incredible mentorship and care for every member of the program. Your support meant oceans to me, and I am so grateful for the opportunity you have provided me (and many) to learn about what goes on in the clinic and to witness how important the work I did is for T1D patients. I also thank my fellow classmate and Leder member Michelle Watts for her constant support and friendship during all of the activities and classes we attended together. Your intellect and drive for your research work are inspiring, thank you for catching up with me once a year and for offering your support during the hard times of my PhD.

I was fortunate enough to work for two years in Shannon Turley's lab prior to the beginning of my PhD and consequently connect with students from the immunology PhD program. I must therefore give a special thanks to the immunology graduate students for welcoming me every year to their annual retreat and for making me feel part of their family throughout my years in graduate school. I especially would like to thank Christin Hong, Rachel Cotton, and Charlie Evavold for their friendship and

essential support on immunology research techniques and knowledge. Christin, thank you for all of your advice on flow cytometry and on life in general, it is a blessing to call you a friend! Charlie, you went above and beyond to help me with the BM-DM experiments, I will forever be grateful for that! Rachel, thank you for sharing your experiences with me, seeing yours and your boyfriend's success inspires me every day to rise above the limitations I often encounter with having ADHD, I am honored to have met you both.

I must also give thanks to all of the teachers, professors, and mentors that encouraged my curiosity and saw my passion for science throughout my forming years in high school and those in college. Some of you discovered my passion for research, even before I understood what that meant, and it is thanks to you I pursued and am so close to completing a doctoral degree in biomedical sciences. I am particularly grateful to Mr. Galán, my 10th grade biology teacher for encouraging me to participate in the science fair amidst my reluctancy and for making biology so interesting and fun. You opened the door to a whole new world, and I have not looked back since. I also want to offer a deep gratitude to Dr. Rosann O'Neil, the first scientist and graduate student I ever met. Thank you for taking me under your mentorship wing at such a young age, for introducing me to research as a career, and for letting me visit your lab and help you do experiments as a high schooler so many times. You made a scientific career seem like something attainable at a time when I was doubting my potential, thank you very much for that. I am also hugely grateful to my honor thesis advisor, mentor and friend Dr. Belinda Román who provided me with an endless amount of opportunities and support to grow as a scientist in a small state college that lacked many resources. Your devotion

for teaching & mentoring, combined with the outstanding generosity you offered me during my college years shaped my scientific career, passion for science, and my path to where I am at this very moment. Thank you for never giving up on me nor letting me give up on myself. I also want to briefly thank all of the professors in the biology department at the University of Puerto Rico at Cayey for allowing me to often disrupt their respective classes to ask questions, and for always being passionate about the subject they were teaching. Each of you ignited my passion for biology and biomedical research and for that I am grateful. I also want to briefly mention and thank my past research mentors: Dr. Irizarry-Ramírez, Dr. Liao, Dr. Gavillán-Suárez, Dr. Martínez-Montemayor and Dr. Turley. Thank you for your mentorship and for opening the doors of your respective labs and giving me the opportunity to grow as a scientist. Thank you also to my peer mentors and friends: Dr. Cremasco, Dr. Fletcher, Dr. Karina González, Dr. Emily Cohen, and Dr. Mónica Feliu-Mojica for your words of wisdom and encouragement throughout my career. A brief thanks to Emily for helping me with generating the FLAG-Tagged Dexi construct, generously gifting the pMSCV-puro and for offering such useful advice on detecting small proteins by western blot. And a very special thanks also to Dr. Sheila Thomas for her mentorship during my post-baccalaureate and beyond, thank you for everything you have done for me. You believed in me even when I didn't and you always encourage me to keep growing and to keep pushing myself, I hold your words of wisdom very close to my heart.

I must thank my close friends and family for helping me, amongst many things to stay sane and at peace. I can't mention you all but know that I am grateful and I love you all. To my community of catholic friends, thank you for fueling my faith and being

there to support me during the times of frustration and to celebrate the blessings that the past 6 years have brought. To my chosen sisters: Yacky, Arlene and Vivi thank you deeply for your support and care for me even while being miles and miles apart. I especially want to thank Arlene who is a T1D patient (and generously allowed me to disclose it here) as well as the motivation behind my interest in this disease. Thank you for sharing your experience as a diabetic, but most importantly thank you for your support, care, and friendship. And to Vivi I want to also offer deep gratitude for her incredible support and help during frustrating times. Thank you for making me laugh, and for constantly reminding me to love myself. As I am sure I have told you many times, your friendship is one of the biggest blessings in my life. I also want to express mountains of gratitude to my siblings Marcos, Alex and Gaby, as well as my stepmom Lizy for their constant love, care and support. I am so close to the finish line because of your continuous believe in me. I love you all so much and I am so grateful to have you in my life. Thank you for always loving me back!

Lastly, I express my deepest and most heartfelt gratitude to the four most important people in my life. To my husband, Kev, I owe you so much gratitude especially for the last 4 months of this journey. Thank you for being so incredibly sacrificial, sweet, generous, supportive, selfless and caring for me as I wrap up my degree. From lending me your ears to listen to my frustrations, to lending your strength to support me in the times where stress and physical illnesses have rendered me weak, to lending your hands to both do chores so I could devote time to my career as well as to embrace me in the hardest of times. You have been a pillar in my life and especially during my PhD. Thank you for not letting me give up on pursuing this degree, I love you so much. I have

also been incredibly blessed with wonderful parents who have always been extremely supportive and generous with me. To my mom, thank you for helping me so much when I struggled in school and college, and for cheering me on every day of my life. I know I have given you many headaches throughout my lifetime, but even when I do, you never tire of showering me with endless amounts of love, care, support, encouragement, joy, and affirmation. Thank you so much for that. To my dad, thank you for encouraging me to be better, for supporting me and for being there for all of my accomplishments. Thank you also for giving me the space to grow into the woman that I am, while still watching out for me. To the both of you, I love you and am so grateful to you for making me into the woman that I am today, I owe it all to you! With deep respect to those believing in other philosophies and/or spirituality, I would like to finish by personally thanking God for loving me into existence, for fueling my faith, for showering me with grace, virtues and endless blessings, and for inspiring me to be the best version of myself. I firmly believe that all of this was made possible by You, and it is all done for You.

Funding for this research was supported by a pre-doctoral training fellowship from NIDDK (T32DK007260), a grant to Dr. Stephan Kissler from NIDDK (R56DK109954-01), and by core facilities funded by the NIDDK Diabetes Research Center award P30DK036836 to the Joslin Diabetes Center.

Dedication

For God, everything I do is for and because of You. For mom and dad, you gave me life so it is my desire to give you my life's work. For my husband, Kev, thank you for loving me and supporting me in everything I do, I love you so much. For Arlene and all T1D patients. And for John Hatch, you and your science will live on forever through every one of us.

A Glossary of Abbreviations

Scientific reports in the biomedical sciences are often filled with an overwhelming amount of abbreviations, and this work is not the exception. For this reason, I opted for including a list of these abbreviations to hopefully aid the navigation of this text.

AhR: Aryl hydrocarbon receptor

ATP: adenosine triphosphate

A1: allele #1 mutation

A2: allele #2 mutation

B_{gc}: germinal center B cells

BLS-II: type II bare lymphocyte syndrome

BM-DM: bone marrow-derived macrophage

B_{mz}: marginal zone B cells

B_{plasma}: plasma B cells

Cas: CRISPR associated

CD: celiacs disease

Cell line abbreviations

A549: alveolar epithelial cell line

Daudi: Burkitt's lymphoma cell line

BGRL-169: EB-transformed lymphocytes

HEL: erythroleukemia cells

H322: adenocarcinoma bronchial epithelial cells

HFL-1: pulmonary fetal fibroblasts

EndoC-βH1: pancreatic β-cell line from rat

MJC1: cortical NOD TEC line.

THP-1: a monocyte-like human cell line

NIT-1: insulin-secreting murine β-cell line from transgenic NOD prone to insulinomas.

HEK293T: Human embryonic kidney 293 transfectable cell line. This cell line, originally referred as 293tsA1609neo, is a highly transfectable derivative of

human embryonic kidney 293 cells, and contains the SV40 T-antigen.

Ch16p13.13: Chromosomal region 16p13.13

CIITA: class II transactivator

CKII: casein kinase II

CPT: camptothecin

CRISPR: clustered regularly interspaced short palindromic repeat

CRISPR/Cas9: CRISPR & Cas9 protein complex. Also referred to as the genome editing tool which uses this complex of nuclease and protein.

cTECs: cortical TECs

CVB5: coxsackievirus B5

CY: cyclophosphamide

DC: dendritic cell

$DC_{I\text{-}Ak}$+: DCs which specifically express the mouse MHC-II molecule: I-A^{g7}. The antibody used is cross reactive with both I-Ak and I-A^{g7} which is why that name was used.

DC_{11b}+: DCs which express the cell surface marker CD11b.

DEL12BP: 12bp deletion in the NOD mice from Davison et al.[9]

DEXI: dexamethasone-induced transcript

DN: double negative; referring to $CD4^{-}CD8^{-}$ double negative thymocytes

DNA: deoxyribonucleic acid

DP: double positive; referring to $CD4^{+}CD8^{+}$ double positive thymocytes

DSB: double stranded break

dsDNA: double-stranded oligonucleotide (i.e. DNA or RNA)

DT_1: developing thymocytes which lack expression of cell surface marker CD69 and TCR-β subunit.

DT_2: developing thymocytes which express of both CD69 and TCR-β.

DT_3: developing thymocytes which express TCR-β, but lack CD69 expression.

EAE: autoimmune encephalomyelitis

EDTA: ethylenediaminetetraacetic acid

eQTLs: expression quantitative loci

FLAG-DEXI: Flagged-tagged Dexi recombinant fusion protein

FSC: forward scatter

GAD: glutamic acid decarboxylase

GFP: green fluorescent protein

GWAS: genome-wide association studies

H: hour(s)

HEPES: 4-(2-hydroxyethyl)-1-piperazineethanesulfonic acid

IBD: Inflammatory Bowel Disease

IF: Immunoflourescence

IFN: interferon

IFN-β: also abbreviated as *Ifnb1* for interferon-β

IFN-γ: interferon-γ

IFNγR: interferon γ receptor

IL-1β: interleukin 1β

IL-17: interleukin 17

IL-21: interleukin 21

IL-21R: IL-21 receptor

IL-22: interleukin 22

IL-23: interleukin 23

IL-23R: interleukin 23 receptor

IL-4: interleukin 4

IL-6: interleukin 6

IL-6R: IL-6 receptor

InDel: Insertion-Deletion mutation

Ins1: Insulin 1 gene

INS1BP: 1bp insertion in the NOD mice described in Davison et al.[9]

IP: Immunoprecipitation

JAK: Janus Kinase

JIA: Juvenile Idiopathic Arthritis

KD: knockdown. Common term used to indicate diminished expression of a gene.

KIR: kinase inhibitory region

KO: knockout. Common term used to indicate absence of a gene.

LDB: Linkage disequilibrium block

LN: lymph node

T1D: type 1 diabetes

Mφ: macrophage

MHC: major histocompatibility complex

MHC-I: major histocompatibility complex class I

MHC-II: major histocompatibility complex class II

min: minute(s)

Mo: monocytes

$MOG_{[35-55]}$: myelin oligodendrocyte glycoprotein

mRNA: messenger RNA

MS: Multiple Sclerosis

mTECs: medullary TECs

NHEJ: non-homologous end joining DNA repair

NK: natural killer cell

NOD: non-obese diabetic

ORF: open reading frame

PAI: Primary Adrenal Insufficiency

PAM: protospacer adjacent motif consisting of 3bp: NGG

PBS: Phosphate-buffered saline

PCR: polymerase chain reaction

pDCs: plasmacytoid DCs

pMSCV-puro: puromycin-resistant murine stem cell virus for retroviral expression plasmid

pMSCV-puro-DEXI-FLAG: expression plasmid containing the flagged-tagged Dexi recombinant fusion protein

Poly(I:C): polyinosinic:polycytidylic acid

pSTAT3-S: STAT3 phosphorylated at the serine 727 site.

pSTAT3-Y: STAT3 phosphorylated at the tyrosine 705 site.

qPCR: quantitative real-time PCR

RA: Rheumatoid Arthritis

RNA: ribonucleic acid

RNAi: RNA interference

RPMI: Roswell Park Memorial Institute

SEM: standard error of mean

sgRNA: single-guide RNA

siRNA: small interfering RNA

SLE: systemic lupus erythematosus

SNP: Single Nucleotide Polymorphism

SOCS1: suppressor of cytokine signaling

SP: single positive; referring to $CD8^+$ or $CD4^+$ single positive (SP) thymocytes

SSC: side scatter

ssDNA: single-stranded oligonucleotide (i.e. DNA or RNA)

STAT: signal transducer and activator of transcription

TBB: 4,5,6,7-tetrabromobenzotriazole

T_c: cytotoxic T cells

TCR-β: β subunit of the T cell receptor complex.

TEC: thymic epithelial cell

TF: transcription factor

T_h: helper T cells

T_{reg}: regulatory T cells

WB: western blot, western blotting, immunoblotting

WT: wild type. In reference to NOD, NOD WT and/or WT mice which are used interchangeably to indicate NOD mice which normally express *Dexi* and/or *Clec16a* and/or *Cd5*.

ZnT8: zinc transporter 8

3C: chomosome conformation capture

Chapter 1

Background and Significance: Laying foundations and understanding the questions motivating the study of T1D-related genes.

1.1 Type 1 Diabetes (T1D): an autoimmune disease of the pancreas

T1D is a chronic autoimmune disease affecting 1 in 300 people in the US before they reach the age of 18[10]. T1D incidence is continuously rising worldwide with a reported rate of about 3-5% more cases reported each year[10-13]. It results from the T cell mediated destruction of β cells within the pancreatic islets, which are the major source of insulin production and release within mammals. Upon abnormal activation of T cells (and/or other immune cells) an inflammatory response is triggered in draining lymph nodes which can escalate to the production of autoantibodies. These antibodies can recognize several self-antigens including the insulin protein, glutamic acid decarboxylase (GAD), zinc transporter 8 (ZnT8) and protein tyrosine phosphatase IA2[11,12]. Upon activation lymphocytes travel to the pancreatic islets and mount a response that ultimately results in the demise of β cells and therefore a lack in pancreatic insulin production. Lack of insulin and the development of T1D results in a chronic hyperglycemia secondary to a lack of glucose uptake by cells and exhaustion of hepatic glucose generation[11-13]. Although T1D has been extensively studied it remains unclear how the initial immune dysregulation occurs as well as the entirety of the elements involved in the process. Moreover, studies have uncovered the participation of both innate and adaptive immune cells in both the onset, development and progression of T1D[11-13]. Like most autoimmune diseases, the risk factors of T1D are both genetic and environmental. T1D is known to be polygenic and modulated by more than 50 genomic regions[14]. Among the known genetic contributors are the loci for major histocompatibility complex class II (MHC-II) and insulin, as well as strong associations

with chromosomal region 16p13.13 (Ch16p13.13)[14]. However, exactly how disease-associated genetic variants affect islet autoimmunity remains largely unresolved.

1.2 GWAS correlate chromosomal region 16p13.13 with autoimmune disease

Ch16p13.13 has been identified in many genome-wide association studies (GWAS). Particularly, this locus contains four genes that form part of a linkage disequilibrium block (LDB) and has been a common hit amongst immune disease GWAS. This region was first associated together with 3 other regions with the autoimmune disease T1D by the work of Todd et al.[15]. Before this study, most studies related to the genetics of polygenic autoimmune diseases (i.e. T1D) focused on understanding the involvement of genes that played major roles on the development of these diseases. Among these were genes within the major histocompatibility complex (MHC or HLA in humans) — HLA class II genes established to have the largest effect on autoimmune disease development — as well as the gene encoding for insulin and three immunoregulatory genes *CTLA4*, *PTPN22*, and interleukin-2 receptor α chain (CD25; *IL2RA*)[15]. While these genes have been well characterized to have a strong influence on the development of T1D and other autoimmune diseases, the model for autoimmune disease development hypothesizes that many other genes are likely also influencing disease development, albeit at a smaller degree than those mentioned above[15]. The ability to identify and characterize those genes has been one of the natural consequences of the great amount of data generated by GWAS. As mentioned above, Ch16p13 was one of the regions of association revealed by the GWAS reported by Todd et al.[15] where single nucleotide polymorphism (SNP) rs12708716 — mapped to intron

18 of *CLEC16A* — was found to have the strongest association within the region[15]. Among the first published GWAS for this region, was the discovery of other SNPs within *CLEC16A* which were present in patients that had T1D or multiple sclerosis (MS)[16,17]. In that same study an association was also described between rheumatoid arthritis (RA) predisposition and one of the other genes in Ch16p13.13: class II transactivator (*CIITA*). Hakonarson et al.[17] also described three additional SNPs (rs2903692, rs725613, rs17673553) within *CLEC16A* to be significantly associated with T1D[17]. The ~530kb LDB in which *CLEC16A* resides within Ch16p13, also happens to be flanked by two candidate genes of known function: *CIITA* and suppressor of cytokine signaling 1 (*SOCS1*), and by dexamethasone-induced transcript (*DEXI*) a gene of unknown function which will be the subject of this dissertation. To this day all four of the genes within the Ch16p13.13 region have been subsequently associated with multiple diseases and a number of functional studies have now been published for most of them.

CIITA composes the beginning portion of the Ch16p13.13 LDB, sitting upstream of *DEXI* and *CLEC16A*[18] and its function as a master regulator of MHC genes has been well established in the more than 20 years of research in the field[19]. CIITA is a transcription factor (TF) which primarily regulates MHC-II-related genes by its ability to induce *de novo* transcription of MHC-II but it can also act to occasionally enhance MHC class I (MHC-I) gene expression[19]. Moreover, CIITA has also been shown to regulate more than 60 immune genes[19]. Like other genes in this region, *CIITA* has been associated with at least 4 autoimmune diseases via GWAS including MS[20], T1D[21], inflammatory bowel disease (IBD)[22], and primary adrenal insufficiency (PAI)[23] by itself or alongside Ch16p13.13 genes. However, due to its major role in the immune response

(via MCH-II expression), *CIITA* has also been linked to other immune-related processes in diseases such as leprosy infection[24], celiacs disease (CD)[25], and cancer[26,27]; with the most significant *CIITA*-associated pathology being type II bare lymphocyte syndrome (BLS-II). BLS-II is a form of combined immunodeficiency that results from *CIITA* deficiency and results in the lack of HLA-II expression. The drastic consequence resulting from its absence showcases *CIITA* as an essential component of HLA-II expression and the immune response[28].

On the other end of the LDB within Ch16p13.13 is *SOCS1*, a gene characterized for the function of its translated transmembrane protein as a negative regulator of cytokine-induced inflammation[29]. The SOCS1 protein contains an amino-terminal kinase inhibitory region (KIR) — commonly referred to as a KIR domain — which allows it to inhibit JAK tyrosine kinase activity[29-31]. Specifically, SOCS1 can inhibit the activity of JAK1, JAK2 and TYK2 via direct interaction with its KIR domain. Using the SOCS-box as an alternate domain (located at the carboxy terminal end of the protein), SOCS1 can also suppress JAK activity via an alternate pathway[29-31]. Janus kinases (JAKs) become activated following receptor oligomerization — in response to cytokine-receptor binding — and consequently phosphorylate the signal transducers and activators of transcription (STATs) to initiate downstream effector functions. Signaling via specific JAKs and STATs is usually related to the downstream effector function and can be restricted to a small number of receptor-cytokine combinations[29-31]. While JAK-STAT signaling will only be briefly addressed during the work of this dissertation, it is necessary to introduce these concepts as they relate to homeostatic SOCS1 function, as well to as its participation in disease. Albeit often associated as a loci, the genes in

Ch16p13.13 have been individually associated with immune diseases that don't always overlap. While *SOCS1* and *CIITA* share leprosy susceptibility[24], CD[25], cancer[32] & IBD[22,33], and all four genes *SOCS1*, *CIITA*, *DEXI* & *CLEC16A* share a strong association with MS[20,34-36]; *SOCS1* has been associated independently with other autoimmune diseases & immune-related events including: psoriasis[33], primary biliary cirrhosis[37,38], serum IgE levels[39] and systemic lupus erythematosus (SLE)[40] — where it negatively correlates with disease activity[29-31]. Studies have uncovered *SOCS1*'s role in the pathogenesis of SLE via multiple immune processes thus emphasizing its essential function in the maintenance of immune homeostasis[29,30]. Moreover, these studies have made *SOCS1* noticeable due to its great therapeutical potential for SLE patients[29-31].

1.2.1 *CLEC16A*, the original GWAS candidate

As mentioned above, *CLEC16A* holds the most significant evidence of variation in this region[41] with variations being abundant in two intronic regions of this gene: introns 10 and 19[3]. Owing to the location of these SNPs, *CLEC16A* has been suggested as the causal gene for the disease association of Ch16p13.13[17,42]. Gene expression analyses have since provided evidence that disease SNPs can affect *CLEC16A* expression[34,43,44]. For example, a significant effect was attributed to SNP rs12708716 which has been associated with T1D & MS risk, and modifies *CLEC16A* expression in the human thymus[43]. *CLEC16A*, like *CIITA* and *SOCS1*, has been associated with multiple autoimmune diseases besides the previously mentioned associations with T1D[13,15,17,41,42,45-53] and MS[34,43,54-58]. These include SLE[59], PAI[23], IBD[60], primary biliary cirrhosis[38], IgA deficiency[61], autoimmune thyroid diseases[62], common variable immunodeficiency disorder[63], juvenile idiopathic arthritis (JIA)[64], and alopecia areata[65].

Interestingly, *CLEC16A* being the largest gene within Ch16p13.13 — with a 238kb sequence— has also been reported to function as an immune modulator in a variety of studies[44,63,66-71]. Work from our lab reported on *Clec16a*'s participation in immunity by its ability to modulate thymic epithelial cell (TEC) autophagy and therefore playing a role in T cell selection[66]. Specifically, silencing of *Clec16a* protected non-obese diabetic (NOD) mice from autoimmune diabetes and reduced the pathogenicity of diabetogenic T cells[66]. *Clec16a* silencing also resulted in the hyporeactivity of T cells, a process that was not T cell intrinsic but instead caused by an alteration of T cell selection in the thymus[66]. Furthermore, knockdown (KD) of *Clec16a* disrupted autophagy both in cortical TECs (cTECs), as well as in the cTEC cell line (MJC1) generated for this study[66]. This role in immunity is further supported by elevated expression of *Clec16a* in both medullary TECs (mTECs) and cTECs of C57BL/6J mice at steady state conditions[72]. Studies in the mononuclear cells found in the peripheral blood of MS patients also showed *CLEC16A* to be upregulated in diseased individuals[67]. In this case, *CLEC16A* was most abundant among the monocyte-derived dendritic cells (DCs) of MS patients, where it appeared to co-localize with the HLA-II cellular compartment[67]. In that study, van Luijn et al.[67] reported *CLEC16A*'s role in the cytoplasmic distribution and formation of HLA-II$^+$ late endosomes where it is part of the dynein motor complex and binds to RILP and the HOPS complex to regulate the HLA-II pathway[67].

Clec16a, a member of the C-type lectin domain family, has also been reported to be a membrane-associated endosomal protein capable of regulating mitophagy in the mouse fibroblast cell line NIH 3T3[44]. In this setting, the neuregulin receptor degradation protein 1 (or Nrdp1) an E3 ubiquitin ligase which targets the mitophagy master regulator

Parkin, was found to interact with Clec16a and regulate its function[44]. Interestingly, a pancreas-specific deletion of Clec16a in C57BL/6 mice led to impaired oxygen consumption and ATP concentration in the mitochondria of β cells[44]. This process was also reported to be regulated by another diabetes susceptibility gene pancreatic and duodenal homeobox 1 (or Pdx1)[73]. These studies in combination with reported data by Pearson et al.[68] in which this Clec16a-Nrdp1 pathway was inhibited by the chemotherapeutic agent lenalidomide and similar impairments were observed in the β cells of both human and mice[68], support a role for *CLEC16A* in T1D development via the regulation of insulin secretion and glucose homeostasis[44] in the pancreas. Additionally, Tam et al.[69] described its role in macroautophagy by starvation-dependent clustering of CLEC16A in the Golgi of HeLa and HEK293 cells, where they suggest it interacts with a yet to be determined mediator to activate the mTORC1 complex following nutrient availability[69]. Taken together, these studies suggest that *CLEC16A* participates in the modulation of HLA-II/MHC-II antigen presentation, through autophagy.

Lastly, recent studies have also elucidated a role for *CLEC16A* in autoimmune development by regulating natural killer (NK) cell function[70,71] and immunoglobulin production in B cells[63]. Notably, Pandey et al.[70] generated an inducible whole organism *Clec16a* knockout (KO) (C57BL/6) mouse and reported that once KO is induced by Tamoxifen injection, these mice have significant weight loss accompanied by thymus and spleen atrophy, a reduction in mitochondria membrane potential among splenocytes, disrupted mitophagy in splenic T and B cells, and an increase in NK cell

cytotoxicity which promotes inflammation[70]. Further studies of *CLEC16A*'s role within NK cells revealed a different subcellular localization for CLEC16A in the cytosol and its ability to associate with a subunit of the class C Vps-HOPS complex — named Vps16A — to regulate the expression of NK cell surface receptors through autophagy[71]. Overall, *CLEC16A*'s role in mitophagy and autophagy within NK cells confers CLEC16A with the ability to regulate NK functions — that include cell surface marker expression, aggregate formation, and granule release of cytokines and chemokines — and thus regulate pro-inflammatory and cytolytic functions which are known to play a role in autoimmune disease development[71]. Although most studies agree that CLEC16A has a role in autophagy and/or mitophagy, the diversity present among all of the data reported on CLEC16A's functions suggests that its role may vary among cell types.

Despite functional data supporting *CLEC16A* as the causal gene for the association of the Ch16p13.13 with T1D and other autoimmune diseases, it has been argued by several groups that its neighbor gene *DEXI* is instead a more likely candidate. This has been the case following reports of disease-associated SNPs within *CLEC16A* also modifying *DEXI* expression[3,41,54]. Specifically, a long-range DNA looping analysis reported that T1D risk alleles in intron 19 of *CLEC16A* act to modulate *DEXI* expression via interactions with its promoter region[3]. While GWAS have and continue to aid the discovery of more genes involved in autoimmune disease pathogenesis, these studies require functional validation in order to understand their causal relationships. Often, GWAS-identified disease variants are within, or have effects on, genes whose function has been poorly characterized in the context of the associated disease or otherwise. That is the case with the smallest gene within Ch16p13.13, *DEXI*, a

transcript first discovered by Edgar et al.[74] in 2001 and the focus of this dissertation.

1.2.2.1 DEXI - A likely candidate; an understudied gene

Identification and cloning of *DEXI* was reported upon differential expression of its mRNA in emphysematous lung* tissue when compared with donor tissue in patients with end-stage respiratory failure. Specifically, *DEXI* mRNA was expressed 147% more in emphysematous tissue than in normal donor tissue and 230% more upon dexamethasone treatment of the adenocarcinoma alveolar epithelial cell line A549[74] with the latter coining its name. In the initial study by Edgar et al.[74], *DEXI* was found to be highly expressed in heart, brain, liver, and lung tissues. *DEXI* was also found to be expressed in several human cell samples which included: a Burkitt's lymphoma cell line (Daudi), EB-transformed lymphocytes (BGRL-169), erythroleukemia cells (HEL), A549 cells, adenocarcinoma bronchial epithelial cells (H322), placental microvascular endothelial cells, umbilical vein endothelial cells, pulmonary fetal fibroblasts (HFL-1), pulmonary artery smooth muscle cells (expressed only 1 of the 2 patients tested), and bronchial smooth muscle cells[74]. Moreover, the Immgen database[72]† shows that *Dexi* is highly expressed in DCs, mTECs and cTECs of mice[72], as well as in human B cells and monocytes (Mo)[3,72]. Data collected in our lab also shows *DEXI* expression in immune organs at steady state conditions which correlates with *Clec16a* and is higher in the pancreata of NOD mice (Figure 1B).

---

* "Pulmonary emphysema is the abnormal, irreversible enlargement of distal air spaces of the lung and the destruction of their walls without obvious fibrosis. It includes respiratory bronchioles and alveolar ducts." It is also a major component of chronic obstructive pulmonary disease[74].

† Immunological Genome Project Database (ImmGen)[72]: https://www.immgen.org.

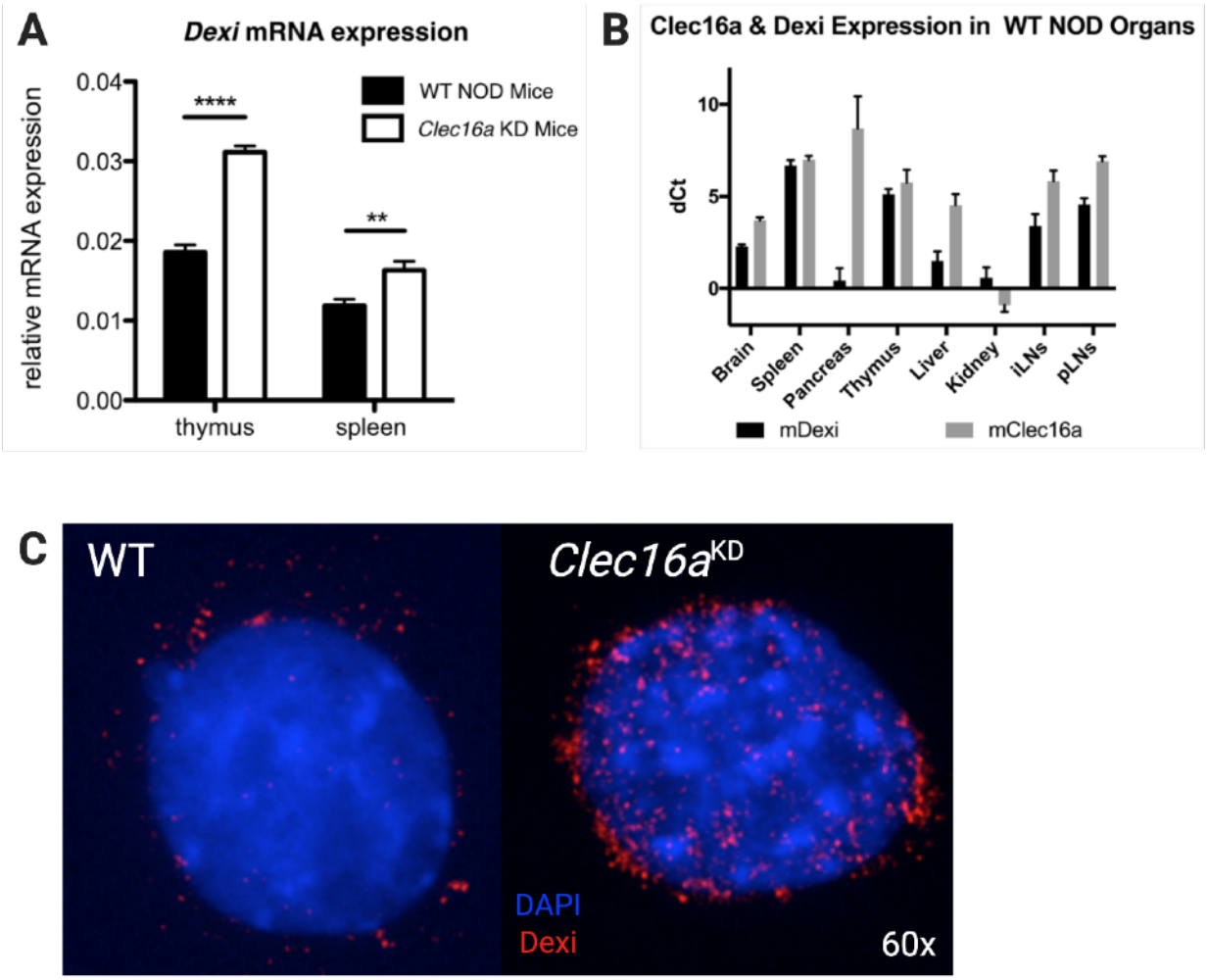

Figure 1. *Dexi* expression is upregulated in NOD.*Clec16a*^{KD} mice and a *Clec16a*^{KD} cTEC line.
A *Dexi* mRNA levels in the thymus and spleen of male NOD and NOD.*Clec16a*^{KD} mice (n=3). **B** Expression of *Dexi* and *Clec16a* at steady state in male NOD mice, as assayed by qPCR (n=4). Expressed as dCt=(*Dexi* CT or *Clec16a* CT)-(β-Actin CT). **C** Immunofluorescence (IF) staining of NOD and NOD.*Clec16a*^{KD} murine cTEC-derived MJC1 cell lines using an anti-Dexi antibody. Representative image shows Dexi protein adjacent to the nucleus of WT MJC1 cells (*left*), and an increase in Dexi detection in *Clec16a*^{KD} MJC1 cells. Samples and data collected by Dr. Cornelia Schuster and Dr. Kevin Boerner.

DEXI protein contains 95 amino acids and is conserved among many species including humans and mice. It has been predicted to contain a transmembrane domain, a carboxy-terminal leucine zipper motif and a casein kinase II (CKII) phosphorylation site suggesting an ability to become phosphorylated[41]. Despite containing a transmembrane domain, DEXI protein is located within the nuclear cellular compartment

reported to co-localize with chromatin in the pancreatic β cell line EndoC-βH1[75] and adjacent to the nucleus in the cTEC line MJC1 (Figure 1C). It is important to note that no other identifiable domains are present in *DEXI* that would suggest its possible function, making it a challenging protein to study.

Until recently, DEXI was a protein of unknown function with its gene having repeated associations to a range of autoimmune & immune-related diseases. Among the first groups to associate *DEXI* with a disease was Miyaki et al.[76], suggesting *DEXI* to be a potential epigenetic biomarker for the detection of chemotherapeutic-resistant colon and gastric cancer patients. In this study, silencing of *DEXI* led to a decrease in fibroblast apoptosis following treatment with the chemotherapeutic drug camptothecin (CPT)[76]. Restored *DEXI* expression following silencing in a colon cancer cell line significantly enhanced the susceptibility of these cells to CPT-induced apoptosis. In this context, the increased CPT susceptibility occurred via methylation, as *DEXI* expression was restored following treatment with a nucleoside antimetabolite which inhibits DNA methyltransferase I activity[76]. As is the case for the other genes in Ch16p13.13, *DEXI* has also been associated with MS in several GWAS studies[3,54,77]. Specifically, changes in *DEXI* expression have been correlated with the presence or absence of MS risk alleles in human thymic samples[54], human Mo[54], and a human lymphoblastoid cell line[20]; but not in peripheral T cells[34]. Studies have also correlated *DEXI* to obesity[78], acute myeloid leukemia (as *CIITA-DEXI* fusion transcript)[79], asthma-related hay fever[80], asthma[81], JIA[81], RA[77], psoriatic arthritis[77], selective IgA deficiency[61], eosinophilic esophagitis[82], and more relevantly T1D[3,15,41,77,83].

1.2.2.2 *DEXI* & T1D

Like with MS, studies have negatively correlated T1D-associated variants with *DEXI* expression. In the case of T1D association, the risk allele correlates with *DEXI* downregulation and the protective allele with *DEXI* upregulation[3,41,77,83]. A majority of the studies which have predicted *DEXI* to be a T1D (or autoimmune disease) risk gene report a type of chromosomal interaction with the *DEXI* promoter matched with differential expression between healthy and diseased patients[3,61,77-82]. The promoter region of *DEXI* has been reported to be highly enriched with histone modifications that are consistent with TF binding events[3,41]. Intron 19 of *CLEC16A* is also enriched with markers associated with enhancer activity[3,41] supporting the claim that the disease-associated variants may modulate *DEXI* expression[3,61,77-82]. This was first reported by Davison et al.[3], where they used chromosome conformation capture (3C) to study the chromosomal interactions in Ch16p13.13. This study correlated two SNPs: rs12708716 and rs8062322 with expression quantitative trait loci (eQTLs) in Ch16p13.13. In this case, T1D protection alleles correlated with increased *DEXI* expression in human Mo samples supporting *DEXI* eQTLs within Ch16p13.13 i.e. intron 19 of *CLEC16A*. Moreover, their study suggested that the fragment within intron 19 of *CLEC16A* measuring 20kb was interacting exclusively with the DEXI promoter region forming a chromosomal loop of >150kb[3]. Lastly, they reported a long-range interaction between a fragment of intron 19 and the promoter region of *DEXI* in an EBV-transformed B cell line, a Mo-like cell line (THP-1), and in A549 cells[3]. This led to the proposition that T1D-associated variants within said fragment of *CLEC16A*'s intron 19 could be influencing *DEXI* transcription via TF interactions between the promoter region of *DEXI* and the

intron 19 fragment[3] (Figure 2). Shortly thereafter, another study confirmed *DEXI* eQTL

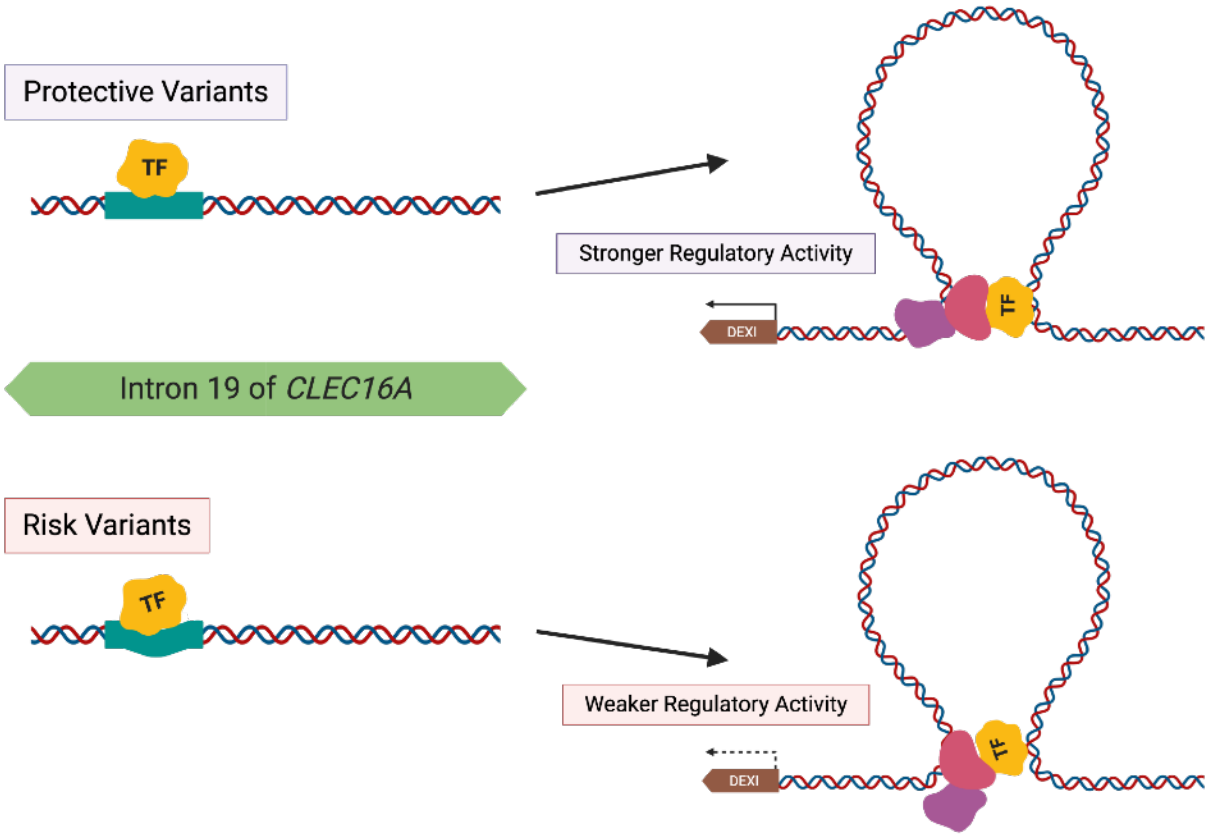

Figure 2. ***CLEC16A* alleles associate with increased *DEXI* expression and T1D protection due to DNA looping interactions.** Adapted from the model proposed by Davison et al.[3] based on chromosome conformation capture and *DEXI* eQTL data, which suggests a DNA loop is formed between the T1D-associated SNPs-containing intronic region of *CLEC16A* (intron 19) and DEXI's promoter region. They postulate that causal variants in this region affect the intron's putative enhancer activity due to allele-specific effects on "chromatin structure and/or recruitment of a multi-protein transcriptional co-activator complex" therefore influencing *DEXI*'s transcription.

correlation with T1D in human Mo from a population in Germany[83]. While a later study was unable to replicate this correlation, it was able to detect two new regions — one proximal to the *RMI2* gene (530kb from *DEXI*) and another proximal to the *ZC3H7A* gene (1.2Mb from *DEXI*) — where T1D disease variants interact with the promoter region of *DEXI*[77]. In this study, T and B cells from diseased individuals and healthy donors were used to identify chromosomal interactions via 3C of known regions containing candidate genomic regions previously identified[77]. Therefore, it remains

controversial which of the two genes (*DEXI* or *CLEC16A*) is causal for the T1D association as well as how they might contribute to T1D disease onset.

Since functional studies for *DEXI* were lacking until recently, whether this gene has any role in autoimmune disease including T1D remained unresolved. A recent study suggests a role for DEXI in the dsRNA-induced type I interferon (IFN) response. However, the experiments in this study were conducted *in vitro* using a human pancreatic β cell line and primary rat β cells[75]. Moreover, whether this gene alone has any role in autoimmunity remains unresolved. This highlights the need for *in vivo* functional and disease related studies for *DEXI*.

1.3 The NOD strain: an in vivo T1D mouse model

The NOD mouse strain is one of the two most commonly used animal models in T1D research next to the bio-breeding rat[84]. This strain of mice developed over 40 years ago originated in Japan from the Jcl:ICR strain which spontaneously develops cataracts[12,85,86]. Much like T1D development in humans, incidence of autoimmune diabetes is influenced by both genetic factors and environmental factors in the NOD mice[12,84-87]. Furthermore, one of the main genetic contributors to autoimmune diabetes incidence in the NOD mice is their MHC haplotype. These mice express the particular MHC-II molecule I-A^{g7} which is the murine ortholog for HLA-DQ in humans, but lack I-E the murine ortholog for HLA-DR in humans. NOD mice also contain a mutation within their I-A^{g7} that results in the substitution of the amino acid at position 57 of the β chain. In this mutation — also found in T1D patients — the charged aspartate residue being

replaced with a serine is sufficient to increase diabetes incidence in these mice[12,84-87]. Other genetic contributions to diabetes onset in NOD are being actively investigated with reports identifying genes such as: *Ctla4*, *Cd28*, *Icos*, *Il21*, *Il2*, insulin (*Ins1*), *Tnfrsf9*, among others[12,84-87].

Spontaneous diabetes onset in NOD mice varies according to sex with an incidence ranging between 50-90% in females and 20-30% in males by 30 weeks of age. Hyperglycemia and glucosuria in NOD mice is detected ~10 weeks at the earliest which is delayed when compared to human T1D onset, commonly diagnosed before adulthood[12,84-88]. However, NOD mice show signs of insulitis — lymphocyte infiltration and islet inflammation — as early as 3-4 weeks of age. Moreover, at around 8-10 weeks of age T cells in NOD mice have been reported to recognize a variety of islet autoantigens such as ZnT8, GAD 65, insulin and chromogranin A[12,84-88]. T1D patients and diabetic NOD mice share a few of these autoantigens, but their requirement for disease development or exacerbation is not fully understood in either setting[12,84-88]. In NOD mice particularly, it is believed that autoantibodies facilitate the propagation of the autoimmune response[12].

Using NOD mice as an animal model for T1D has aided a deeper understanding of the key players in disease pathogenesis. Among those is the requirement of innate and adaptive immune cells including: $CD4^+$ T, $CD8^+$ T, B cells, macrophages (Mφs), neutrophils and DCs in disease development[12,84-88]. This makes the NOD mouse strain a favored animal model for the study of potential immune modulatory elements that might affect T1D development.

1.4 Experimental Question & Rationale

DEXI's repeated association with T1D protection warrants the investigation of this gene's functional participation in T1D[3,34,41,54] as it could shed new insights on the development of T1D. For this reason, the work herein focuses on answering the following question: does *Dexi* contribute to the development of T1D? Describing the role of *DEXI* in the context of T1D would broaden our understanding of disease onset, of the involvement of Ch16p13.13 in disease and of *DEXI*'s role in autoimmunity.

Chapter 2

Generation & Immune Cell Characterization of *Dexi*-deficient NOD mice to study the role of *Dexi* in autoimmune diabetes development.

2.1 Contributions

Janice Marie Nieves-Bonilla performed experiments, analyzed data, and wrote the text for this chapter. Badr Kiaf harvested and isolated islets from pancreata of mice. Cornelia Schuster helped with experimental design and data interpretation. Stephan Kissler supervised the study, analyzed data, and wrote the published manuscript.

This chapter is partially adapted from the published manuscript Nieves-Bonilla, J.M., et al. The type 1 diabetes candidate gene Dexi does not affect disease risk in the nonobese diabetic mouse model. *Genes Immun* 21, 71–77 (2020). https://doi.org/10.1038/s41435-019-0083-y

2.2.1 Introduction

GWAS have implicated LDB genes within Ch16p13.13 with T1D and a variety of autoimmune diseases[3,10-17,21,41,42,77,83]. Among the four genes in this region is *DEXI*, a gene encoding a small conserved protein of 95 amino acids predicted to contain a transmembrane domain, a carboxy-terminal leucine zipper motif and a CKII phosphorylation site[41]. *DEXI* has been predicted to be a T1D risk gene by a variety of studies which have reported chromosomal interactions between disease variants and the *DEXI* promoter region that result in the modulation of *DEXI* expression[3,61,77-82](Figure 2). Until recently, functional studies for DEXI were lacking making it difficult to understand its involvement in autoimmunity. Association of DEXI with more than 5 autoimmune diseases[3,15,20,41,54,77,81] and a variety of immune-related diseases or events[61,79-83] suggest *DEXI* could be modulating disease through a role in immunity. This is strengthened by data from the Immgen database[72] which shows high *DEXI* expression among mice DCs and monocytes, as well as in human B cells[72]. Describing a role of *DEXI* in autoimmunity, specifically in the context of the autoimmune

disease T1D, would thus broaden our understanding of this disease's onset as well as the involvement of Ch16p13.13 in autoimmunity.

2.2.2 Specific Aim & Rationale

Despite the array of functional data supporting *CLEC16A* to be the causal gene for autoimmune disease association among Ch16p13.13[44,63,66-71], a dichotomy exists owing to disease-associated SNPs modulating both *CLEC16A*[34,43,44,67] and *DEXI*[3,61,77-82] expression. In order to fully understand the involvement of Ch16p13.13 in autoimmune disease onset it is imperative to unveil if *DEXI* has role in autoimmunity. *DEXI*'s previous association with T1D risk[3,15,41,77,83] and the availability of well-established rodent models of disease[12,84-87] justify a focus in the study of *DEXI*'s potential participation in T1D development. Moreover, *Dexi* is expressed in both immune organs[72](Figure 1) and immune cells[72] of NOD mice suggesting that *Dexi* KO in NOD mice could potentially alter T1D by immune related effects. For this reason, we set out to first generate a *Dexi* KO NOD mouse using CRISPR/Cas9 genome editing. This chapter describes the resulting work from experimental efforts aimed towards the characterization of CRISPR/Cas9-generated *Dexi* KO NOD mice.

2.3.1 NOD.*Dexi*$^{-/-}$ mice were generated using CRISPR/Cas9 as a genome editing tool

The discovery of the function of clustered regularly interspaced short palindromic repeat (CRISPR) and its associated (Cas) proteins ~15 years ago[89,90] gave rise to one of the most currently used genome editing tools. Part of a prokaryotic acquired immune system against virus and plasmids, CRISPR and Cas proteins work together to induce a

DNA double stranded break (DSB) by identifying homologous nucleotide sequences[89,90]. Specifically, the combination of CRISPR & Cas protein 9 (CRISPR/ Cas9) is necessary for the recognition of target nucleotides, i.e. RNA, and the effective formation of the nuclease complex that will cleave the target DNA sequence[89,90]. The CRISPR/Cas9 system has now been optimized and is used widely among the scientific community to engineer genomic mutations in both cell-based and whole organism animal models. This method is now preferred over the two other nuclease-based methods of genome editing zinc-finger nucleases and transcription activator-like effector nucleases (TALENs) due to its higher efficiency and efficacy[89,90]. For effective genome editing, CRISPR/Cas9 requires a fusion single-guide RNA (sgRNA) that contains the complementary genomic DNA sequence of the target followed by a protospacer adjacent motif (PAM) sequence which is a 3bp NGG motif[89,90]; along with the expression of a functional Cas9 protein. sgRNAs can be synthesized and purified *in vitro* and subsequently injected along with Cas9 mRNA or protein into the pronucleus of zygotes for the generation of mutant mice[90] or transfected into cells for the generation of mutant cell lines[91]. This system's rapid efficiency made it an ideal choice for the generation of a *Dexi*-deficient NOD mice in the current study.

Therefore, the CRISPR/Cas9 genome editing tool was used to generate an NOD mouse line which lacked *Dexi*. Initial attempts using a single sgRNA containing a sequence homologous to the beginning of *Dexi*'s coding region proved unsuccessful. To increase the chances of obtaining a complete deletion of *Dexi*'s protein-coding genomic sequence, two sgRNAs with corresponding PAM sequences (Table 1) were designed

Table 1. Nucleotide sequences used for the generation, genotyping, and gene expression analysis of *Dexi* KO mice. PAM sequences are marked in red.

Name	Sequence
mDexiKO-g1-Forward	5'-CACCGATGGGCAGTGAGCCTGCGG-3'
mDexiKO-g1-Reverse	5'-AAACCCGCAGGCTCACTGCCCATC-3'
mDexiKO-g2-Forward	5'-CACCGGGATGGGACCCCAGGAAG-3'
mDexiKO-g2-Reverse	5'-AAACCTTCCTGGGGTCCCATCCC-3'
T7_mDexiKO_g1-Forward *(In Vitro Transcription)*	5'-TTAATACGACTCACTATAGGATGGGCAGTGAGCCTGCGG-3'
T7_mDexiKO_g2-Forward *(In Vitro Transcription)*	5'-TTAATACGACTCACTATAGGGGGATGGGACCCCAGGAAG-3'
T7_mDexiKO-Reverse *(In Vitro Transcription)*	5'-AAAAGCACCGACTCGGTGCC-3'
mDexiKO_genoA1-Forward	5'-ACAAAGGTGGTCTGTAAACCG-3'
mDexiKO_genoA1-Reverse	5'-TGGCAATGTTGGCAATCAGG-3'
mDexiKO_genoA2-Forward	5'-CTTTTCCACCCGGCATCATT-3'
mDexiKO_genoA2-Reverse	5'-TTGACACCCCGAGATGCT-3
m*Actb*-Forward	5'-GGCTGTATTCCCCTCCATCG-3'
m*Actb*-Reverse	5'-CCAGTTGGTAACAATGCCATGT-3'
m*Dexi*-Forward	5'-CTGCTGCCCTCTATGTTCTACG-3'
m*Dexi*-Reverse	5'-GCCAGGGTCTGAAAGTACGC-3'
m*Clec16a*-Forward	5'-CCTGATTTGGGGCGATCAAAA-3'
m*Clec16a*-Reverse	5'-CATAACGGCCTGATTTCTGCC-3'
m*Socs1*-Forward	5'-CTGCGGCTTCTATTGGGGAC-3'
m*Socs1*-Reverse	5'-AAAAGGCAGTCGAAGGTCTCG-3'
m*Ciita*-Forward	5'-TGCGTGTGATGGATGTCCAG-3'
m*Ciita*-Reverse	5'-CCAAAGGGGATAGTGGGTGTC-3'
m*Ins1*-Forward	5'-ACCCACCCAGGCTTTTGTC-3'
m*Ins1*-Reverse	5'-TCCCCACACACCAGGTAGAGA-3'
m*Glucagon*-Forward	5'-TCACAGGGCACATTCACCAG-3'
m*Glucagon*-Reverse	5'-CATCATGACGTTTGGCAATGTT-3'

Table 1. (Continued)

Name	Sequence
m*Ifnb1* (IFN-β)-Forward	5'-CAGCTCCAAGAAAGGACGAAC-3'
m*Ifnb1* (IFN-β)-Reverse	5'-GGCAGTGTAACTCTTCTGCAT-3'
m*Rsad2*-Forward	5'-TGCTGGCTGAGAATAGCATTAGG-3'
m*Rsad2*-Reverse	5'-GCTGAGTGCTGTTCCCATCT-3'
pMSCV-Forward	5'-CCCTTGAACCTCCTCGTTCGACC-3'
pMSCV-Reverse	5'-GAGACGTGCTACTTCCATTTGTC-3'

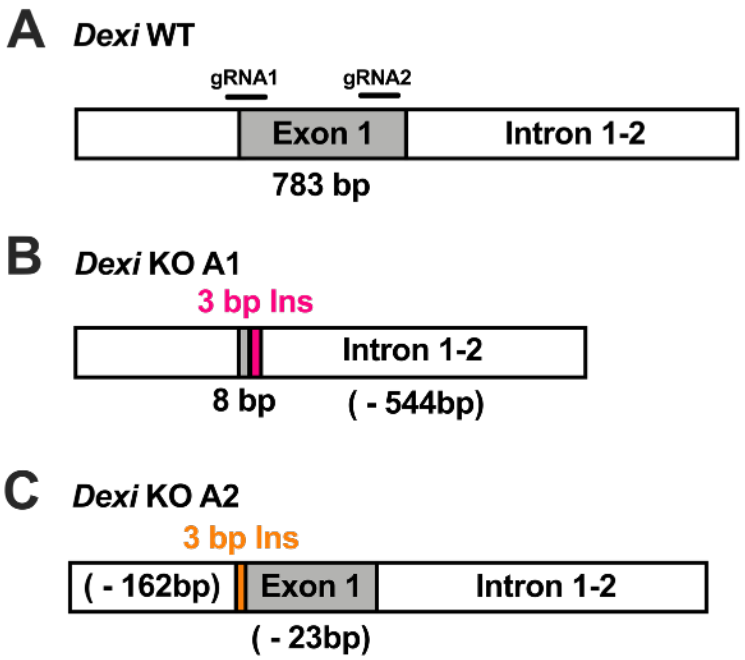

Figure 3. Generation of NOD.*Dexi*$^{-/-}$ mice. A Shows a schematic representation of the region targeted by the sgRNAs used for CRISPR/Cas9 genome editing in the *Dexi* genomic region. **B** This schematic represents the *Dexi* KO A1 mutation. In the case of this mutation, only the first 8 bp of exon 1 remain, followed by a 3 bp insertion and a 544 bp deletion at the start of intron 1–2. **C** Similar schematic representation of the *Dexi* KO A2 mutation in which 162bp prior to *Dexi*'s exon were deleted along with 23bp extra within the start of exon 1. A 3bp insertion was also observed in these mutant mice.

and selected using a published algorithm by Xu et al.[92‡] The first sgRNA: mDexiKO-g1 contained a sequence homologous to the beginning of *Dexi*'s unique coding exon while

‡. accesible at: http://crispr.dfci.harvard.edu/SSC/

a second sgRNA — mDexiKO-g2 — included a homologous sequence present near the end of *Dexi*'s exon 1, flanking the whole exon (Figure 3A). Both sgRNAs and Cas9 mRNA were injected into into the pronucleus of NOD zygotes to generate DNA DSB at either end of the protein-coding exon. Injected NOD zygotes were then implanted into Swiss-Webster surrogate foster mice.

2.3.2 Genotyping & Propagation of NOD.*Dexi*$^{-/-}$ mice

The resulting seven founder pups were genotyped to identify possible *Dexi* mutants. Genotyping polymerase chain reaction (PCR) using primers homologous to the beginning and end of the targeted region (Figure 4D) revealed a potential founder mouse which lacked an intact *Dexi* band (Figure 4A). Sanger sequencing confirmed a 1330bp near complete disruption of *Dexi*'s genomic sequence (Figure 3B) which spanned most of exon 1 and included the protein-coding open reading frame (ORF) (Figure 4B). Following mating of the founder mutant mouse with a wild type (WT) NOD, genotyping of F1 progeny proved challenging. This was due to the inability of the PCR protocol to distinguish between heterozygote and homozygote mutations in these mice (Figure 4E). Thus, a second PCR protocol was developed to make feasible the detection of these genotypes. By using a set of primers that were homologous to a small target sequence within the start of *Dexi*'s exon 1 and running mouse DNA samples through both of these protocols separately, the distinction between heterozygote and homozygote mutations was finally achieved (Figure 4F). The second PCR protocol also aided in the identification of a second mutation generated in the founder mouse (Figure 3C). This deletion mutation spanned only 185bp along the start of *Dexi*'s exon 1, leaving the protein-coding ORF intact (Figure 4C). The 1330bp

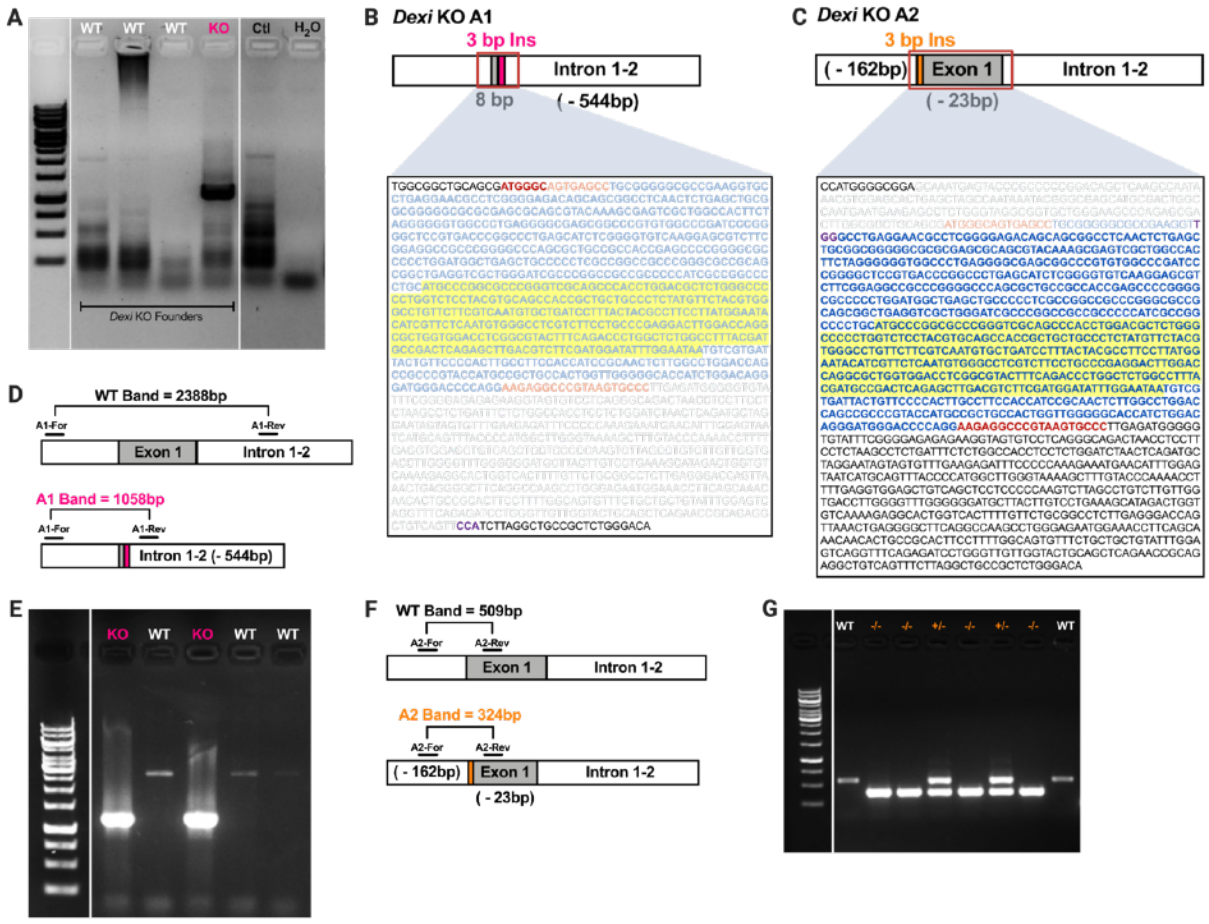

Figure 4. NOD.*Dexi*$^{-/-}$ mice genotyping requires two PCR protocols. **A** Genotyping results for 4 of the 7 pups following CRISPR/Cas9 genome editing. Only the mouse in lane 4 showed a smaller for *Dexi* following PCR amplification. An NOD mouse was used as positive control and nuclease-free water as a negative control. **B** Detailed genomic sequence of NOD.*Dexi*$^{-/-}$ A1 as mapped by Sanger sequencing using the primers described below for genotyping. Exon 1 is shown in red, the CRISPR/Cas9 targeted region in blue, and the coding ORF is highlighted in yellow. The shaded area maps the 1330bp deletion found in the founder mouse. **C** Genomic sequence detailing the NOD.*Dexi*$^{-/-}$ A2 mutation which consists of a ~185bp deletion. Both mutations also resulted in 3bp insertion (shown in purple) upon DNA repair. *Dexi* KO mice are genotyped using 2 PCR protocols with primers that target different sections of the coding region of *Dexi* allowing for the distinction between heterozygote vs homozygote mutant mice and between each respective mutation. **D** Schematic representation of the first genotyping PCR protocol which uses a set of primer spanning a large portion of *Dexi*'s genomic sequence and yields ~2Kb bands for WT NOD mice and a ~1Kb for NOD.*Dexi*$^{-/-}$ A1 mutant mice. **E** Representative 1% agarose gel of genotyping results for NOD.*Dexi*$^{+/-}$ A1 progeny using the primers described in **D**. **F** Schematic representation of the second genotyping PCR protocol which uses a set of primer spanning only a small portion within the start of *Dexi*'s genomic sequence. This PCR protocol yields a band WT band that is ~500bp in size bands and can be used to determine heterozygosity in NOD.*Dexi*$^{+/-}$ A1 mice which posses a single WT allele. This PCR protocol also led to the discovery of a second allele mutation in the founder *Dexi* KO mouse, and it is simultaneously used for genotyping the NOD.*Dexi*$^{-/-}$ A2 mice which show a single band at ~300bp. **G** Representative 1% agarose gel of genotyping results for NOD.*Dexi*$^{+/-}$ A2 progeny using the primers described in **F**.

deletion was then referred to as the allele #1 (A1) mutation and the 185bp deletion as allele #2 (A2) mutation. Moreover, due to the evident lack of portions of the *Dexi* genomic sequence these mice were referred to as *Dexi* knockout (KO) or *Dexi*-deficient NOD (NOD.*Dexi*$^{-/-}$) mice moving forward.

Breeding of the *Dexi* KO founder mouse containing both mutated alleles with NOD WT mice to expand and establish two separate NOD.*Dexi*$^{-/-}$ mice lines led to an unexpected genotype segregation within the F1 pups. Contrary to the expected 50% NOD.*Dexi*$^{+/-}$ A1 vs NOD.*Dexi*$^{+/-}$ A2, each of the mutant alleles segregated into ~25% of the progeny, while the remaining pups (~50%) carried only WT alleles (Figure 5A). These data indicate that the original founder mutant mouse was chimeric, specifically containing chimeric germ cells (Figure 5B). Taking this together, it is likely that the observed germ cell chimerism resulted from single CRISPR/Cas9-induced DSBs occurring simultaneously at each cell during the two-cell stage of embryonic development.

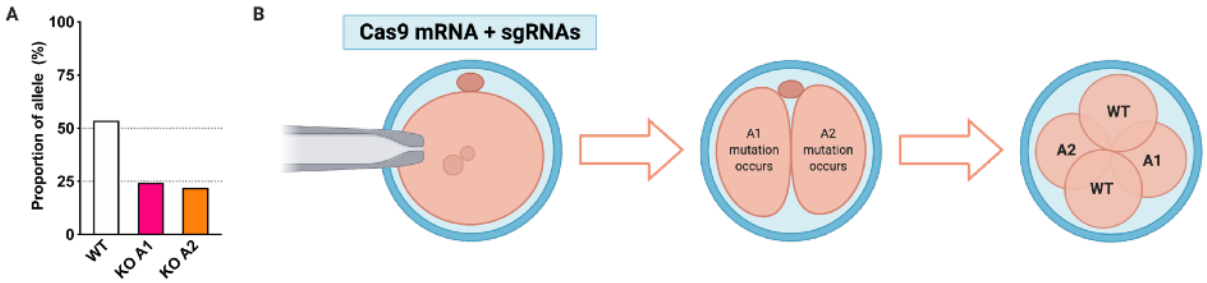

Figure 5. <u>Generation of a *Dexi* KO via CRISPR/Cas9 results in chimeric founder germ cells.</u> A The male founder was bread with 3 different NOD females which birthed a total of 5 F1 litters. The inheritance pattern is graphed as the proportion of wild-type and mutant alleles inherited from the founder mouse (total 41 mice, of which 10 carried the A1 mutation and 9 carried the A2 mutation). **B** Schematic representation of the CRISPR/Cas9 events which led to chimeric germ cells in the founder and consequently resulted in the F1 progeny distributions shown in **A**.

2.3.3 Generation, Genotyping & Propagation of NOD.*Dexi*$^{-/-}$*Clec16a*^{KD} mice

To test for possible interactions between *Clec16a* and *Dexi*, NOD.*Dexi*$^{-/-}$ mice were intercrossed with NOD.*Clec16a*^{KD} mice, which were previously generated in our lab[66], to generate double-mutant mice. Whole-mouse constitutive KD of *Clec16a* in NOD.*Clec16a*^{KD} mice is mediated by a lentiviral transgene that is not in proximity of Ch16p13.13, making it possible to combine these mutations by breeding. The lentiviral transgene used in these mice also confers the expression of green fluorescent protein (GFP) as a marker which correlates well with transgene expression[66,93]. For this reason, NOD.*Clec16a*^{KD} mice were genotyped based on GFP expression among lymphocytes via flow cytometry (Figure 6). Mice expressing from 50-75% of GFP were considered to contain only a single transgene allele (Figure 6C), while mice expressing >75% of GFP were considered homozygous for the lentiviral transgene (Figure 6D) and referred to as NOD.*Clec16a*^{KD} or NOD.*Clec16a*$^{KD/KD}$ mice. NOD.*Clec16a*$^{KD/KD}$ mice were bred with NOD.*Dexi*$^{-/-}$ A1 and A2 mice to create two different lines of double-deficient mice: NOD.*Dexi*$^{-/-}$*Clec16a*^{KD} A1 and NOD.*Dexi*$^{-/-}$*Clec16a*^{KD} A2. These mice were genotyped using both flow cytometry for GFP detection as well as the genotyping PCRs previously described for *Dexi* detection. NOD.*Dexi*$^{-/-}$*Clec16a*^{KD} mice were considered as such only when mice were homozygous for each *Dexi* KO mutation and expressed >85% of GFP among lymphocytes. Double mutant mouse lines were propagated further by intercrossing NOD.*Dexi*$^{-/-}$*Clec16a*^{KD} mice with each other.

2.4.1 *Dexi* deficiency was validated in NOD.*Dexi*$^{-/-}$ and NOD.*Dexi*$^{-/-}$*Clec16a*^{KD} mice

To validate each *Dexi* KO mouse line mutation, *Dexi* mRNA expression was

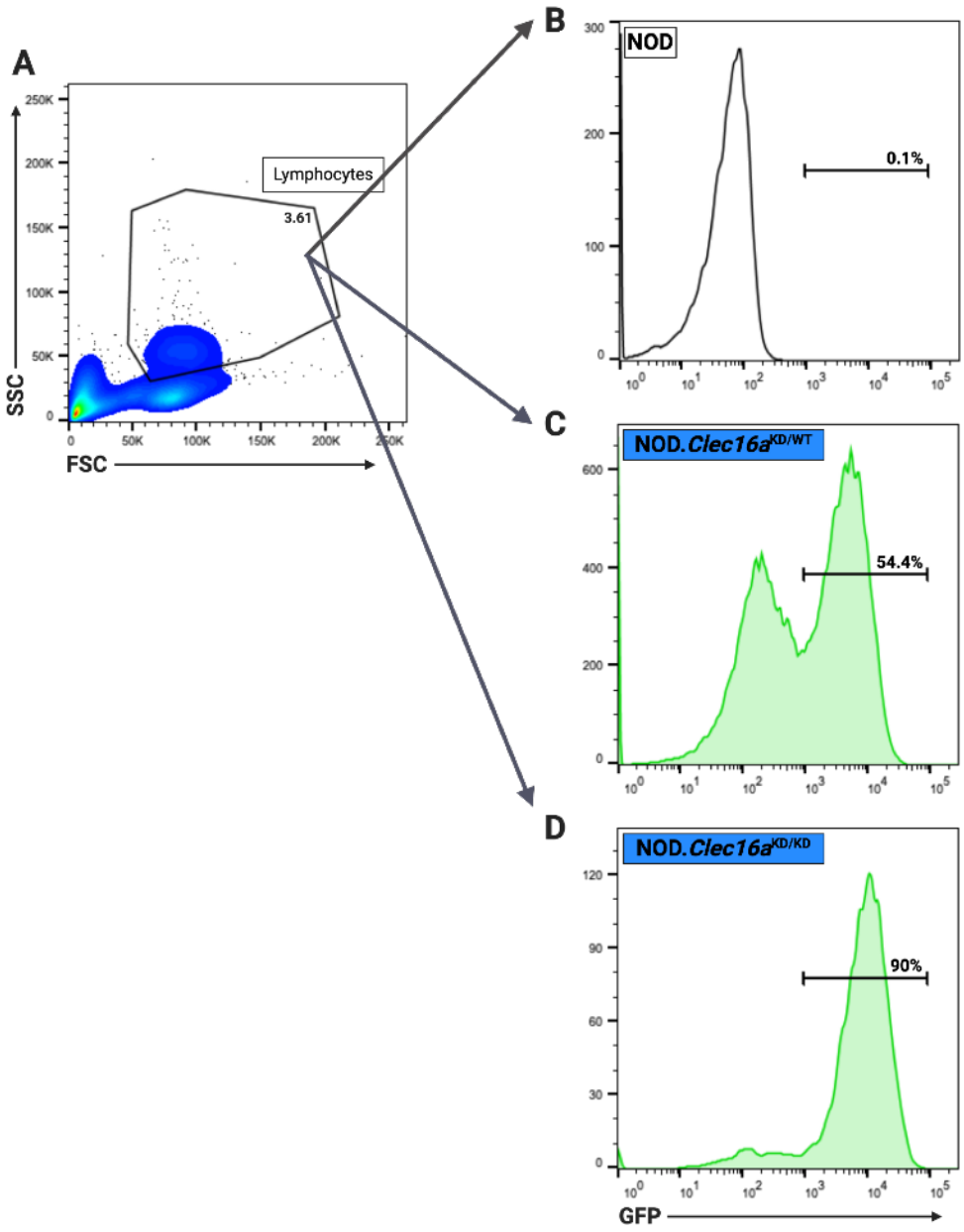

Figure 6. <u>Genotyping NOD.*Dexi*$^{-/-}$*Clec16a*^{KD} mice by assessing GFP expression with flow cytometry.</u> **A** Pseudocolor dot plot example of the gate used to quantify GFP expression among the selected circulating lymphocytes for genotyping of *Clec16a*^{KD} within the analyzed mice. Expression of GFP can be more easily quantified when gating for granule-containing lymphocytes which present at a slightly higher location within the side scatter (SSC). The SSC discriminates cells by internal complexity, where components such as granules and the nucleus can increase the SSC. The forward scatter (FSC) discriminates cells by size with its intensity being propositional to cell diameter. **B** Example of a histogram plot for GFP expression among lymphocytes obtained from the blood of a WT NOD mouse which lacks GFP expression. An example for mice containing only a single allele of the *Clec16a*^{KD} transgene is shown in **C**. **D** Histogram plot example for the GFP expression within lymphocytes of a mouse with both alleles of the *Clec16a*^{KD} transgene.

measured via quantitative real-time PCR (qPCR) in relevant organs of homozygous mutant mice. Data confirmed the absence of *Dexi* transcript in the spleen, thymus, lymph nodes (LNs), and pancreatic islets (Figure 7A) of female (Figure 7B) and male (Figure 7C) NOD.*Dexi*$^{-/-}$ A1 mice. Despite the smaller mutation, male and female

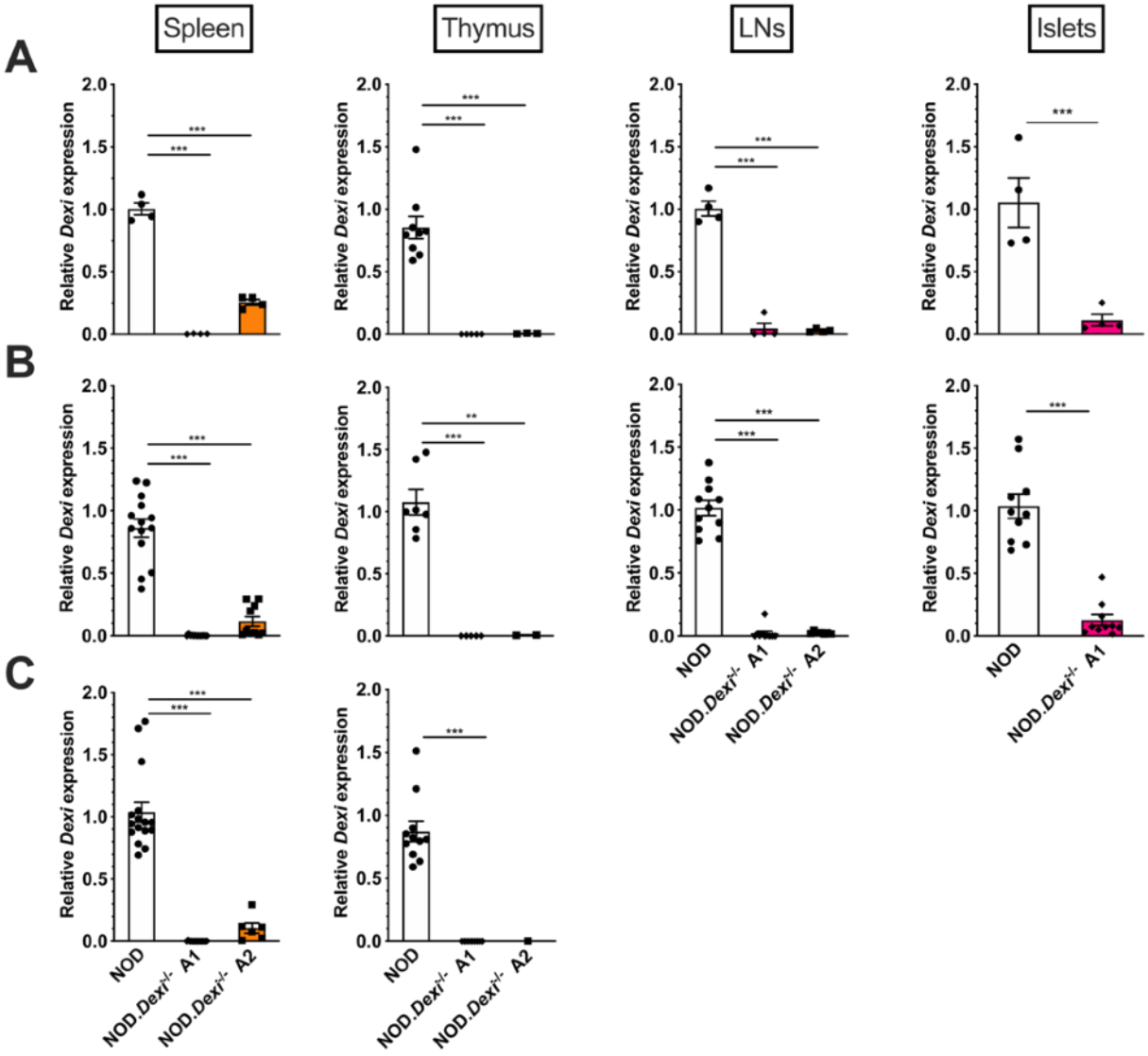

Figure 7. <u>NOD.*Dexi*$^{-/-}$ A1 mice lack *Dexi* mRNA expression.</u> **A** Quantification of *Dexi* transcript levels within spleen, thymus, LNs, and pancreatic islets of NOD WT and *Dexi* KO mice by quantitative PCR. Results for spleen, LNs, and pancreatic islets are n=4 mice per group, while for thymus are n=9 (NOD), n=5 (A1), and n=3 (A2). Data show individual values and mean±SEM and are representative of at least three similar experiments. *Dexi* transcript levels for all female samples studied are shown **B**, while male samples for spleen and thymus are depicted in **C**. **P<0.01, ***P<0.001, ns=not significant; P>0.05 (two-tailed t-test). Relative expression was determined as $2^{[-(Dexi\ Ct\ -\ \beta\text{-}Actin\ Ct)]}$ using NOD mouse samples as a baseline.

NOD.*Dexi*$^{-/-}$ A2 mice also lacked *Dexi* transcript in thymus and LN and to a lesser degree in the spleen (Figure 7). *Dexi* transcript was not measured in the islets of NOD.*Dexi*$^{-/-}$ A2 mice. Lastly, splenic lysates of NOD.*Dexi*$^{-/-}$*Clec16a*^{KD} A1 (Figure 8A) and A2 (Figure 8B) mice also lacked *Dexi* transcript.

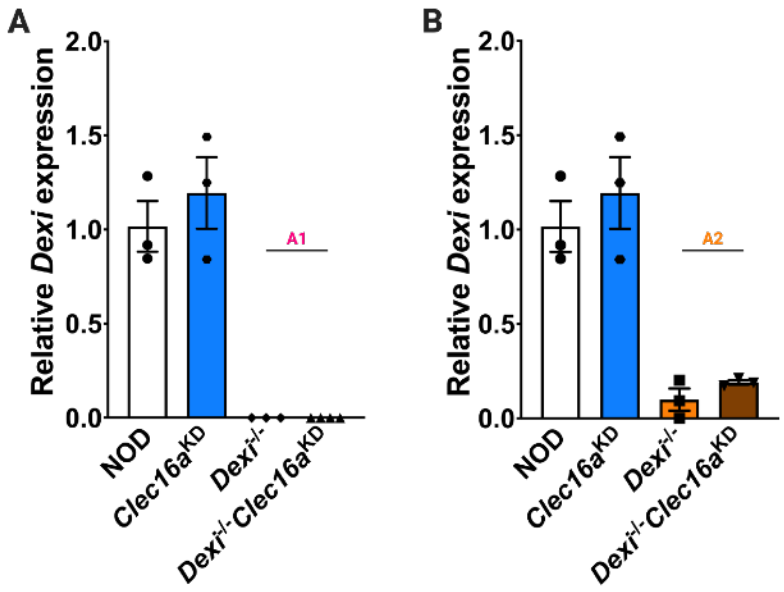

Figure 8. NOD.*Dexi*$^{-/-}$*Clec16a*^{KD} mice also lack *Dexi* mRNA expression. **A** Quantification of *Dexi* transcript levels within spleen of NOD WT, NOD.*Clec16a*^{KD}, NOD.*Dexi*$^{-/-}$ A1, and NOD.*Dexi*$^{-/-}$*Clec16a*^{KD} A1 mice by quantitative PCR. Results are n=3-4 mice per group. Data show individual values and mean±SEM in a single experiment. *Dexi* transcript levels for NOD, NOD.*Clec16a*^{KD}, NOD.*Dexi*$^{-/-}$ A2, and NOD.*Dexi*$^{-/-}$*Clec16a*^{KD} A2 mice are shown in **B**. Results are n=3 mice per group. Data show individual values and mean±SEM in a single experiment that was conducted simultaneously with samples shown in **A**. Relative expression was determined as $2^{[-(Dexi\ Ct - CyclophilinA\ Ct)]}$ using NOD mouse samples as a baseline.

Measuring the levels of Dexi protein proved difficult due to the small size of the protein (~10kDa), its low abundance in relevant tissues and the low availability of validated mouse-reactive antibodies. Initial attempts using Dexi antibodies from two different companies were inconsistent and difficult to interpret due to the high levels of unspecific binding by each antibody (Figure 9). In order to validate the specificity of the existing antibodies for mouse Dexi protein detection, the generation of a tagged Dexi fusion protein was necessary. Therefore, the genomic sequence for the generation of a

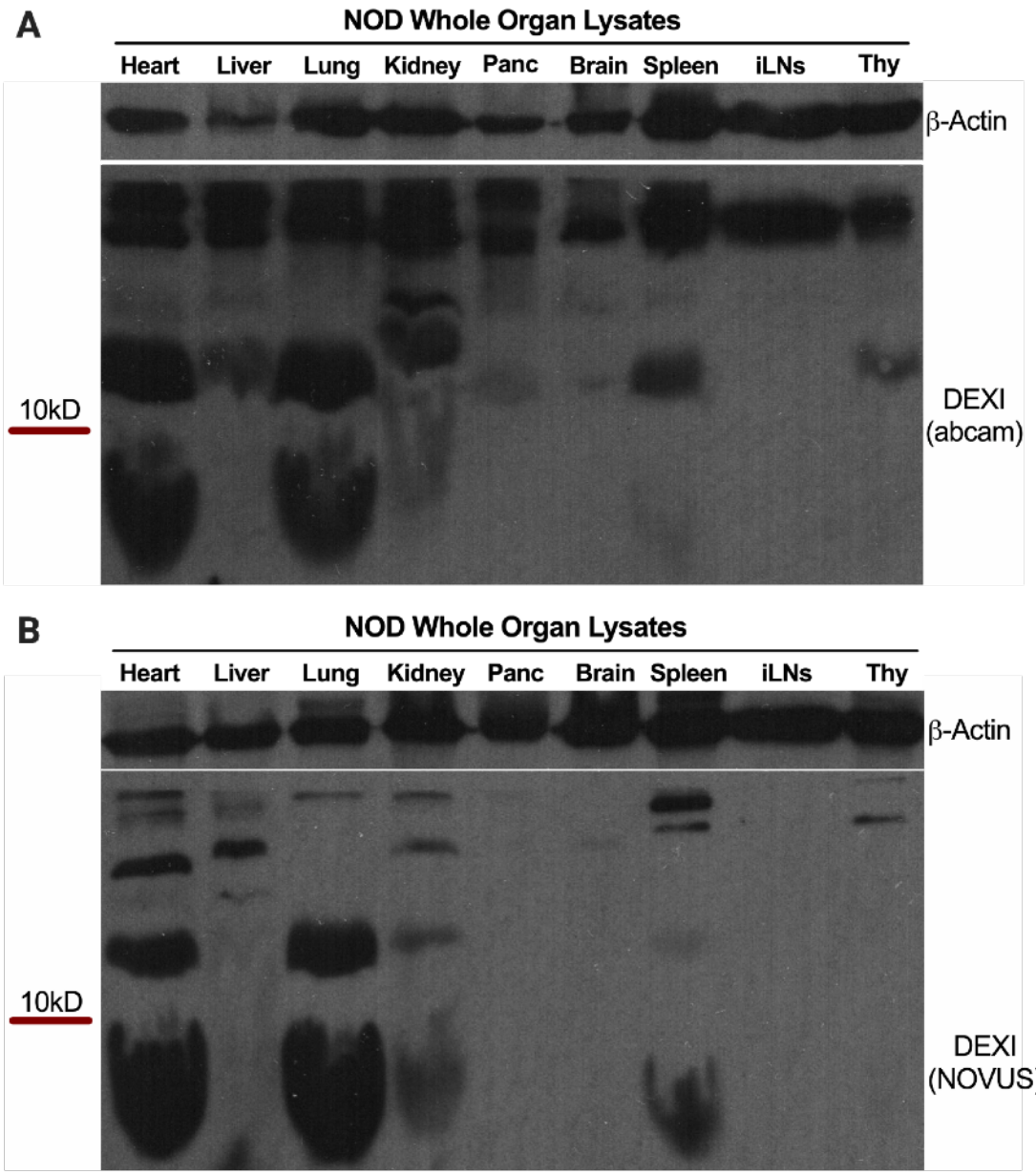

Figure 9. **Failure of simple detection of DEXI protein expression via western blot.** **A** Detection of Dexi protein in mechanically-disrupted organ lysates of NOD mice. Abcam anti-DEXI antibody (ab130511) was used and 60µg of protein were loaded onto an 15% SDS-PAGE gel. **β**-Actin was used as a loading control. The same samples were tested using the NOVUS anti-DEXI antibody (NBP1-81015) under the same conditions and are shown in **B**. While it is expected for Dexi to be highest in in the lung, kidney and heart of mice, the expression of Dexi in the pancreas, which should also be among the highest, is barely observed with either antibody. It is also unclear which of the bands seen above or below the 10kD mark are the correct indicators of Dexi as they are not consistently expressed among samples.

FLAG-Tagged Dexi recombinant protein was cloned into the puromycin-resistant murine stem cell virus for retroviral expression plasmid (pMSCV-puro) which allowed for

puromycin selection when expressed. This sequence consisted of the genomic mouse sequence for *Dexi*'s protein coding ORF preceded by the genomic sequence for the FLAG tag and a flexible linker between Dexi's N-terminal domain and FLAG (Figure 10A-B). In a preliminary attempt to detect FLAG, HEK293T cells and the insulin-secreting murine β cell line NIT-1, were transiently transfected with the FLAG-DEXI plasmid and selected for using puromycin treatment. The NIT-1 cell line is derived from the insulinomas of transgenic NOD mice which harbor a hybrid rat insulin-promoter/ SV40 large T antigen gene that results in the spontaneous development of β cell adenomas[94] and is used as an *in vitro* model of insulin-secreting murine β cells. Immunoblotting of total protein lysates for FLAG, showed unspecific binding and lacked bands near the DEXI protein region which is predicted to be 10kDa in size (Figure 10C). However, immunoprecipitation (IP) and western blotting for FLAG in transfected cells showed less unspecific binding and a band about 10kDa in size was observed (Figure 10D).

Figure 10. <u>Generating a FLAG-Tagged Dexi recombinant protein for the validation of anti-DEXI antibodies.</u> A The genomic sequence for the generation of a FLAG-Tagged DEXI recombinant protein depicted was cloned into the expression plasmid pMSCV-puro. Dexi's protein coding sequence (blue) is preceded by the sequence for the FLAG tag (green) and a flexible linker (brown). **B** Visual representation of the expected recombinant FLAG-tagged Dexi protein used to validate anti-Dexi antibodies for the detection of Dexi in mice. **C** Whole protein lysates from pMSCV-puro-DEXI-FLAG transfected HEK293T & NIT-1 cells were immunoblotted for FLAG and β-actin. **D** Lysates from pMSCV-puro-DEXI-FLAG transfected HEK293T & NIT-1 cells were used to IP using an anti-FLAG antibody followed by immunoblotting for FLAG. **E** Protein lysates from retrovirus-infected NIT-1s selected via two subsequent rounds of puromycin treatment were collected and used for IP with anti-FLAG antibody. Immunoblotting with anti-FLAG antibody failed to detect stable expression of the recombinant FLAG-tagged Dexi protein in NIT-1 cells. **F** Whole protein lysates and lysates following IP with anti-FLAG antibody from pMSCV-puro-DEXI-FLAG transfected and puromycin-selected HEK293T were blotted using the anti-DEXI antibody from NOVUS. These lysates were also blotted with the anti-DEXI antibody from abcam which is shown **H**. The NOVUS anti-DEXI antibody was selected for further studies due to its specificity in detecting the FLAG-DEXI fusion protein in whole protein lysates as well as flowing IP using anti-FLAG. Immunoblotting with anti-FLAG antibody was used to confirm FLAG detection among whole protein lysates (**G**) and lysates following IP with anti-DEXI antibody (**I**) in pMSCV-puro-DEXI-FLAG transfected and puromycin-selected HEK293T cells. **J** Lysates from pMSCV-puro-DEXI-FLAG transfected puromycin-selected were once again used to IP using an anti-FLAG antibody or the anti-DEXI antibody. Clear detection of the mouse FLAG tagged Dexi recombinant protein was observed upon western blotting using the anti-FLAG or anti-DEXI antibodies in both IP samples as well as in whole protein lysates. Data shown is representative for at least two similar experiments.

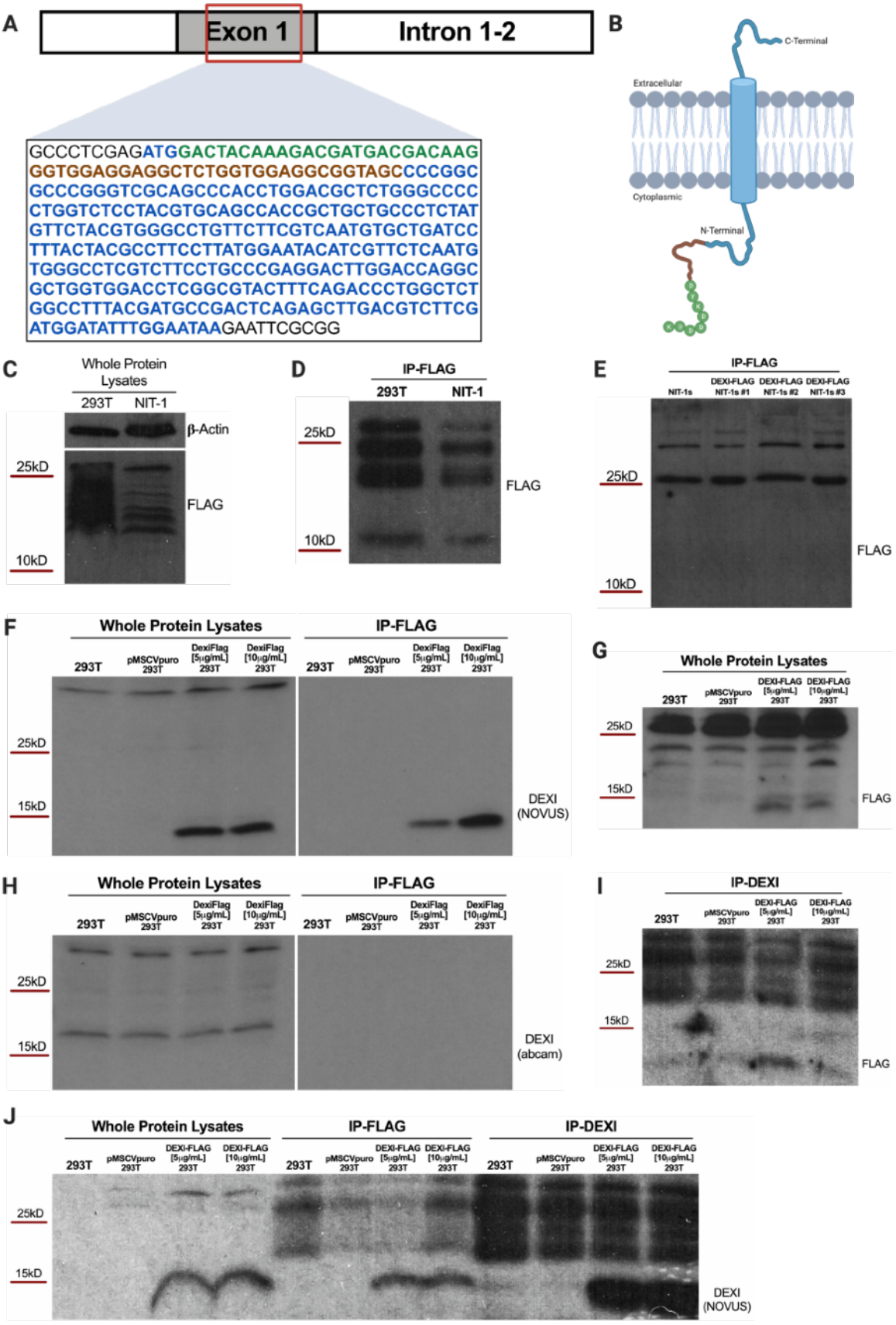
A
Exon 1
Intron 1-2
GCCCTCGAGATGGACTACAAAGACGATGACGACAAG
GGTGGAGGAGGCTCTGGTGGAGGCGGTAGCCCCGGC
GCCCGGGTCGCAGCCCACCTGGACGCTCTGGGCCCC
CTGGTCTCCTACGTGCAGCCACCGCTGCTGCCCTCTAT
GTTCTACGTGGGCCTGTTCTTCGTCAATGTGCTGATCC
TTTACTACGCCTTCCTTATGGAATACATCGTTCTCAATG
TGGGCCTCGTCTTCCTGCCCGAGGACTTGGACCAGGC
GCTGGTGGACCTCGGCGTACTTTCAGACCCTGGCTCT
GGCCTTTACGATGCCGACTCAGAGCTTGACGTCTTCG
ATGGATATTTGGAATAAGAATTCGCGG
B
C-Terminal
Extracellular
Cytoplasmic
N-Terminal
C
Whole Protein Lysates
293T
NIT-1
β-Actin
25kD
FLAG
10kD
D
IP-FLAG
293T
NIT-1
25kD
10kD
FLAG
E
IP-FLAG
NIT-1s
DEXI-FLAG NIT-1s #1
DEXI-FLAG NIT-1s #2
DEXI-FLAG NIT-1s #3
25kD
10kD
FLAG
F
Whole Protein Lysates
IP-FLAG
293T
pMSCVpuro 293T
DexiFlag [5μg/mL] 293T
DexiFlag [10μg/mL] 293T
25kD
15kD
DEXI (NOVUS)
G
Whole Protein Lysates
293T
pMSCVpuro 293T
DEXI-FLAG [5μg/mL] 293T
DEXI-FLAG [10μg/mL] 293T
25kD
15kD
FLAG
H
Whole Protein Lysates
IP-FLAG
293T
pMSCVpuro 293T
DexiFlag [5μg/mL] 293T
DexiFlag [10μg/mL] 293T
25kD
15kD
DEXI (abcam)
I
IP-DEXI
293T
pMSCVpuro 293T
DEXI-FLAG [5μg/mL] 293T
DEXI-FLAG [10μg/mL] 293T
25kD
15kD
FLAG
J
Whole Protein Lysates
IP-FLAG
IP-DEXI
293T
pMSCVpuro 293T
DEXI-FLAG [5μg/mL] 293T
DEXI-FLAG [10μg/mL] 293T
25kD
15kD
DEXI (NOVUS)

In order to generate a murine cell line which stably expresses the FLAG-Tagged Dexi recombinant protein and therefore allow for rapid and consistent sample collection in subsequent experiments, HEK293T cells were transfected with the retroviral packaging plasmid pCL-eco and the FLAG-DEXI expression plasmid to generate virus. The FLAG-DEXI-containing retrovirus produced was used to generate FLAG-DEXI-expressing NIT-1 cells. Infected cells were selected using two subsequent puromycin treatments. Unexpectedly, puromycin-resistant NIT-1s lacked expression of the FLAG-DEXI fusion protein (Figure 10E). While further validation using NIT-1s would have been ideal, the established and highly transfectable cell line HEK293T was selected for subsequent experiments. It should be noted that pMSCV-puro is optimized for the stable expression of murine genes in mostly murine cell lines. Therefore, in order to avoid further complications, the pMSCV-puro-FLAG-DEXI construct was instead transiently expressed in HEK293Ts in all further experiments. FLAG-DEXI was clearly detected in whole protein lysates of transfected cells when western blotting with the anti-FLAG antibody (Figure 10G) or the anti-Dexi antibody from NOVUS biologics (Figure 10F), but was not detected when the anti-Dexi antibody from abcam was used (Figure 10H). Additionally, IP of FLAG-DEXI using the FLAG antibody or the anti-Dexi antibody, enhanced Dexi protein detection with the Dexi antibody from NOVUS (Figure 10J). Lastly, to confirm the anti-Dexi antibody from NOVUS was indeed pulling down the fusion protein in addition to any endogenous DEXI, lysates from IP using the anti-Dexi antibody were immunoblotted for FLAG detection. As shown in Figure 10I, FLAG was detected in transfected samples following IP with the anti-Dexi antibody.

Since previous attempts at detecting Dexi in whole protein lysates of mouse

organs had been unsuccessful — likely due to the low abundance of *Dexi* protein *in vivo* — IP using the Dexi antibody was used as an enrichment method. IP and western blot (WB) using the Dexi antibody resulted in the successful and clear detection of Dexi protein in transfected HEK293T cells (Figure 10J), as well as in the pancreas (Figure 11A) of NOD mice. This was also observed to a lesser degree in the spleen of NOD mice (Figure 11B). Importantly, pancreas — containing high levels of Dexi — and spleens of NOD.*Dexi*$^{-/-}$ A1 as well as NOD.*Dexi*$^{-/-}$*Clec16a*^{KD} A1 mice lacked Dexi protein expression (Figure 11) confirming the complete abrogation of *Dexi* in these transgenic mice. Lastly, preliminary results from whole protein lysates of NOD.*Dexi*$^{-/-}$ A2 and NOD.*Dexi*$^{-/-}$*Clec16a*^{KD} A2 pancreas (Figure 11C) and spleen (Figure 11C) suggest that these mice also lack Dexi protein. IP with Dexi antibody in these samples was not

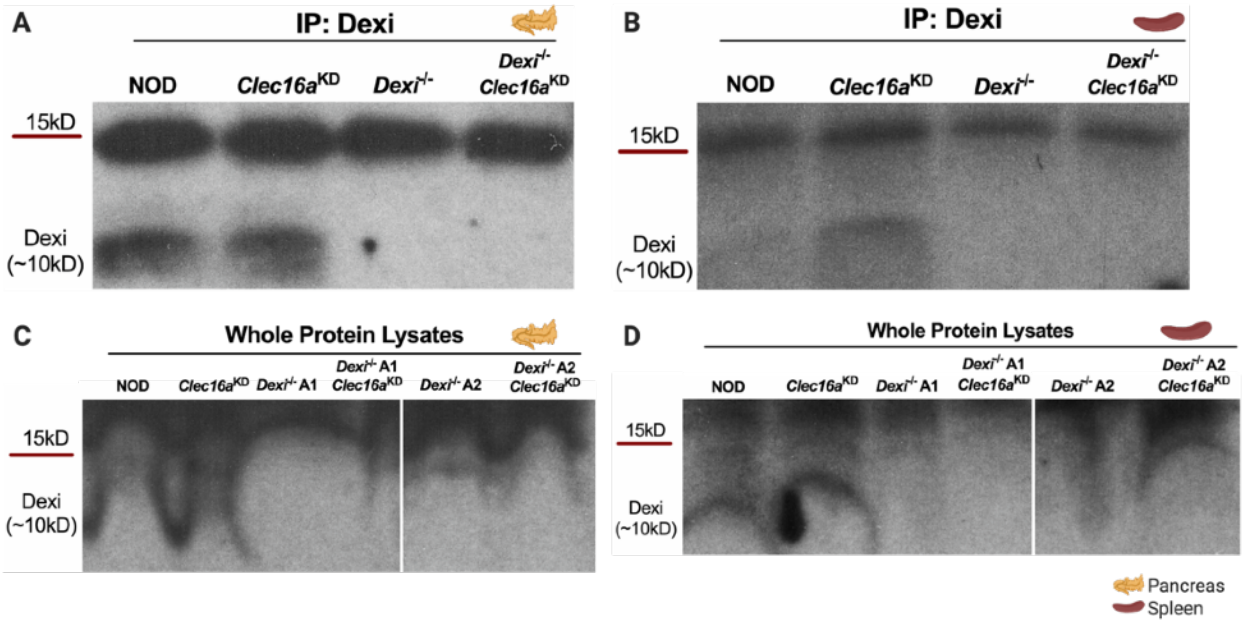

Figure 11. <u>Validated anti-DEXI antibody allows clear protein detection of Dexi in NOD WT, but not in NOD.*Dexi*$^{-/-}$ or NOD.*Dexi*$^{-/-}$*Clec16a*^{KD} mice.</u> A Protein lysates collected from the pancreas of NOD, NOD.*Dexi*$^{-/-}$ A1, NOD.*Clec16a*^{KD}, and NOD.*Dexi*$^{-/-}$*Clec16a*^{KD} A1 mice were immunoprecipitated using anti-DEXI antibody. Mouse Dexi protein was clearly detected in IP lysates by western blotting with the anti-DEXI antibody. Spleen lysates were also collected and are shown in **B**. **C** Expression of Dexi protein in whole protein lysates from the pancreas of NOD, NOD.*Dexi*$^{-/-}$ A1 & A2 mice, NOD.*Clec16a*^{KD}, and NOD.*Dexi*$^{-/-}$*Clec16a*^{KD} A1 & A2 mice. Whole protein lysates from the spleen of these mice were also collected and are depicted in **D**. Data shown are representative for two similar experiments.

employed and would thus be necessary to confirm Dexi protein levels in the NOD.*Dexi*$^{-/-}$ A2 mice.

2.4.2 The expression of Ch16p13.13 genes is not affected in NOD.*Dexi*$^{-/-}$ mice

The mRNA levels of the three other Ch16p13.13 genes were measured in both *Dexi* KO mutant lines by qPCR. Data collected using samples from spleen, islets, thymi and LNs of NOD.*Dexi*$^{-/-}$ A1 mice show no significant alterations to the expression of *Clec16a* (Figure 12A) upon *Dexi* deletion. Similarly, qPCR data from spleen, and LNs of NOD.*Dexi*$^{-/-}$ A2 mice suggest no significant changes in *Clec16a* mRNA. It should be noted that there is low expression of *Clec16a* in LN lymphocytes[72], which can make Ct values vary among samples.

Socs1 mRNA levels were also measured in the spleen, thymi, islets and LNs of NOD.*Dexi*$^{-/-}$ A1 mice. No significant changes were observed in samples from spleen, thymi, and islets of NOD.*Dexi*$^{-/-}$ A1 mice (Figure 12B). Variability in the mRNA levels of *Socs1* was observed among the LN lymphocytes samples. Representative data suggest small upregulation of *Socs1* in the LNs of NOD.*Dexi*$^{-/-}$ A1 mice but not in the LNs of NOD.*Dexi*$^{-/-}$ A2 mice. It should be noted that similar to *Clec16a*, *Socs1* is not highly expressed in LN lymphocytes[72] during steady state conditions which could explain the slight differences observed in these organs. *Socs1* mRNA levels were also unaltered in splenic samples of NOD.*Dexi*$^{-/-}$ A2 mice (Figure 12B).

Lastly, the mRNA levels of *Ciita* were also measured in both *Dexi* KO mouse lines. No significant expression changes were observed in samples from spleen, islets, thymi of NOD.*Dexi*$^{-/-}$ A1 mice (Figure 12C). This was also observed among spleens of

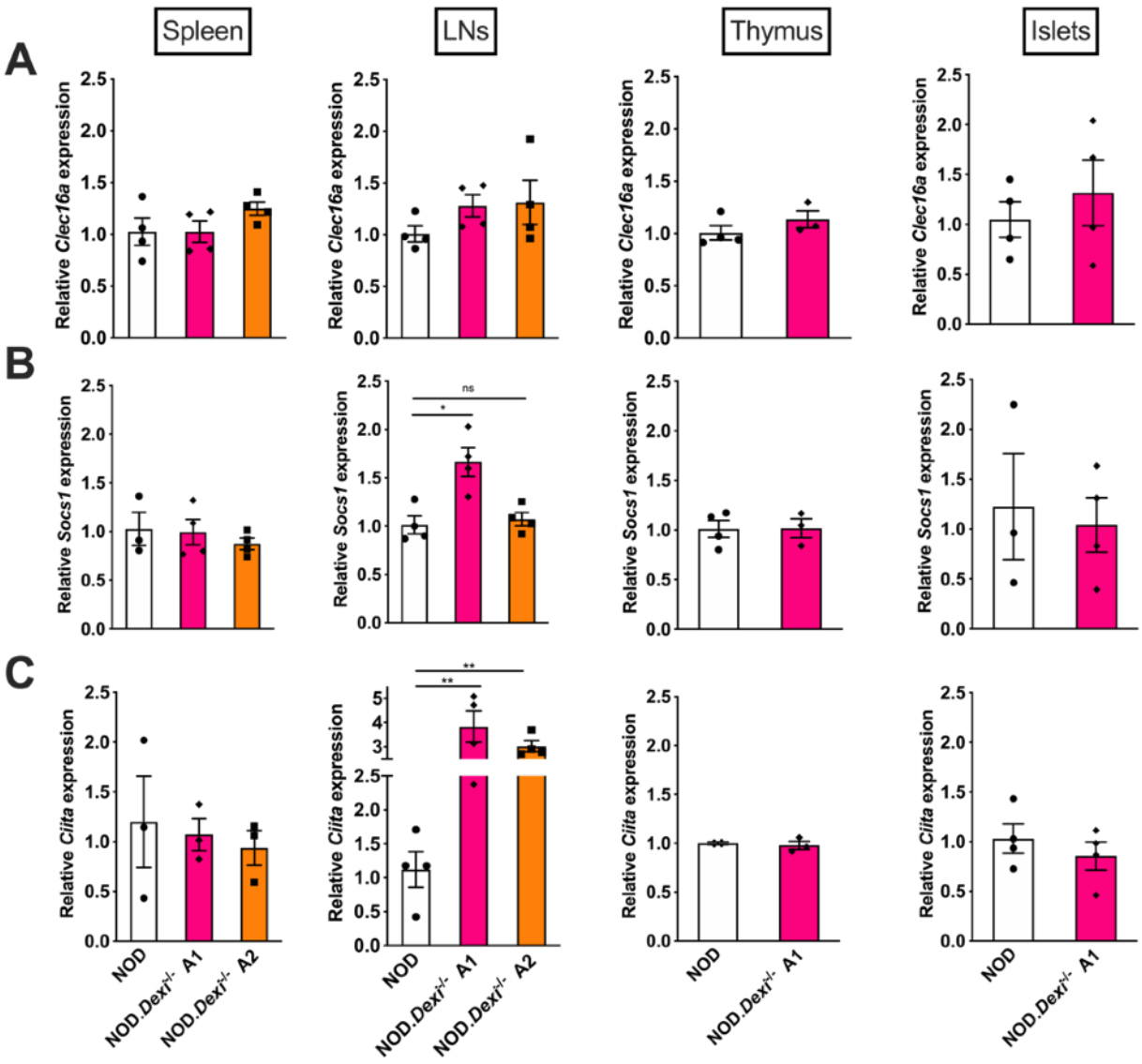

Figure 12. <u>Expression of Ch16p13.13 genes is not affected in the thymus, spleen and islets of NOD.*Dexi*$^{-/-}$ mice.</u> A-C Quantification of *Clec16a* (**A**), *Socs1* (**B**), and *Ciita* (**C**) mRNA by quantitative PCR in the spleen, thymus, LNs and pancreatic islets of NOD, NOD.*Dexi*$^{-/-}$ A1 and NOD.*Dexi*$^{-/-}$ A2 mice. n=3-4 mice per group. Data show individual values for a single mouse, mean ± SEM and are representative of at least two similar experiments, with the exception of the levels of *Ciita* in LN samples which were assayed only once. Relative expression was determined as $2^{[-(Dexi\ Ct\text{-}\beta\text{-}Actin\ Ct)]}$ using NOD mouse samples as a baseline. *P<0.05, **P<0.01, ns=not significant; >0.05.

NOD.*Dexi*$^{-/-}$ A2 mice (Figure 12C). In a preliminary experiment, high mRNA levels of *Ciita* were observed among LNs lymphocytes of both *Dexi* mutant line. Since this difference was exclusive to the LNs, confirmation of data was deferred with the intent of repeating this experiment in the event of a significant phenotype observed in the

diabetes development of these mice. The expression of Ch16p13.13 genes was not assessed in NOD.*Dexi*$^{-/-}$*Clec16a*^{KD} mice.

2.5.1 Characterization of NOD.*Dexi*$^{-/-}$ mice

In order to characterize any potential physiological changes or immune phenotypes upon *Dexi* deletion, several traits were assessed. Initially, mice were carefully monitored and showed no observable signs of disease before diabetes development. Furthermore, the total weights of mice between 8-12 weeks of age remained normal in both NOD.*Dexi*$^{-/-}$ mutant mouse lines when compared to NOD (Figure 13A). Surprisingly, the spleens of NOD.*Dexi*$^{-/-}$ A1 and A2 mice weighed significantly less than NODs (Figure 13C), although they did not appear to be smaller in size (Figure 13D). This was accompanied with a significant reduction of the amount of total splenocytes in *Dexi*-depleted mice (Figure 13E). This difference in total cellularity appeared to be restricted to the spleen, as it was not observed in total thymocytes or pooled LN lymphocytes (Figure 13F-G). The weight and size of other immune organs and pancreas were not visually different and therefore not assessed.

2.5.2 Characterization of immune cell populations in NOD.*Dexi*$^{-/-}$ mice

When looking at the percentages of T cell subsets in the spleen, LNs (Figure 14), and thymi (Figure 15) of these mice by flow cytometry no significant differences where observed. Moreover, total T cell subset cellularity was only significantly reduced in naîve CD4^{+} T cells among the splenocytes of both NOD.*Dexi*$^{-/-}$ A1 and A2 mice. However, this effect was not observed in developing thymocytes (Figure 15) or LN lymphocytes (Figure 14). A small percent of thymic regulatory T cells appeared reduced in

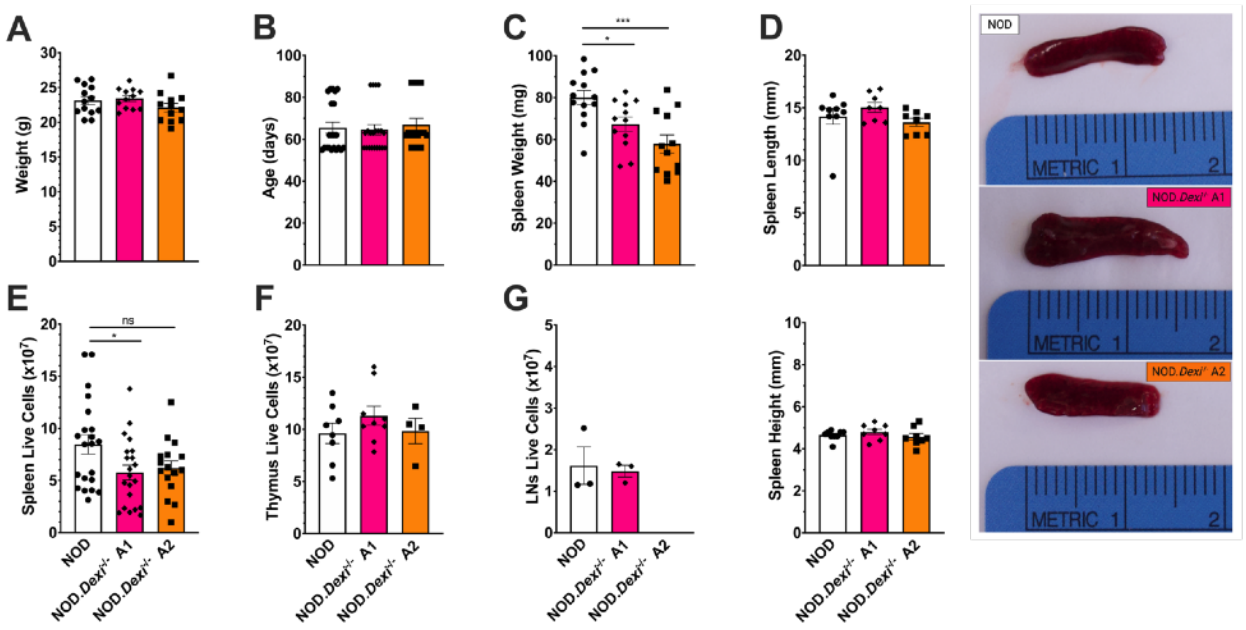

Figure 13. *Dexi* KO leads to a reduction in the spleen weight and total splenocytes of NOD mice. **A** Each studied mouse was weighted prior to harvest of organs. Data show individual values for a single mouse, mean ± SEM and are combined from two similar experiments. n=12-13 mice per group. **B** Combined age distribution within the mice used for phenotyping experiments. Data show individual values for a single mouse and mean ± SEM. n=16-21 mice per group. **C-D** Spleen weight (**C**), length and height (**D**) were also determined in two similar experiments and values were combined. Data show individual values for a single mouse with the mean ± SEM. Representative pictures of spleens for each study group are also shown in **D** (*right*). n=12-13 mice per group. **E-G** Total viable spleen (**E**), thymus (**F**), and LN (**G**) cellularity was determined using a hematocytometer and trypan blue staining. Data show individual values for a single mouse, mean ± SEM and are combined from at least two similar experiments, with the exception of LNs which were only assessed once in NOD.*Dexi*$^{-/-}$ A1 mice, as well as of NOD.*Dexi*$^{-/-}$ A2 thymi which were only assessed once. *P<0.05, ***P<0.001, ns=not significant; >0.05.

NOD.*Dexi*$^{-/-}$ A2, but not A2 mice (Figure 15D). Specifically, frequencies and absolute numbers of the following T cell subsets within the spleen and LNs of NOD, NOD.*Dexi*$^{-/-}$ A1 and A2 mice: all TCR-β^+ T cells (Figure 14A), cytotoxic T (T_c) cells (Figure 14B), naïve T_c cells (Figure 14C), helper T (T_h) cells (Figure 14D, naïve T_h cells (Figure 14E), and regulatory T (T_{reg}) cells (Figure 14F). Developing thymocytes specifically assessed within thymi of NOD and NOD.*Dexi*$^{-/-}$ A1 and A2 mice were as follows: $CD4^+CD8^+$ double positive (DP) thymocytes (Figure 15A), $CD8^+$ single positive (SP) thymocytes (SP_{CD8+}; Figure 15B), $CD4^+$ SP thymocytes ($SP_{CD4+;}$ Figure 15C), double negative (DN)

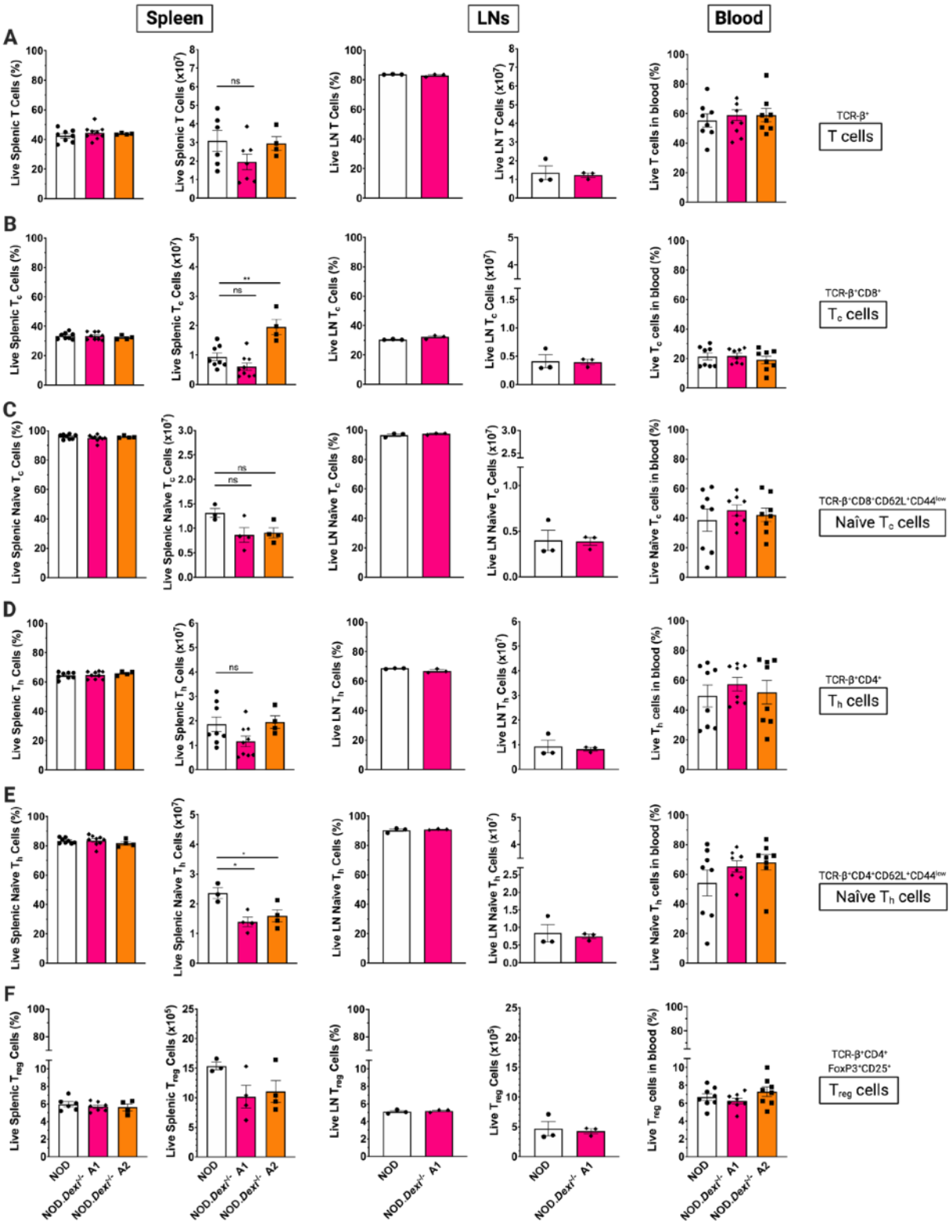

Figure 14. ***Dexi*** **KO mice have a relatively normal distribution of spleen, LN and circulating T cells.** **A-F** Graphs depicting the frequency and total cellularity of T cell subsets within spleen, LNs and blood of NOD, NOD.*Dexi*$^{-/-}$ A1 and NOD.*Dexi*$^{-/-}$ A2 age-matched female mice within 8-10 weeks of age.

Figure 14 (Continued)
The following subsets were evaluated **A** TCR-β$^+$ T cells, **B** T_c cells, **C** naïve T_c cells, **D** T_h cells, **E** naïve T_h cells, and **F** T_{reg} cells. Blood was collected via cardiac puncture. Data show individual values for a single mouse, mean ± SEM, and are either representative of at least two similar experiments or are combined data from two similar experiments. Data for LNs was only collected once. n=3-9 mice per group. *P<0.05, **P<0.01, ns=not significant; >0.05.

thymocytes (Figure 15H), 3 subsets of developing thymocytes (DT_1: CD69$^-$TCR-β$^-$; DT_2: CD69$^+$TCR-β$^+$; DT_3: CD69$^-$TCR-β$^+$; Figure 15E-G) and thymic T_{reg} cells (Figure 14D).

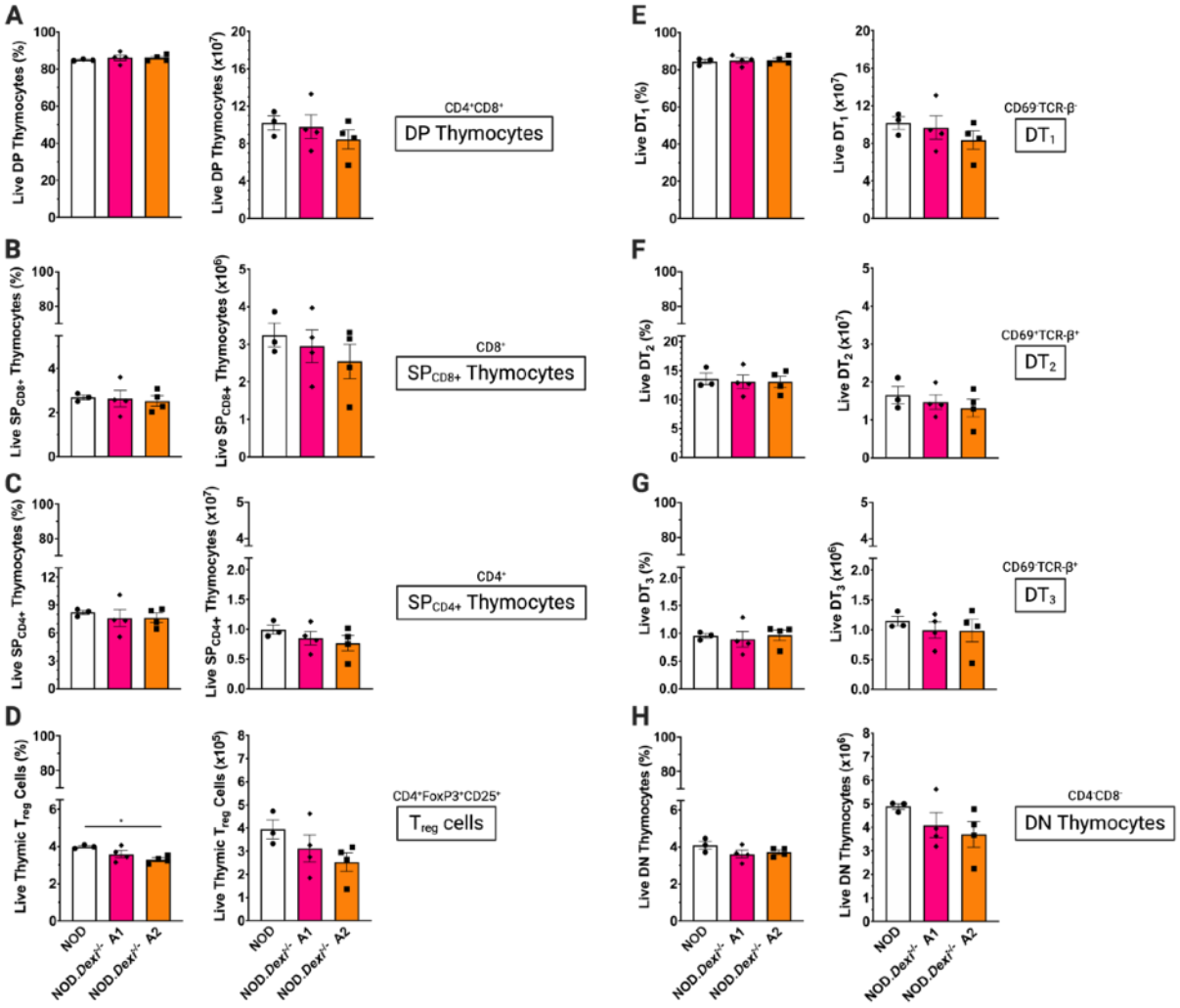

Figure 15. <u>*Dexi* KO mice have a normal distribution of developing thymocytes.</u> A-H Graphs depicting the frequency and total cellularity of thymocyte cell subsets in NOD, NOD.*Dexi*$^{-/-}$ A1 and NOD.*Dexi*$^{-/-}$ A2 age-matched female mice. The following subsets were evaluated **A** double-positive thymocytes, **B-C** single-positive thymocytes, **D** thymic T_{reg} cells, **E-G** three subsets of early development thymocytes (DT_{1-3}), and **H** double-negative thymocytes. Data show individual values for a single mouse, mean ± SEM, and representative of at least two similar experiments. n=3-4 mice per group. *P<0.05.

Flow cytometry was also used to assess the frequencies of B cell subsets and total B cells from the spleen of NOD and NOD.*Dexi*$^{-/-}$ A1 and A2 mice. Both the frequency and total number of B cells (Figure 16A), plasma B (B_{plasma}) cells (Figure 16B), germinal center B (B_{gc}) cells (Figure 16C), and marginal zone B (B_{mz}) cells (Figure 16D) remained mostly unaltered in both *Dexi* mutant mouse lines. A significant, yet small, increase in B_{gc} accompanied by a similarly sized decrease in B_{mz} was observed between NOD and NOD.*Dexi*$^{-/-}$ A1 mice, but this was not observed in NOD.*Dexi*$^{-/-}$ A2 mice.

Splenic myeloid cells were assessed via flow cytometry as well and included the following antigen presenting cells (APCs): Mo (Figure 17A), red pulp Mφs (Figure 17B), DCs (Figure 17C), CD11b^{+} DCs (DC_{11b}+; Figure 17D), MHC-II/I-Ag^{7} DCs ($DC_{I\text{-}Ak}$+; Figure 17E), and plasmacytoid DCs (pDCs; Figure 17F). No significant frequency changes were noted between the myeloid cells of NOD and NOD.*Dexi*$^{-/-}$ A1 and A2 mutant mice. Absolute numbers within splenic myeloid cells were also comparable between NOD and *Dexi* KO mice (Figure 17). Importantly, splenocytes analyzed where obtained by physical disruption of the corresponding spleens. In the event of a disease phenotype, this assessment would have been repeated using enzymatic digestion in order to increase the quantity, quality and accuracy of myeloid cell detection, as well as to allow for the detection of specific and less abundant DC and Mo cell subsets which have been predicted to have higher expression of *Dexi* mRNA.

Assessment of the frequencies of *in vivo* circulating T (Figure 14) and B (Figure 16E) cells suggests no significant differences among NOD and NOD.*Dexi*$^{-/-}$ A1 and A2

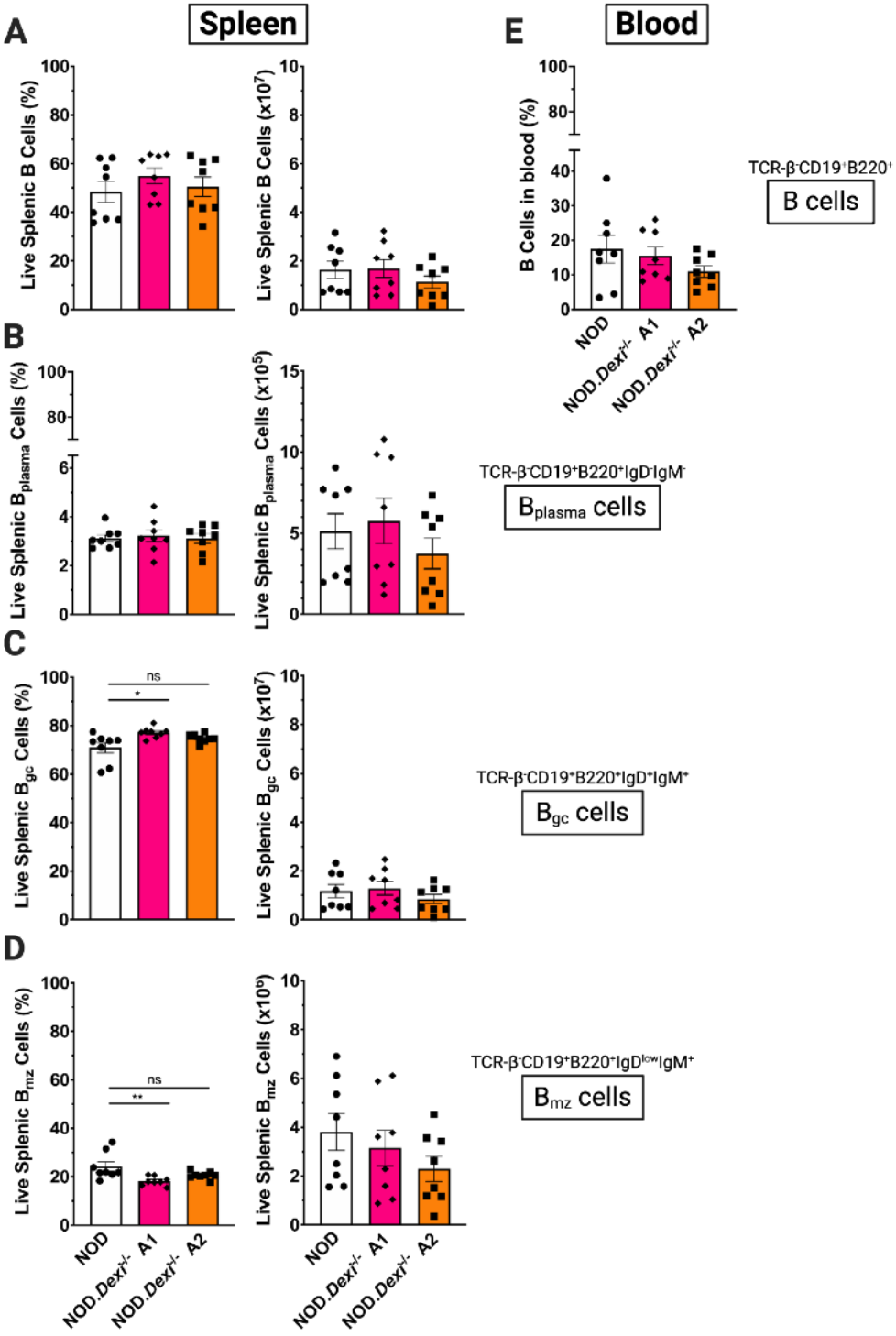

Figure 16. *Dexi* KO mice have a normal distribution of splenic and circulating B cells. A-E Graphs depicting the frequency and total cellularity of B cell subsets within NOD, NOD.*Dexi*$^{-/-}$ A1 and NOD.*Dexi*$^{-/-}$ A2 age-matched female mice (8-9 weeks of age). The following subsets were evaluated **A** CD19^{+}B220^{+} splenic B cells, **B** splenic plasma B cells, **C** germinal center B cells, **D** marginal zone B cells, and **E** circulating B cells. Blood was collected via cardiac puncture. Data show individual values for a single mouse, mean ± SEM, and are combined from two similar experiments. n=8 mice per group. *P<0.05, **P<0.01.

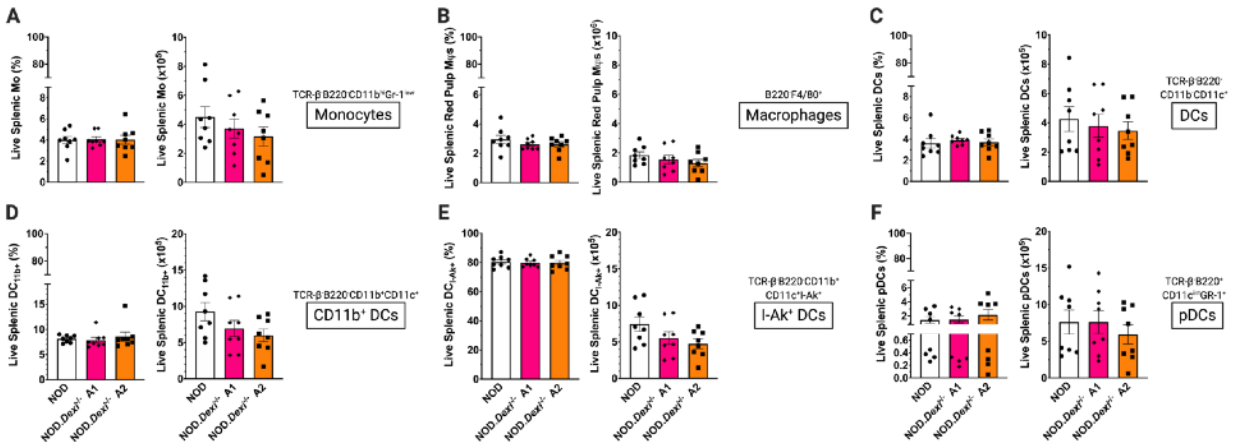

Figure 17. *Dexi* KO mice have normal splenic myeloid cell distribution. A-E Graphs depicting the frequency and total cellularity of **A** monocytes, **B** macrophages, **C-E** three subsets of DCs, and **F** plasmacytoid DCs within NOD, NOD.*Dexi*$^{-/-}$ A1 and NOD.*Dexi*$^{-/-}$ A2 age-matched female mice (8-9 weeks of age). Data show individual values for a single mouse, mean ± SEM, and are combined from two similar experiments. n=8 mice per group.

mutant mice. However, assessing the total amount of circulating was unattainable due to high levels of variability obtained between blood samples when collected with an aqueous solution of EDTA to prevent clotting. Collecting blood samples into tubes lined with soluble EDTA would have overcome this hurdle. Additional attempts to measure the total amount of circulating immune cells and factors with this more accurate methodology were planned in the event of a significant diabetes-related phenotype. Lastly, the gating strategies used for all data acquired via flow cytometry are also depicted in Figure 18.

Figure 18. <u>Gating strategies used for flow cytometry analysis</u> A-K Pseudocolor dot plot examples of the gating strategies used for the data depicted in Figures 12-15. **A** naîve T_c cell gating (spleen, LNs and blood), **B** naîve T_h cell gating (spleen, LNs and blood), **C** T_{reg} cell gating (spleen, LNs and blood), **D** developing thymocytes gating **E** thymic T_{reg} cell gating, **F** macrophages gating, **G** monocytes gating, **H** DCs and $CD11b^+$ DCs gating, **I** $I\text{-}A^{g7}$ DCs gating, **J** pDCs gating, and **K** gating of B cells in blood and spleen of NOD, NOD.*Dexi*$^{-/-}$ A1 and NOD.*Dexi*$^{-/-}$ A2 mice. Plot values are representative of all data analyzed.

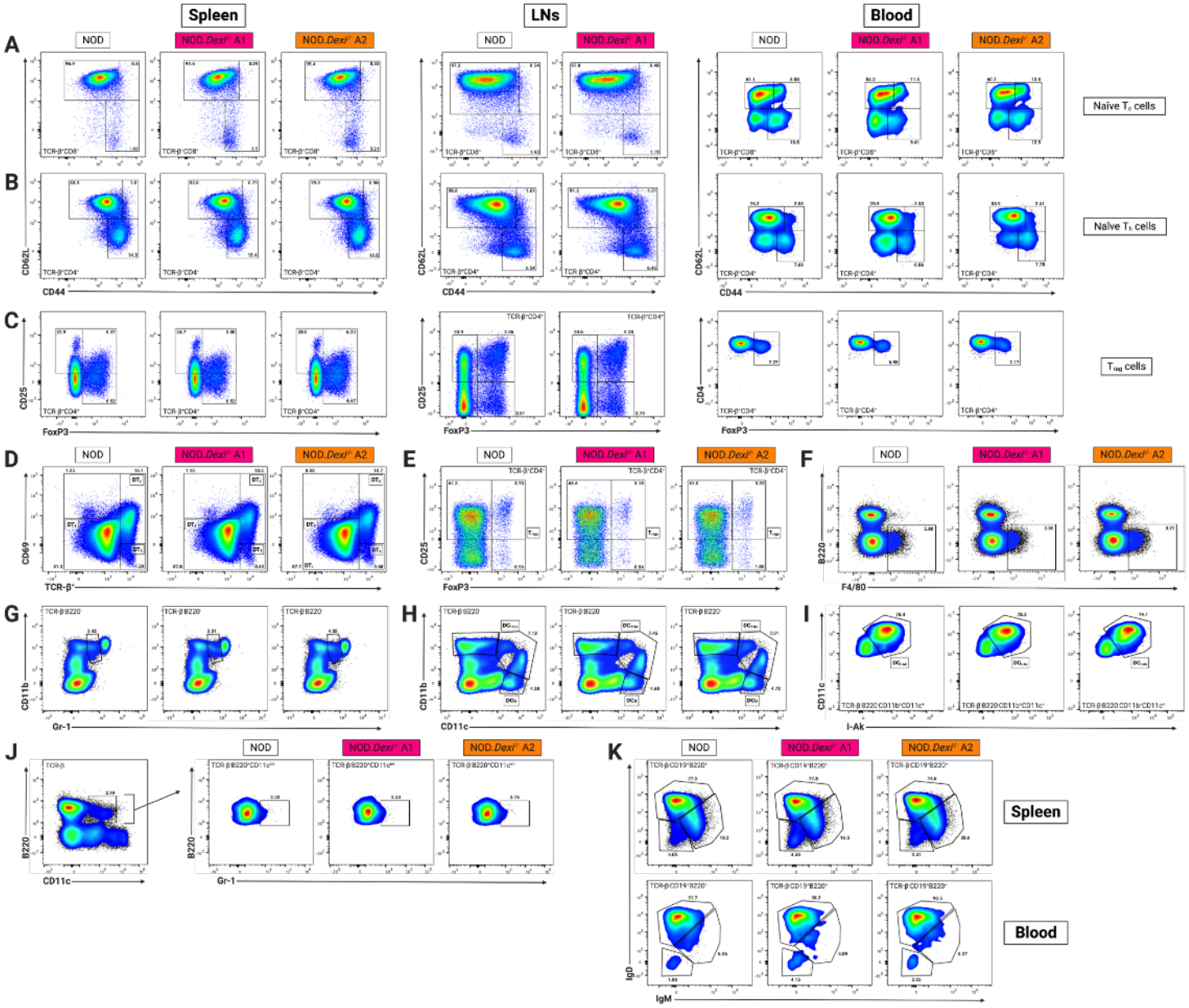
Spleen
LNs
Blood
NOD
NOD.Dexi-/- A1
NOD.Dexi-/- A2
A
B
C
D
E
F
G
H
I
J
K
Naïve Tc cells
Naïve Th cells
Treg cells
CD62L
CD44
CD25
FoxP3
CD4
CD69
TCR-β
B220
F4/80
CD11b
Gr-1
CD11c
I-Ak
IgD
IgM
Spleen
Blood

2.6 Summary of findings

Overall, the generation of a *Dexi*-deficient NOD founder mouse was successful using CRISPR/Cas9 genome editing. Chimerism among the founder's germ cells facilitated the propagation of two distinct *Dexi*-deficient mouse lines which were backcrossed with NOD mice to eliminate any potential off-target effects. While genotyping was initially challenging, designing two PCR protocols targeting different genomic regions within *Dexi* allowed efficient genotyping and characterization of the mutated genomic sequences in both NOD.*Dexi*$^{-/-}$ A1 and A2 mice. To explore the effects of potential interactions between *Dexi* and *Clec16a*, previously generated NOD.*Clec16a*^{KD} mice were intercrossed with NOD.*Dexi*$^{-/-}$ mice to generate double mutant NOD.*Dexi*$^{-/-}$*Clec16a*^{KD} mice. Assessment of *Dexi* mRNA and protein levels provided evidence of complete ablation of Dexi in both NOD.*Dexi*$^{-/-}$ and NOD.*Dexi*$^{-/-}$ *Clec16a*^{KD} mutant mice. Moreover, the expression of neighboring genes within Ch16p13.13 did not appear to be significantly affected among the spleen, thymus and pancreatic islets of *Dexi* KO mice. While NOD.*Dexi*$^{-/-}$ A1 and A2 mice weighed the same as NOD mice, their spleens were significantly lighter and contained less total splenocytes than NOD mice, albeit the size of their spleens was not affected. Immune characterization of *Dexi*-deficient mice did not show evidence of changes in the percentage of T cell populations within the blood, spleen or LNs. However, a small but significant change was observed in the total amount of splenic naîve T_h cells in *Dexi* KO mice as well as an increased total amount of T_c when this values were compared to those of NOD mice. Similarly, the percentages of developing thymocyte populations displaying established cell surface marker combinations were not affected upon *Dexi*

deletion. While the percentage of thymic T_{regs} were similar between NOD and NOD.*Dexi*$^{-/-}$ A1 mice, a small but significant decrease was observed among the percentage, but not the total amount, of thymic T_{regs} in NOD.*Dexi*$^{-/-}$ A2 mice. The percentage of circulating B cells did not appear to differ between blood samples of NOD and NOD.*Dexi*$^{-/-}$ mice. Interestingly, assessment of splenic B cell subsets revealed that while the percentage of $CD19^{+}B220^{+}$ B and B_{plasma} cells do not change, the percentage of germinal center B cells as well as that of marginal zone residing B cells is significantly changed in NOD.*Dexi*$^{-/-}$ A1 mice. Specifically, the percentage of B_{gc} cells is increased while the percentage of B_{mz} cells is decreased within the spleens of NOD.*Dexi*$^{-/-}$ A1 mice. However, these changes were not observed following the assessment of total splenic B cell subsets. Lastly, no evidence of changes among the percentage of or total amount of monocytes, macrophages or DC subsets were observed among the spleens of NOD.*Dexi*$^{-/-}$ mice when compared to their WT counterparts. The effective generation of NOD.*Dexi*$^{-/-}$ mice via CRISPR/Cas9 described in this chapter made it possible to study the effect of organism-wide *Dexi* depletion on immune cell populations as well as in autoimmune diabetes development the latter will be discussed in the following chapter.

Chapter 3

"Is *DEXI* or *CLEC16A* causal for T1D-association?": Studying the role of *Dexi* in a mouse model of T1D development.

3.1 Contributions

Janice Marie Nieves-Bonilla performed experiments, analyzed data, and wrote the text for this chapter. Badr Kiaf harvested and isolated islets from pancreata of mice. Cornelia Schuster helped with experimental design and data interpretation. Stephan Kissler supervised the study, analyzed data, and wrote the published manuscript.

This chapter is partially adapted from the published manuscript Nieves-Bonilla, J.M., et al. The type 1 diabetes candidate gene Dexi does not affect disease risk in the nonobese diabetic mouse model. *Genes Immun* 21, 71–77 (2020). https://doi.org/10.1038/s41435-019-0083-y

3.2.1 Introduction

The most significant T1D-associated SNPs within Ch16p13.13 are located in introns 8, 10 and 19-22 of *CLEC16A*[41] some of which have been reported to have a significant effect on *CLEC16A* expression[34,43,44]. Despite variations affecting its own expression and the available functional data[44,63,66-71] strongly suggesting *CLEC16A* to be the causal gene for T1D association within Ch16p13.13, it has been argued that *DEXI* is instead a more likely candidate due to variations also affecting *DEXI* expression[3,41,54]. *DEXI* has been predicted to be a T1D risk gene in a variety of studies where risk variants correlated with differential expression of *DEXI* among healthy and diseased patients[3,61,77-82]. Association of *DEXI* with disease has been reported as a result of variations modifying chromosomal interaction between TFs and *DEXI*'s promoter region, which is reported to be highly enriched with histone modification typically observed during TF-binding events[3,41,61,77-82]. In order to clarify if one or both of these two genes are causal for the T1D association within Ch16p13.13, evidence of a role for *DEXI* in T1D or autoimmunity is necessary.

3.2.2 Specific Aim & Rationale

As previously mentioned, *DEXI*'s repeated association with T1D[3,34,41,54] and the lack of functional data for DEXI warrant the study of its participation in T1D development. Studying DEXI's functional role in T1D could shed new insights on the development of T1D and other autoimmune disease while also providing clarity on whether *CLEC16* or *DEXI* are causal for the T1D association reported in Ch16p13.13[3,41,54]. The generation of *Dexi* KO NOD and double-deficient *Dexi* KO *Clec16a* KD NOD mice described in the previous chapter provide the necessary tools to study the effects of *Dexi* on autoimmune diabetes development. Moreover, the generation of this *Clec16a* KD *Dexi* KO double mutant mouse line provides the unique opportunity to study the joint contribution of *Clec16a* & *Dexi* to diabetes onset, as well as *Dexi*'s role in *Clec16a* KD's protection against diabetes onset in NOD mice. Therefore, this chapter describes the resulting work from experimental efforts aimed towards studying the effect of *Dexi* KO on autoimmune diabetes development using the NOD mouse model.

3.3 *Dexi* deletion does not affect autoimmune diabetes risk in NOD mice.

To understand the effects of *Dexi* KO on autoimmune diabetes development cyclophosphamide (CY)-accelerated diabetes onset was initially tested in 2 small cohorts of mice. These initial cohorts only included 10 NOD and 11 NOD.*Dexi*$^{-/-}$ A1 female mice. During the initial days of diabetes onset following CY injection, NOD.*Dexi*$^{-/-}$ A1 mice appeared to have a higher incidence when compared to NODs. However, this difference was not significant nor did it remain consistent throughout the study (Figure

19A). Spontaneous diabetes incidence was simultaneously tested weekly for about 6 months in slightly larger cohorts of mice which did include the NOD.*Dexi*$^{-/-}$ A2 mice in addition to the previously tested NODs and NOD.*Dexi*$^{-/-}$ A1 mice. In this case, no significant differences in diabetes incidence were observed despite results suggesting a trend towards higher incidence in *Dexi*-deficient NOD mice (Figure 19E). It is important to consider that for these two initial experiments the overall diabetes incidence (~30%) was lower in our NOD mice than what typically results in these mouse colonies[12,84-88]. To address these inconsistent data, adult NOD mice were ordered from The Jackson Laboratories and bred in house with our existing colony for several generations before use in further experiments. These mice were also incorporated in the last few generations of the mutant mice backcrosses.

Larger cohorts where used when assessing spontaneous diabetes onset in a later experiment which consisted of 54 NOD, 39 NOD.*Clec16a*^{KD}, 47 NOD.*Dexi*$^{-/-}$ A1, 49 NOD.*Dexi*$^{-/-}$*Clec16a*^{KD} A1, 30 NOD.*Dexi*$^{-/-}$ A2, and 28 NOD.*Dexi*$^{-/-}$*Clec16a*^{KD} A2 females. Glucosuria was assessed weekly for 18 weeks starting at 10 weeks of age. The diabetes endpoint for each mice was defined as 2 consecutive readings of 250mg/dL or higher glucose in the urine. At this point, diabetic mice were euthanized to minimize disease burden. Once again, no significant differences in spontaneous diabetes incidence were observed for either NOD.*Dexi*$^{-/-}$ A1 or NOD.*Dexi*$^{-/-}$ A2 mice when compared to NOD mice (Figure 19F). NOD.*Clec16a*^{KD} mice had a significant delay in diabetes onset, as has been reported[66]. Dexi KO did not have an effect on this phenotype, as both NOD.*Dexi*$^{-/-}$*Clec16a*^{KD} A1 and A2 mice were similarly protected from diabetes (Figure 20G-H). Additionally, the NOD mouse cohort had a higher incidence

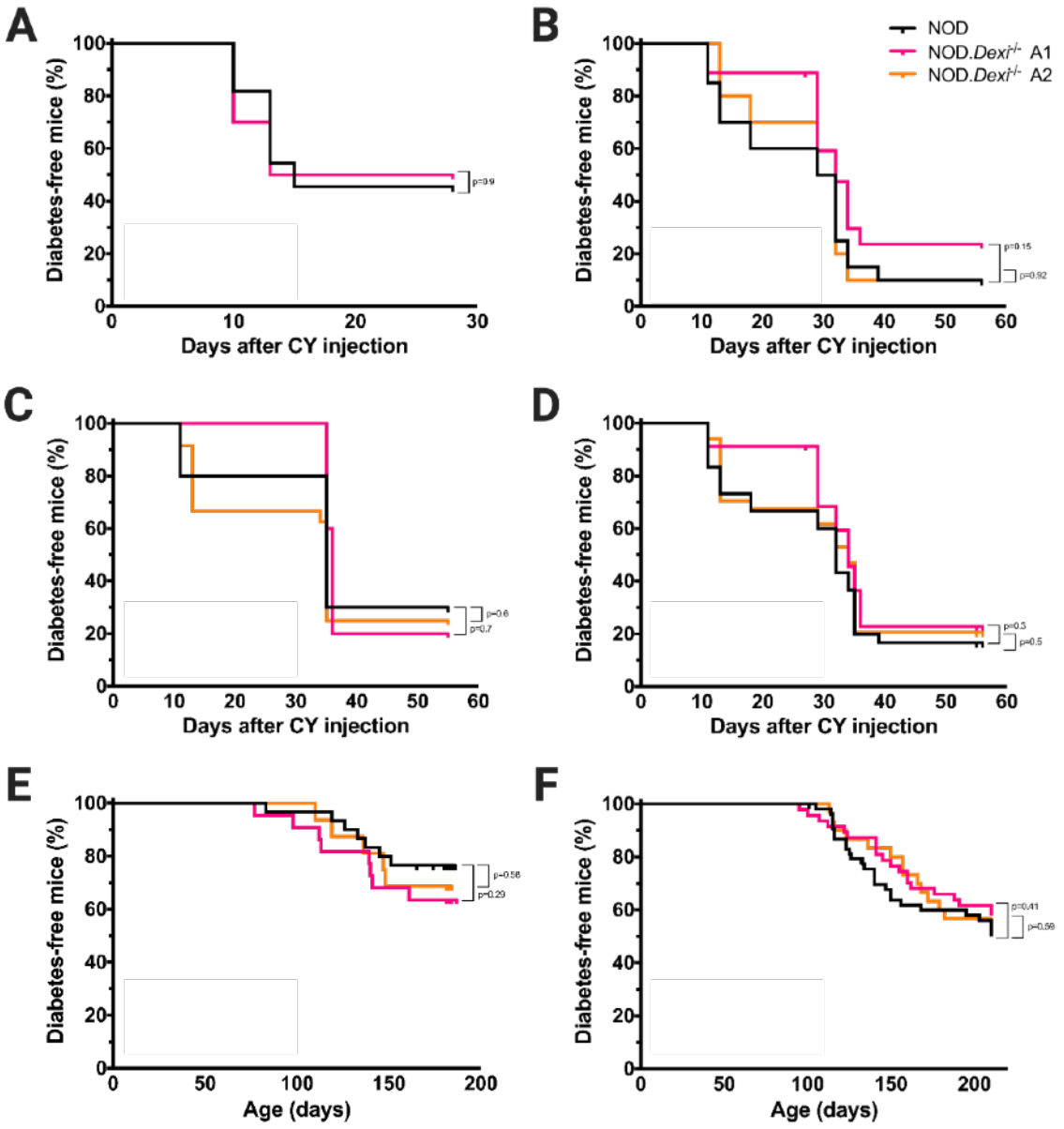

Figure 19. <u>*Dexi* KO in NOD mice does not modify the frequency of spontaneous or CY-accelerated diabetes.</u> **A-D** CY-accelerated diabetes incidence was measured in female NOD (n=10) and NOD.*Dexi*$^{-/-}$ A1 (n=11) mice injected intraperitoneally with CY. (**B-C**) Larger cohorts of male mice were later tested in two back to back experiments with an initial CY injection at 8 weeks of age and a secondary equal dose of CY 21 days after. In the first experiment cohorts consisted of 20 NOD, 18 NOD.*Dexi*$^{-/-}$ A1, and 10 NOD.*Dexi*$^{-/-}$ A2 age-matched males. The second cohort also contained NOD (n=10), NOD.*Dexi*$^{-/-}$ A1 (n=5), and NOD.*Dexi*$^{-/-}$ A2 (n=24) age-matched males. The second CY injection for the first male tested cohort was simultaneous with the first CY injection for the second cohort. Data from CY-accelerated diabetes incidence in males is combined in **D**. **E-F** Spontaneous diabetes incidence was measured once-weekly for six months in two cohorts of female mice from 10 weeks of age. The initial cohort (**E**) consisted of 30 NOD, 22 NOD.*Dexi*$^{-/-}$ A1, and 16 NOD.*Dexi*$^{-/-}$ A2 mice. **F** A larger cohort of NOD (n=54), NOD.*Dexi*$^{-/-}$ A1 (n=47), and NOD.*Dexi*$^{-/-}$ A2 (n=30) mice was used to measure to the effects of *Dexi* KO on spontaneous diabetes incidence in NOD mice. Differences between groups were measured using the Log-rank test.

(50%) of diabetes than previously observed which falls under the typical range for these mice.

CY-accelerated diabetes was simultaneously assessed in two subsequent experiments with slightly larger cohorts of male mice than previously tested. These amounted to a total of 30 NOD, 26 NOD.*Clec16a*^{KD}, 23 NOD.*Dexi*$^{-/-}$ A1, 31 NOD.*Dexi*$^{-/-}$ *Clec16a*^{KD} A1, 34 NOD.*Dexi*$^{-/-}$ A2, and 22 NOD.*Dexi*$^{-/-}$*Clec16a*^{KD} A2 mice between both cohorts. Males were age-matched between both experiments and were injected with an initial dose of 250mg/kg of CY intraperitonealy when they reached 8 weeks of age. An equal dose of CY was also injected 21 days after the initial injection. In this case, glucosuria was assessed three times a week for 4 weeks post CY injection. As previously, diabetic mice were euthanized following 2 consecutive readings of >250mg/dL glucose in the urine. CY-accelerated diabetes onset was not significantly affected upon *Dexi* KO, in either experiment as shown in Figures 19B-C. Furthermore, *Dexi* KO did not alter the protective effects previously reported following *Clec16a* KD in NOD mice[66] (Figure 20A-B). Strangely, during the second experiment executed, NOD.*Dexi*$^{-/-}$ *Clec16a*^{KD} A1 were not protected from diabetes while NOD.*Dexi*$^{-/-}$*Clec16a*^{KD} A2 were less protected than in the previous experiment. It is unclear why these results were inconsistent between experiments. Data obtained from both of these experiments was then combined to analyze as a whole and is depicted in Figures 19D and 20E-F. Combined data results more closely resembled what was observed during the first experiment, as well as what was observed when measuring spontaneous diabetes. For this reason, it was presumed that results from the second CY treated groups were unreliable and ineffective in the replication of effects seen when measuring spontaneous

diabetes incidence (Figure 20G-H).

Figure 20. *Dexi* KO in NOD.*Clec16a*^{KD} mice does not alter the spontaneous or CY-accelerated diabetes protection conferred by *Clec16a*^{KD}. CY-accelerated diabetes incidence was assessed in male mice by performing two back to back experiments with an initial CY injection at 8 weeks of age and a secondary equal dose of CY 21 days after. The following cohorts were used in the first experiment plotted in **A**-**B**: 20 NOD (**A**-**B**), 20 NOD.*Clec16a*^{KD} (**A**-**B**), 18 NOD.*Dexi*$^{-/-}$ A1 (**A**), 17 NOD.*Dexi*$^{-/-}$*Clec16a*^{KD} A1 (**A**), 10 NOD.*Dexi*$^{-/-}$ A2 (**B**), and 7 NOD.*Dexi*$^{-/-}$*Clec16a*^{KD} A2 (**B**) age-matched males. For the second experiment (plotted in **C-D**) the same genotype groups were used including: NOD (**C-D;** n=10), NOD.*Clec16a*^{KD} (**C-D;** n=6), NOD.*Dexi*$^{-/-}$ A1 (**C**; n=5), NOD.*Dexi*$^{-/-}$*Clec16a*^{KD} A1 (**C**; n=14), NOD.*Dexi*$^{-/-}$ A2 (**D**; n=24), and NOD.*Dexi*$^{-/-}$*Clec16a*^{KD} A2 (**D**; n=15) age-matched males. The second CY injection for the first group of males tested was simultaneous with the first CY injection for the second group of tested males. Data from CY-accelerated diabetes incidence in males with the A1 mutation is combined in **E** and for those with A2 mutation in **F**. **G-H** Spontaneous diabetes incidence was measured once-weekly for six months in cohorts of female mice starting at 10 weeks of age. NOD (**G-H**; n=54), NOD.*Clec16a*^{KD} (**G-H;** n=39), NOD.*Dexi*$^{-/-}$ A1 (**G**; n=47), NOD.*Dexi*$^{-/-}$*Clec16a*^{KD} A1 (**G**; n=49), NOD.*Dexi*$^{-/-}$ A2 (**H**; n=30), and NOD.*Dexi*$^{-/-}$*Clec16a*^{KD} A2 (**H**; n=28) mice were used and are graphed accordingly. Data collected simultaneously for all groups and graphed separately here and in Figure 19 for ease of interpretation. Differences between groups were measured using the Log-rank test. *P<0.05, **P<0.01, ***P<0.001.

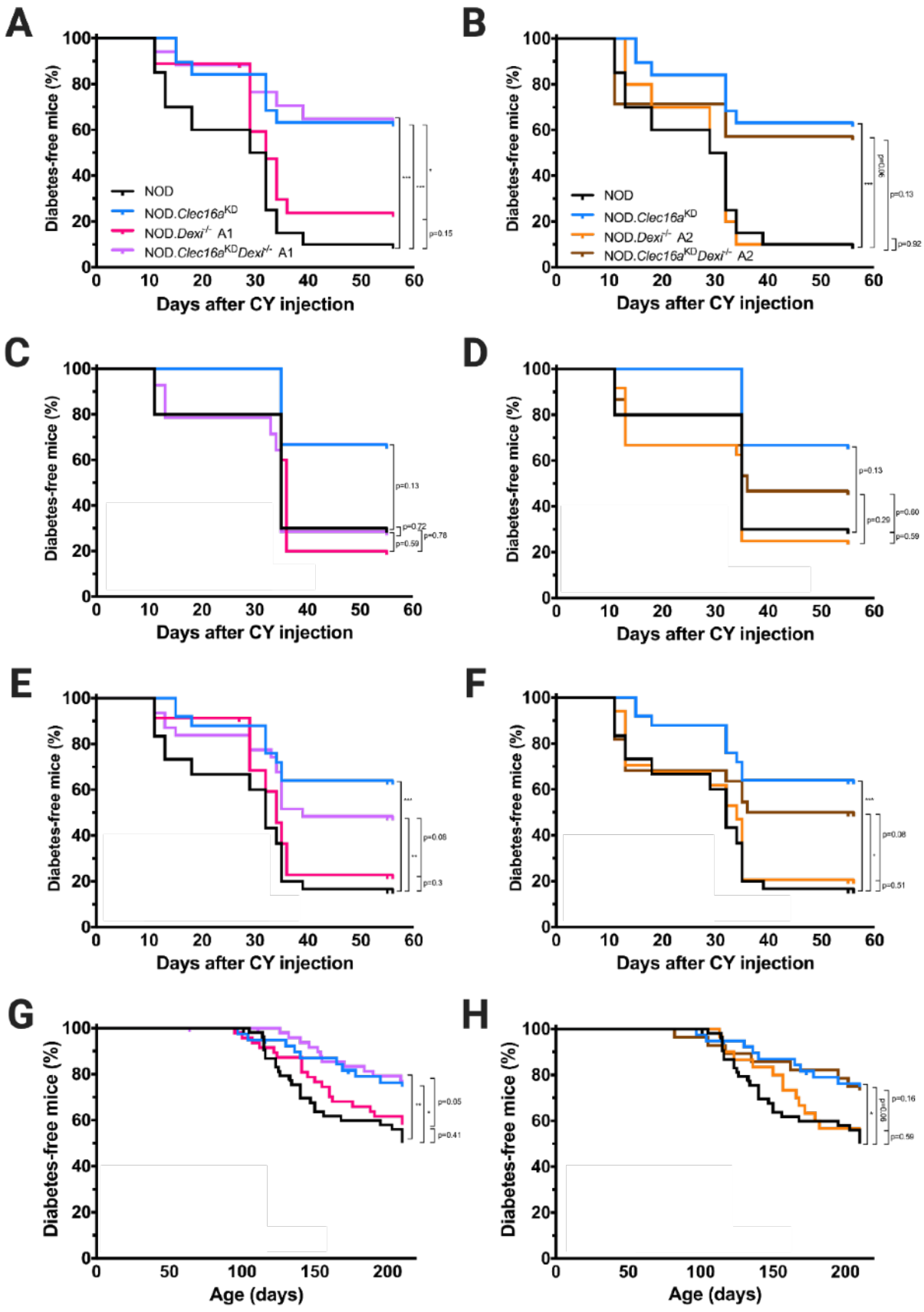
A
B
C
D
E
F
G
H
Diabetes-free mice (%)
Days after CY injection
Age (days)
NOD
NOD.Clec16a^KD
NOD.Dexi^-/- A1
NOD.Clec16a^KDDexi^-/- A1
NOD.Dexi^-/- A2
NOD.Clec16a^KDDexi^-/- A2
p=0.15
p=0.13
p=0.92
p=0.72
p=0.78
p=0.59
p=0.29
p=0.60
p=0.08
p=0.3
p=0.51
p=0.05
p=0.41
p=0.16
p=0.56

Two other diabetes-related pathophysiological features were measured in NOD and *Dexi* KO mutant mice to rule out a role for *Dexi* in autoimmune diabetes in this mouse model. Insulitis severity was first measured by a histological analysis of lymphocyte infiltration in the islets of 10-week old NOD and NOD.*Dexi*$^{-/-}$ A1 mice. Pancreata were harvested from mice and individually fixed overnight in a 10% Paraformaldehyde-PBS solution. Samples were embedded, processed, mounted onto slides and stained with H&E by the Rodent Histopathology [DF/HCC] Core. The degree of insulitis in each islet was quantified in a blinded experiment using the following categories: (1) no insulitis - islet had no infiltrating lymphocytes and showed no perinsulitis; (2) moderate insulitis - islet had perinsulitis and/or less than half of the islet infiltrated; (3) severe insulitis - more than half of the islet was infiltrated with lymphocytes. No significant differences were detected between the levels of insulitis in NOD and NOD.*Dexi*$^{-/-}$ A1 mice. Overall, both NOD and *Dexi*-deficient mice had ~50% insulitis-free islets, ~30% islets with moderate insulitis, and ~20% severely infiltrated islets (Figure 21A).

Additionally, the effects of *Dexi* KO on glucose tolerance were measured in pre-diabetic mice. For this experiment, both NOD and NOD.*Dexi*$^{-/-}$ A1 mice were fasted overnight and blood glucose levels were measured in 30 minute (min) increments from 30mins before an intraperitoneal injection of glucose (2g/kg body weight) until 120mins post-injection. As expected, pre-diabetic NOD mice showed an insignificant level of hyperglycemia at 60mins post-injection while being still able to reach normoglycemia an hour later. Likewise, pre-diabetic NOD.*Dexi*$^{-/-}$ A1 mice were able to reach normoglycemia 2 hours following glucose injection (Figure 21B). Of note, *Ins1* and

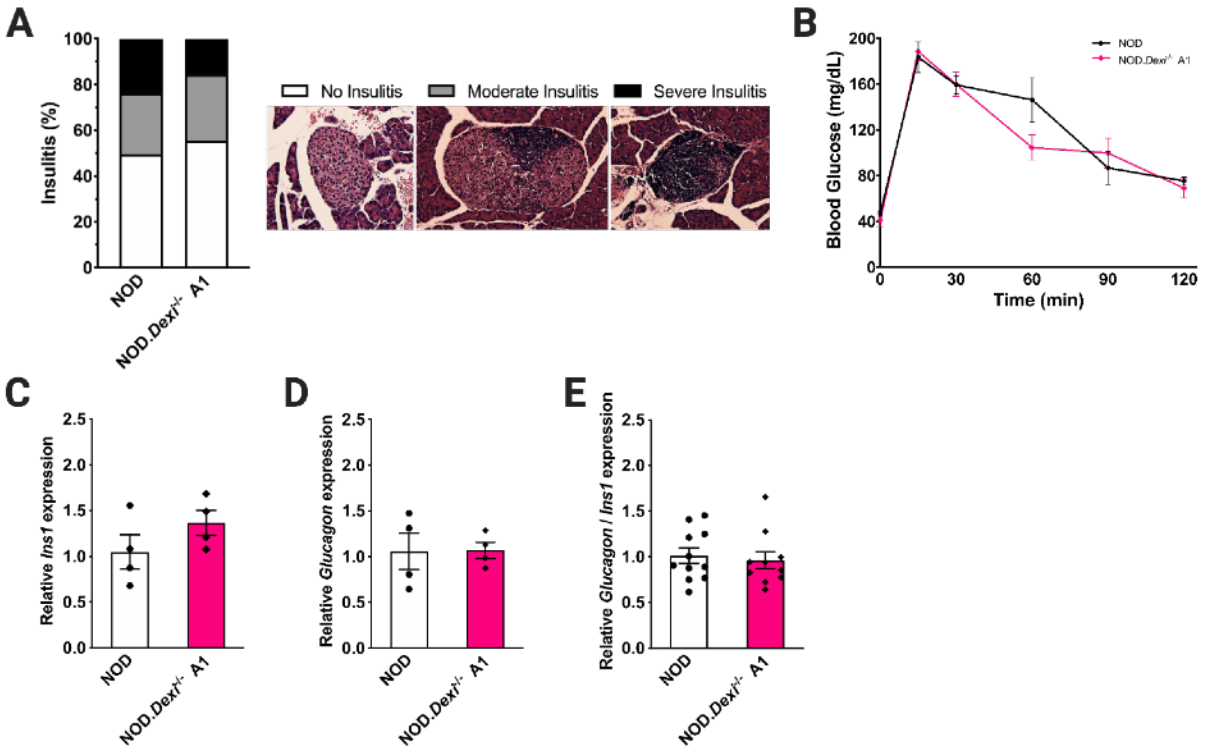

Figure 21. *Dexi* KO in NOD mice does not alter β cell function. **A** Histological analysis of 10-week-old NOD and NOD.*Dexi*$^{-/-}$ A1 pancreatic sections to quantify the degree of insulitis. Data show the proportion of NOD islets (n = 402) and NOD.*Dexi*$^{-/-}$ A1 islets (n = 354) with no lymphocytic infiltration, moderate or severe insulitis from three mice per group. Fisher's exact test P = 0.1 comparing the proportion of infiltrated islets in NOD and NOD.*Dexi*$^{-/-}$ A1 mice. **B** Pre-diabetic NOD and NOD.*Dexi*$^{-/-}$ A1 mice (9 weeks old) were injected with glucose intraperitoneally to test their glucose tolerance. Data show mean ± SEM values from six mice per group. **C-E** Quantification of *Ins1* (**C**), *Glucagon* (**D**), *Glucagon*/*Ins1* (**E**) mRNA by qPCR in the pancreatic islets of NOD, NOD.Dexi-/- A1 and NOD.Dexi-/- A2 mice. n=3-4 mice per group per experiment. Data show individual values for a single mouse, mean ± SEM and are representative of at least two similar experiments, with the exception of the *Glucagon*/*Ins1* ratio which was calculated using the combined results from three similar experiments.

Glucagon mRNA transcript levels were also measured in the islets of NOD and NOD.*Dexi*$^{-/-}$ A1 mice. *Ins1* (Figure 21C) and *Glucagon* (Figure 21D) levels remained similar in both NOD and NOD.*Dexi*$^{-/-}$ A1 mice. The ratio of glucagon to insulin (*Glucagon*/*Ins1*) was also calculated for all samples tested and no significant differences were observed (Figure 21E). Overall, *Dexi* deficiency had no significant effect on β cell function or on autoimmune diabetes onset.

3.4 Summary of findings

The successful generation of NOD.*Dexi*$^{-/-}$ and NOD.*Dexi*$^{-/-}$*Clec16a*^{KD} mutant mice described in the previous chapter allowed for the study of potential effects resulting from *Dexi* ablation on diabetes development in NOD mice. CY-accelerated diabetes incidence was not significantly different in either mouse lines of NOD.*Dexi*$^{-/-}$ mice when compared to their NOD counterparts. Moreover, NOD.*Clec16a*^{KD} mice still appeared to be protected following CY-induced diabetes acceleration[66] as was previously reported. This protection was not significantly impaired in NOD.*Dexi*$^{-/-}$*Clec16a*^{KD} A1 or A2 mice. Although there appears to be a trend towards less mice being protected following both *Dexi* KO and *Clec16a* KD, the differences observed are neither significant nor consistent among experiments. Importantly, these differences are not observed when measuring spontaneous diabetes incidence in these mice. While NOD.*Clec16a*^{KD} mice showed delayed spontaneous diabetes incidence as previously[66], *Dexi* ablation alone was not sufficient to alter the spontaneous diabetes incidence in NOD mice. An initial experiment suggested a trend towards higher incidence of spontaneous diabetes incidence among *Dexi* KO mice, but this was clearly due to control NOD mice in that cohort having an overall reduced diabetes incidence. Re-introducing pure NODs from Jackson Laboratories into the in-house colony breeding reversed this effect.

To measure the effects of *Dexi* KO on β cell function — which when disrupted can result in a higher pre-disposition to autoimmune diabetes onset — the levels of insulitis, blood glucose following fasting and a single glucose injection, and the levels of islet insulin and glucagon mRNA where tested in NOD and NOD.*Dexi*$^{-/-}$ A1 mice. As expected, no difference were observed in these mice suggesting that *Dexi* KO is not

sufficient to cause and/or accelerate β cell function impairment in pre-diabetic NOD mice. Taken together, the data in this chapter provide evidence supporting a role for *Clec16a*, but not *Dexi*, on the development of autoimmune diabetes in NOD mice. While the data herein strongly suggest that *DEXI*, which is conserved among a variety of species, does not have a role in T1D, it could still be likely for this gene to have a role in other autoimmune diseases or immune diseases not addressed here and thus explain its association with autoimmune disease. However, since disease association studies are insufficient to establish causality and previous reports on CLEC16A's immune function[44,63,66-71] provide strong evidence for an involvement of this gene in T1D development, *CLEC16A* is likely to be the causal gene for Ch16p13.13's T1D-disease association.

Chapter 4

Understanding the role of CD5 in JAK-STAT signaling.

4.1 Contributions

Cornelia Schuster and Badr Kiaf designed and performed experiments, and analyzed data as indicated below. Janice Marie Nieves-Bonilla performed experiments depicted in Figures 24-26, analyzed data, and wrote the text for this chapter. Ogechi Obed and Otutochukwu Nwagbata helped perform experiments depicted in Figures 24-26 and interpret data. Stephan Kissler supervised the study, analyzed data, and edited this chapter.

4.2 Author's note

A deep sense of curiosity has served as motivation and inspiration since my very first years in life. It has informed many of the decisions I have made throughout my short lifetime and it is ultimately the source of my interest and excitement in becoming a scientist. It was due to that curiosity that I jumped at the opportunity to participate and contribute to one of the other projects in our lab. Albeit my contribution to this project is small in comparison to all the interesting findings others in the lab have contributed, this opportunity has greatly influenced my growth as a scientist during the last two years and is therefore worth mentioning. Participating in this project came with two greatly appreciated benefits the first being an expanded knowledge of immune regulation in the gut, autoimmunity, and immunology in general. The second and most important reward that resulted from my participation in this project was the opportunity to mentor two undergraduate students. A majority of the results presented in this chapter came from joint efforts between the two of them and myself and are a tangible outcome of my efforts to pass on the excitement I feel for biomedical research. Upon self-reflection of the year and a half I spent training Ogechi Obed and the summer I spent training Otutochukwu Nwagbata, I became aware of a deep desire to dedicate a majority of my

time to teaching and mentoring others in science. It is this desire that will guide the next steps of my scientific career as I apply for and hopefully experience jobs in teaching and curriculum development. For these reasons, both Stephan and I agreed it was important to include a short chapter in this dissertation describing our joint contribution to this project. In honor of Otuto and Ogechi, I present this small digression from the topic of the preceding chapters of this dissertation. Enjoy!

4.3 Introduction

CD5, alternatively known as Ly-1 in mice, is a member of the scavenger receptor cysteine-rich (or SRCR) protein family first discovered over 30 years ago. Known to be a type I transmembrane glycoprotein of 67kDa, CD5 is typically expressed on the surface of developing T cells (also referred to as thymocytes), mature T cells and a subset of B cells[95]. CD5 has been proposed to participate in T cell stimulation via co-stimulation, as anti-CD5 antibody has the ability to augment TCR signaling in vitro[95-99]. Subsequently, it was proposed that CD5 can also function as a negative regulator of thymocyte stimulation during T cell development in the thymus, yielding the function of this co-receptor conflicting[95,100-103]. CD5 has also been linked to the regulation of extra-thymic Foxp3^{+} T_{reg} cell differentiation[104,105] suggesting its participation in various levels of immune regulation. Surprisingly, *Cd5*$^{-/-}$ mice do not have an apparent immune pathology or greatly altered lymphocyte function[103,106]. In an effort to better understand the extent of CD5's function in immunity, our lab generated a doxycycline-inducible *Cd5* KD mouse model in the NOD background (NOD.*Cd5*^{KD} mice) to test whether *Cd5* silencing has a greater impact in immune regulation under this immunocompromised system. Previously collected data by Dr. Schuster revealed that induction of *Cd5*

silencing beginning at 3 weeks of age led to a spontaneous sub-clinical gut inflammation that caused mice to loose weight (Figure 22A). This pathology, termed wasting disease, was T cell-driven (Figure 22B), but not due to a loss in extra-thymic T_{regs} (Figure 22C) in the NOD.*Cd5*^{KD} mice. Moreover, *Cd5* KD exacerbated colitis in the DSS and T cell transfer models (Figure 22D-E) suggesting that CD5 has the potential to act as a regulator of gut immunity and whose participation likely becomes critical when other mechanisms of immune tolerance are compromised. Previously collected RNA-seq data from purified T cells of intra-epithelial lymphocytes, payer's patches, mesenteric lymph nodes and spleen revealed a variety of transcriptional differences between NOD and NOD.*Cd5*^{KD} mice. Among those differences, STAT1-regulated genes appeared to be upregulated, whilst STAT6- and Aryl hydrocarbon receptor (AhR)-regulated transcripts were downregulated in NOD.*Cd5*^{KD} mice (data not shown), suggesting an intersection of CD5 with immune pathways signaling via JAK/STAT. This led to my interest in studying how JAK/STAT signaling is altered in NOD.*Cd5*^{KD} mice as this could aid in understanding the observed pathology, as well as in potentially unveiling a role for CD5 in the regulation of gut T cell immunity.

Levels of cell surface CD5 differ among T cell subsets with thymic and splenic T_h cells expressing the highest levels[1]. Additionally, CD5 is reported to signal via association with CKII (Figure 23B), which phosphorylates CD5 itself as well as downstream effectors, in both T and B cells[1,107]. As has been reported, signaling via CKII is an important component in T_h17 cell differentiation via phosphorylation of STAT3 and activation of the PI3K/AKT/mTOR pathways[1,108](Figure 23B). Similarly, signaling via CD5 has been reported to be necessary for $CD4^+$ T cells to efficiently differentiate into

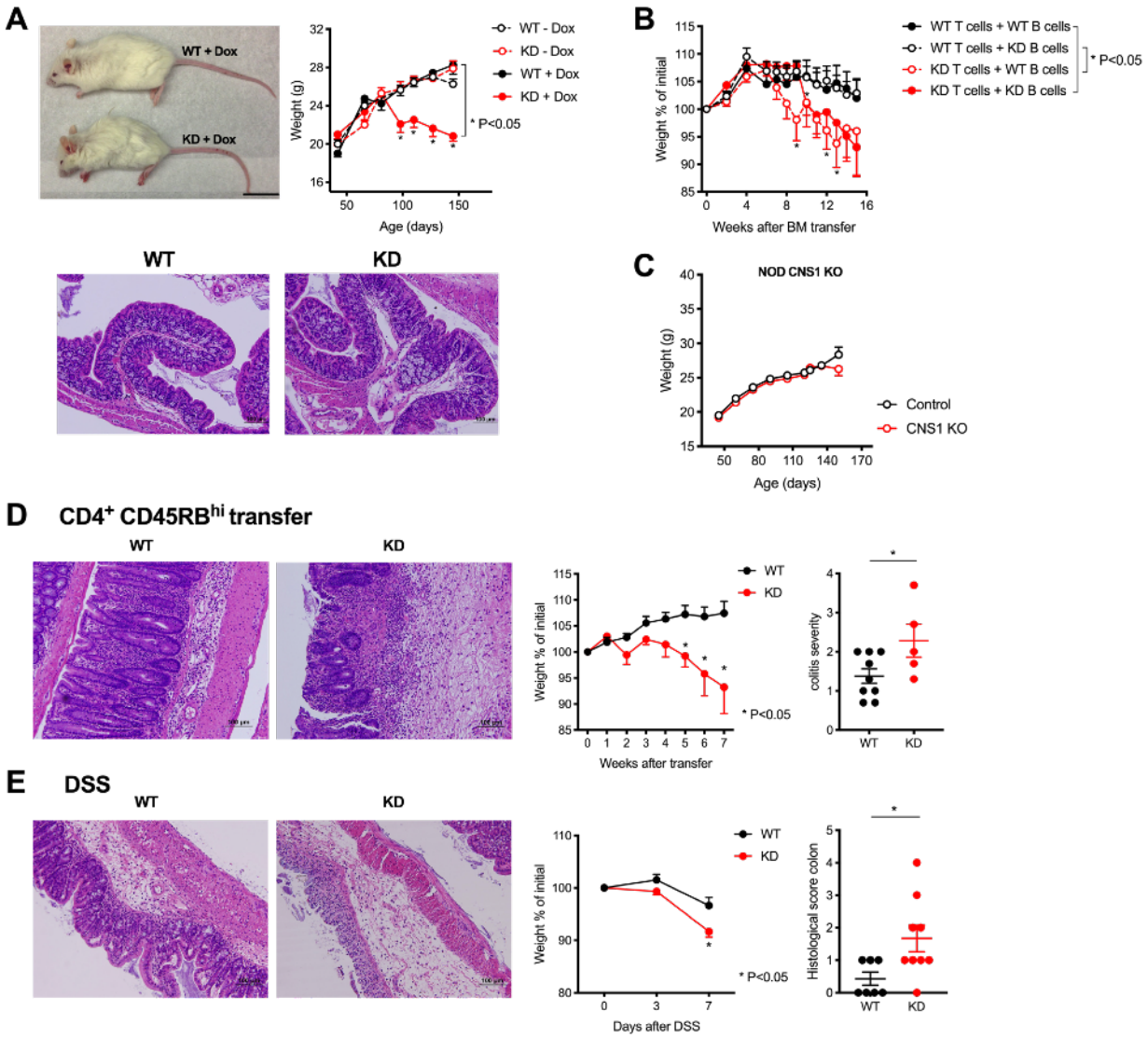

Figure 22. ***Cd5*KD in NOD mice results in a T cell-driven wasting disease.** **A** NOD.*Cd5*KD mice develop a wasting disease from ~3 months of age, which is characterized by weight loss (*top*; n=17-21) and gut inflammation (*bottom*; H&E stained histological sections of the colon). 5 months old mice are pictured and were used for histological analysis. **B** Weight curves for bone marrow (BM) chimeric mice, shown as percent of initial weight. NOD.*Rag*$^{-/-}$ mice (n=11-12) were reconstituted with a mixture of BM from NOD or NOD.*Cd5*KD T-cell deficient (NOD.*Tcr*$^{-/-}$) and B-cell deficient (NOD.*Igm*$^{-/-}$) mice. **C** Weight curves for NOD.*Cns1*$^{-/-}$ mice[2] which have reduced extra-thymic T_{reg} cells and NOD female mice (n=16-29) show that extra-thymic T_{reg} alone are not sufficient to cause the wasting disease seen in NOD.*Cd5*KD mice[2]. **D** CD4^{+}CD45RB^{hi} T cells were FACS-sorted from spleens of NOD & NOD.*Cd5*KD mice (n=5-9) and transferred into NOD.*Rag*$^{-/-}$ mice. **E** The effects of DSS-induced colitis on NOD & NOD.*Cd5*KD mice (n=6-8) was also assessed. Colitis severity was calculated using a combined score including the following criteria: Weight loss, colon length, macropathology (diarrhea, bloody stool) and histological scores[5]. Data collected and analyzed by Dr. Cornelia Schuster.

the T_h17 subset, a process that requires CD5-CKII binding and that is similarly required

in polarization of $CD4^+$ T cells into the T_h2 subtype[1,6]. Although no conclusive data has been reported regarding CD5's involvement in T_h1 differentiation, reports support CD5-CKII binding's ability to activate the AKT pathway — which can inhibit GSK3β, reduce STAT1 phosphorylation (and consequently T-bet levels) and promote efficient nuclear translocation of RORγt (Figure 23B-C) — to promote T_h17 polarization by suppression of T_h1-differentiation-required IFN-γ-mediated responses[1,7]. It remains unknown whether CD5 association with CKII, or another protein kinase, can directly phosphorylate other STATs to promote or suppress the different T_h differentiated subsets. T_h17 cells are a T_h cell subset which produce IL-17, a cytokine that among other functions, has a role in maintaining intestinal barrier integrity[4]. It is established that STAT3 phosphorylation and activation drives T_h17 polarization, and that the activation of this JAK/STAT pathway can be stimulated via several different receptors[4]. The most common example is STAT3's ability to become activated by IL-6 binding to IL-6R for the induction of T_h17 cell differentiation via the release of several cytokines such as IL-17a[4]. Other receptors, such as the IL-21R and IL23R(Figure 23A), can also activate JAK/STAT via STAT3 to promote T_h17 cell differentiation[109]. However, IL-6R-driven activation of JAK/STAT via STAT3 is not restricted to T_h17 polarization or T cells for that matter. In 2016, Zhang et al.[8] reported that in mouse tumor $CD5^+$ B cells, IL-6 can associate with CD5 and gp130 to activate STAT3 and amplify *Cd5* expression. In this context, activation of STAT3 results in a feed-forward loop which promotes tumor growth via upregulation of *Cd5*[8]. While Rozovski et al.[107] reported that CD5 forms a complex with CKII and BLNK in B cells to constitutively phosphorylate STAT3 at its serine (S727; pSTAT3-S) site during chronic lymphocytic leukemia, the study by Zhang et al.[8] looked

at CKII-bound CD5's ability to phosphorylate STAT3 at its tyrosine (T705; pSTAT3-Y) site upon association with JAK2 and in response to IL-6 binding[8].

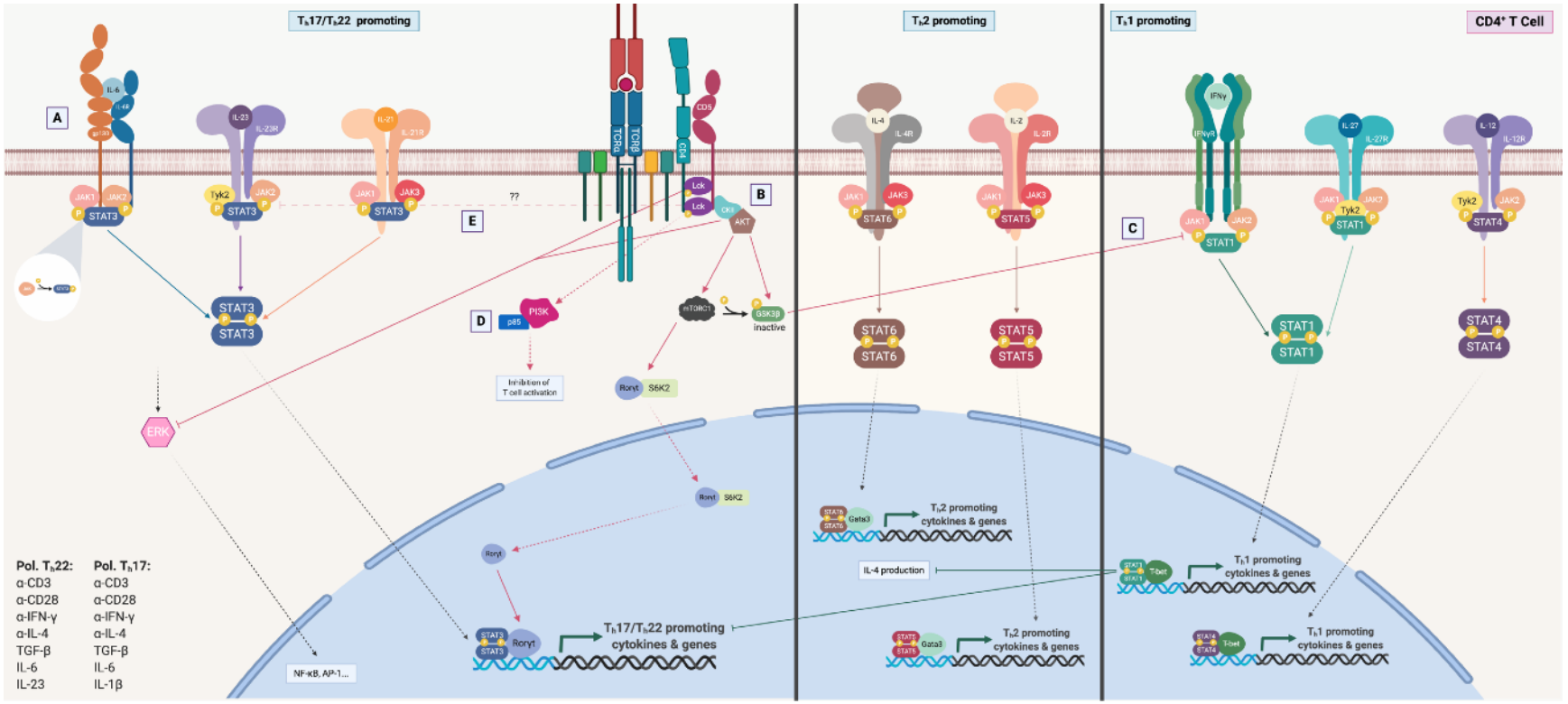

Figure 23. **<u>CD5 signaling promotes T_h17 cell differentiation.</u>** This cartoon diagram models the immunological synapse, IL-17 signaling and activation of STAT3 via IL-6R/IL23R/IL21R and CD5 signaling via CKII in the promotion of T_h17 cells[1]. **A** IL-17 signaling begins upon TCR engagement in $CD4^+$ T cells accompanied by cytokine-cytokine receptor binding which include IL-6-IL-6R, IL-21-IL-21R, and IL-23-IL-23R[4]. Binding recruits protein kinases that vary upon each receptor. In the case of IL-6R — which associates with gp130 to begin signaling — JAK1 and JAK2 are recruited for the phosphorylation of STAT3 and downstream translocation of transcription factor RORγt which binds to promoters of T_h17-promoting genes[4]. **B** CD5 — which can bind Lck and other molecules upon TCR or its own engagement — recruits CKII for activation of AKT[1]. Consequently, AKT activates mTORC1 which promotes RORγt-S6K2 binding for its translocation into the nucleus, as well as the phosphorylation of GSK3β which renders it inactive[6,7]. **C** Inactivation of GSK3β inhibits IFNγR-driven STAT1 signaling[6,7]. **D** CD5 can also recruit CKII to activate the PI3K pathway and inhibit T cell activation[1]. **E** While a direct association between CD5 and JAK2 been reported in B cells[8] this association has yet to be reported in T cells.

4.4 Results & Discussion

In an effort to understand the molecular mechanism by which NOD.*Cd5*^{KD} mice develop wasting disease, we first aimed to verify if STAT3 or its phosphorylation was altered in *Cd5*^{KD} T cells similar to what was described in studies by Zhang et al.[8] and Rozovski et al.[107] The total levels of STAT3 remained constant following TCR engagement with anti-CD3 and/or anti-CD5 antibody in T cells from both NOD and NOD.*Cd5*^{KD} mice stimulated overnight (Figure 24A). This was also the case for T cells stimulated for shorter time points (Figure 24B-C). This result is expected as STAT3 is constitutively present in both stimulated and unstimulated cells. Quantification of the intensity of STAT3 WB bands also provide consistent evidence for normal STAT3 levels among stimulated NOD and NOD.*Cd5*^{KD} T cells (Figure 25A). Moreover, STAT3 also appears to be constitutively phosphorylated at its serine site in stimulated T cells of both NOD and NOD.*Cd5*^{KD} mice, albeit data suggest a small increase of pSTAT3-S in NOD.*Cd5*^{KD} T cells stimulated for longer than 1h (Figure 24). In order to confirm if the observed increase in pSTAT3-S is significant, T cell stimulation experiments can be repeated and data collected can be quantified accordingly. However, since STAT3 is constitutively phosphorylated at its serine site it is less likely that the small difference observed herein will provide relevant information regarding a role for CD5 in the JAK/ STAT signaling pathway.

Furthermore, purified T cells isolated from NOD.*Cd5*^{KD} mice appear to have higher pSTAT3-Y when stimulated for ≥3 hours *in vitro* following TCR engagement with anti-CD3 alone or in combination with anti-CD5(Figure 24A; 24C). However, quantification data suggest this difference is not significant (Figure 25B). Moreover, the observed

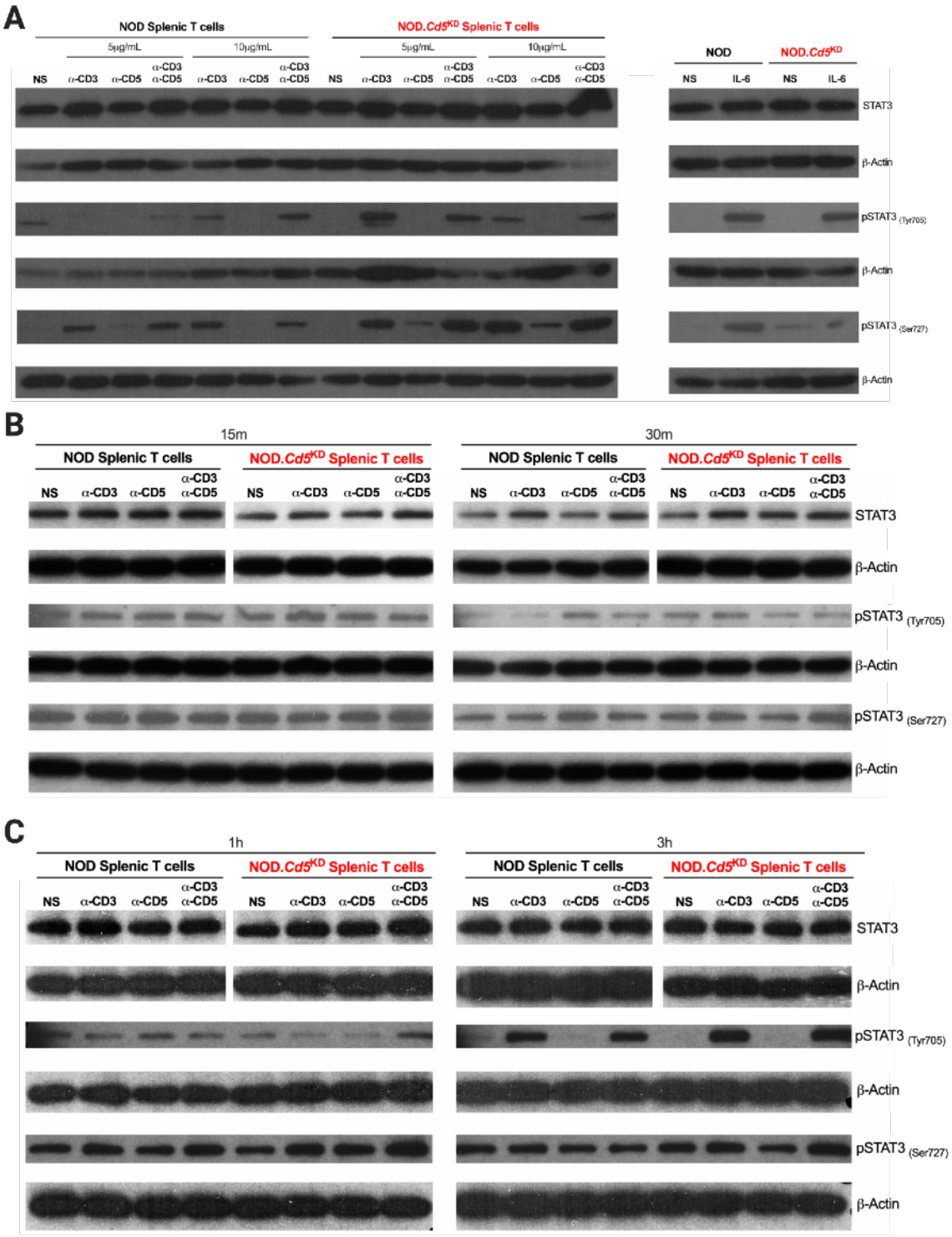

Figure 24. <u>T cells from NOD.*Cd5*^{KD} mice have higher pSTAT3-Y.</u> A Immunoblotting of purified splenic T cells from NOD and NOD.*Cd5*^{KD} mice stimulated *in vitro* with IL-6, ***α***-CD5, ***α***-CD3 or both ***α***-CD5 & ***α***-CD3 overnight (16 hours). **B-C** Cells were also stimulated under these conditions for 15 minutes, 30minutes, 1 hour (**C**) or 3 hours (**C**). NS = not stimulated; ***α***=anti.

effect within NOD.*Cd5*^{KD} T cells on pSTAT3-Y was dampened by treatment with a CKII inhibitor (Figure 25C). Interestingly, phosphorylation of STAT3 at either of the sites was consistent when both NOD and NOD.*Cd5*^{KD} T cells were stimulated via the IL-6R by addition of IL-6 (Figure 24A). While the discordance between the WB images and quantification efforts suggest that perhaps lysates from NOD.*Cd5*^{KD} mice have higher protein content, the same amount of protein was added for each condition. An alternative methodology for pSTAT3-Y quantification is flow cytometry. Therefore, current efforts by Dr. Kiaf in our lab have focused in using this technique to confirm the observed results regarding pSTAT3-Y in NOD.*Cd5*^{KD} mice. Of note, an increase in pSTAT3-Y has been consistently reported upon silencing of CD5-dependent CKII

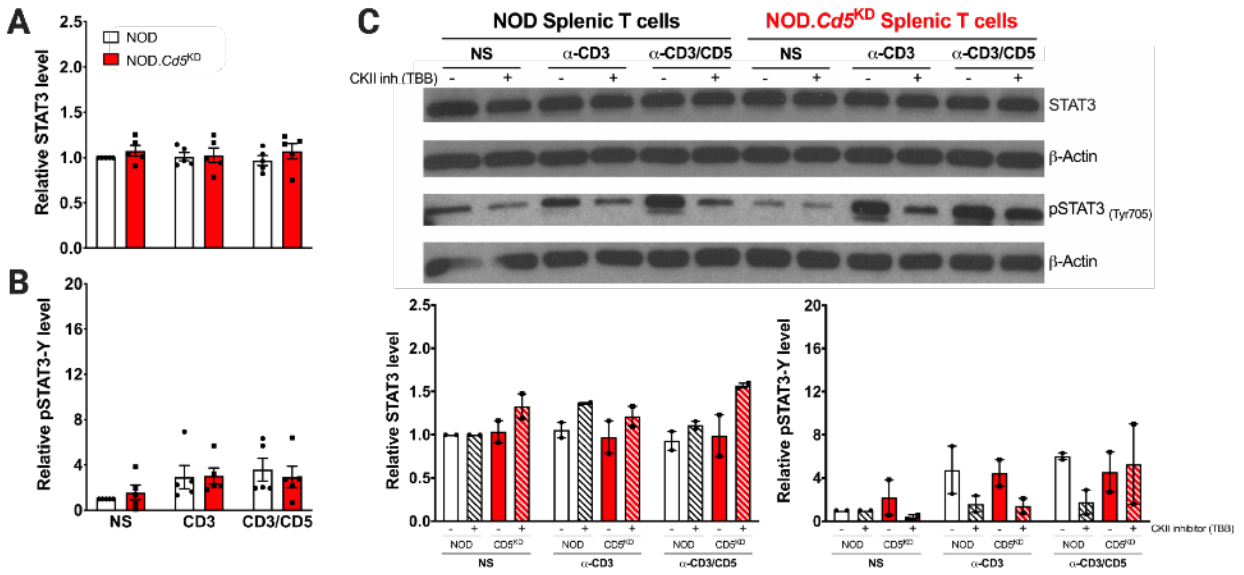

Figure 25. <u>CKII inhibition reduces the effects of CD5 KD on pSTAT3-Y.</u> A-B Western blot band intensity was measured using the ImageJ/Fiji software. Relative protein levels were calculated as the ratio of STAT3 (**A**) or pSTAT3-Y (**B**) to the loading control **β**-Actin and normalized to NOD NS samples are depicted here. Calculation formula: x=[(band intensity of STAT3 or pSTAT3-Y)/(band intensity of **β**-Actin)]/[x for NOD NS]. Figure 24C is representative of all experiments plotted. Plotted data is combined from 3 independent experiments. **C** *In vitro* TCR engagement of NOD and NOD.*Cd5*^{KD} mice splenic T cells with CD5 co-stimulation using ***α***-CD5 and ***α***-CD3 antibodies for 3 hours. Cells were stimulated in the presence or absence of TBB to inhibit CKII. Western blot picture is representative of two independent experiments. Data for these experiments was also quantified, combined and plotted. NS=not stimulated; ***α***=anti.

activation in T_h cells[6,7]. In both reports by Sestero et al. [6] and McGuire et al.[7] this effect is significantly observed following T_h cell differentiation into the T_h17 cell subset[6,7]. This provides a possible explanation as to why the differences observed herein are not significant, since T_h17 polarized conditions were not used for these experiments. Since CD5 binding to CKII plays a role in T_h17 differentiation, stimulating pan T cells instead of differentiated T_h cells likely diminished the strength of the expected difference between genotypes. Interestingly, a preliminary study where NOD.*Cd5*^{KD} T_h cells were cultured under T_h17 and T_h22 polarizing conditions for ~48h hours (Figure 26) suggests that T_h22-polarized cells have higher levels pSTAT3-Y (Figure 26C-D) and to a lesser extent STAT3 (Figure 26D) than T_h17-polarized cells (Figure 26). Furthermore, preliminary quantification following cellular fractionation of polarized cells suggest that the observed increase in both STAT3 and pSTAT3-Y levels within T_h22-polarized cells is sustained in the nucleus. However, this experiment has to be repeated in order to make definitive conclusions.

CD5 has been reported to regulate T_h17 cell differentiation in a variety of ways[6,7,110-112]. In the reports by Sestero et al.[6] and McGuire et al.[7] CD5-dependent activation of CKII was reported to intersect with JAK/STAT signaling at several points throughout the pathway[6,7]. Specifically, ablation of CD5-dependent activation of CKII was found to enhance both the activation of STAT3 and STAT1, as well as the production of IL17a and IL-6 cytokines while reducing T_h17 cell proliferation[6,7]. In the case of these two studies, the authors claim that the increase in STAT3 activation[6,7] is due to the overproduction of IL-6[6], the hyperactivation of STAT1[6] which has been reported to inhibit T_h17 proliferation[6,7,113], and the ability of CKII to bind and

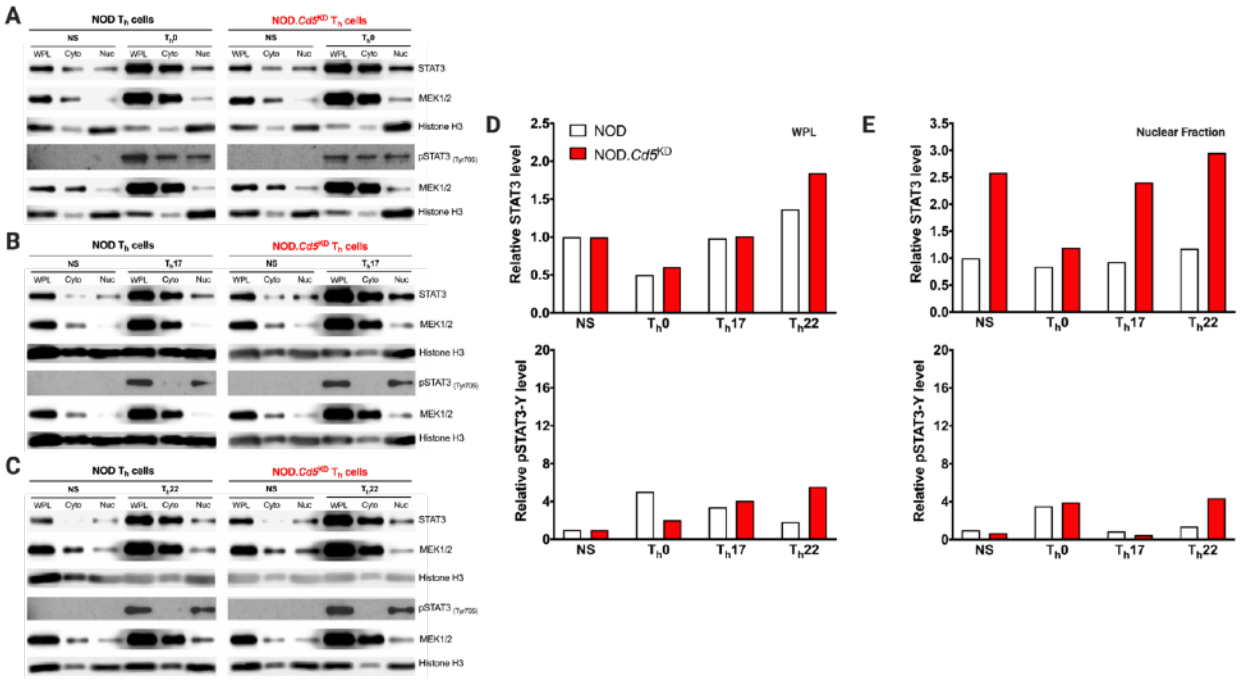

Figure 26. <u>Preliminary data suggest T_h22-polarized cells from NOD.*Cd5*^{KD} mice also have higher pSTAT3-Y.</u> **A-C** Purified naïve T_h cells from the spleen of NOD and NOD.*Cd5*^{KD} mice were incubated under T_h0-polarizing (TCR engagement with plate-bound ***α***-CD3, and co-stimulation with ***α***-CD28; **A**) , T_h17-polarizing (TCR engagement with plate-bound ***α***-CD3, co-stimulation with ***α***-CD28 and addition of TGF-**β**1/IL-6/IL-1**β**/***α***-IFN-**γ**/***α***-IL-4; **B**) and T_h22-polarizing (TCR engagement with plate-bound ***α***-CD3, co-stimulation with ***α***-CD28 and addition of IL-6/IL-23/***α***-IFN-**γ**/***α***-IL-4; **C**) conditions for ~48 hours. Preliminary quantification of whole protein lysates is shown in **D**, while quantification of lysates from the nuclear fraction collected following subcellular fractionation is shown in **E**. This experiment was only performed once. NS=not stimulated; ***α***=anti.

phosphorylate JAK1 and JAK2 which activate STAT3[114]. Moreover, they see a reduction in AKT activation[7], nuclear Ror**γ**t[7] accompanied by an increase in cell death[6] when the binding of CD5 and CKII are abrogated which they attribute to CD5's participation mTOR-driven nuclear translocation of Ror**γ**t and inhibition of GSK3**β**[7]. Co-stimulation with CD5 has also been found to stably induce T_h17 differentiation by increasing IL-23R expression and in that way promoting STAT3 activation[110], a process which is likely CKII-independent[6] but IL-6-dependent[111]. The data presented in this chapter is somewhat consistent with previous reports regarding an increase in STAT3 activation

via pSTAT3-Y upon costimulation with CD5 or under T_h17/22 polarizing conditions. Moreover, current efforts by Dr. Kiaf in our lab have also confirmed a significant reduction in T_h17/22 differentiation, IL-17 and IL-22 production and even IL-23R expression in NOD.*Cd5*^{KD} mice. Interestingly, while CKII inhibition with 4,5,6,7-tetrabromobenzotriazole (TBB) was able to diminish the increased STAT3 activation resulting from a 3h costimulation with CD5, it was not able to completely abrogate STAT3 activation in NOD mice. Moreover, treatment with TBB following CD5 costimulation did not consistently diminish STAT3 activation in T cells from NOD.*Cd5*^{KD} mice (Figure 25). These data, in combination with previous reports, suggest that CD5 can modulate JAK/STAT signaling, i.e. STAT3, in both a CKII-independent as well as in a CKII-dependent manner and consequently influence T_h17/22 differentiation. Given that CD5 has been reported to form a complex with IL-6, gp130 and JAK2 to consequently phosphorylate STAT3 in B cells[8], I propose that in T cells CD5 has a potential dual role in the differentiation of T_h17/22 cells where it can act via CKII to induce downstream mTOR signaling which enhances Rorγt translocation and inhibition of the T_h1 phenotype as previously reported[6,7,113], and independently of CKII by responding to IL-6 and binding JAK2, which has been reported to induce activation and downstream signaling of STAT3 in CD5$^+$ B cells[8]. Signaling downstream of STAT3 activation also results in the promotion of IL-23R expression which CD5 has been reported to participate in[110]. However, evidence of CD5's ability to bind IL-6 and JAK2 in T_h17/22-polarized cells is lacking and would be necessary to confirm this proposed dual role of CD5 in STAT3 activation. Additionally, evidence of significant STAT3 activation and upregulation of IL-23R expression in purified NOD T_h cells treated with IL-6R

neutralizing antibody and TBB upon T_h17/22 polarization while using CD5 instead of CD28 costimulation would also be necessary to implicate this alternative role for CD5 in T_h17/22 differentiation. Efforts by Dr. Kiaf have also revealed that NOD.*Cd5*^{KD} mice have significantly increased gut permeability (data not shown) which has been reported to result following dysregulation of IL-17 and/or IL-22 signaling[115,116], supporting a role for CD5 in gut immunity via modulation of IL-17/IL-22 signaling. Overall, further describing CD5's role in IL-17 & IL-22 signaling, gut immunity and the spontaneous wasting disease developed in NOD.*Cd5*^{KD} mice would deepen the current understanding of CD5's role in immune regulation and expand its potential use as a therapeutic target for the immune modulation of autoimmune diseases.

Chapter 5

Discussion

5.1 Summary and discussion of dissertation findings

The repeated association of Ch16p13.13 with multiple autoimmune diseases, T1D in particular, has lead to an ongoing debate over which of the genes within the region is causal for disease associations. This debate stems from the ambiguous effects disease-associated SNPs can have on gene expression and protein function[3,34,41,43,54]. While there is an adequate amount of reports on the role of 3 genes from Ch16p13.13 (i.e. *CIITA*[19], *CLEC16A*[44,63,66-71], *SOCS1*[29-31]) in autoimmunity and/or T1D, functional data for *DEXI* and its role in T1D[75] is still quite limited. The genomic sequence coding for this small protein of ~10kDa in size which co-localizes with chromatin within the nucleus[75] (Figure 1C) is conserved among species[3], making it possible to study its function in mouse models of disease. To describe a potential role for *DEXI* in T1D onset, CRISPR/Cas9 genome editing was used in diabetes-prone NOD mice to excise *Dexi*'s protein-coding genomic sequence. An initial attempt to create a *Dexi* mutant mouse using a single sgRNA was unsuccessful. Using one sgRNA should result in a single DSBs in the *Dexi* DNA at which point the DNA mismatch machinery would act to repair the DNA. Since it was desired to obtained a KO mutation, a homologous sequence was not provided along with the sgRNA and Cas9 mRNa, making it more likely that the DSB would be repaired using the non-homologous end joining (NHEJ) pathway[89,90]. It was expected that this error-prone repair system would incorrectly assemble the genomic sequence of *Dexi*, creating an Insertion-Deletion (InDel) mutation, but this was not the case. It is likely that using a single sgRNA allowed the CRISPR/Cas9 complex to make a DSB, however, the NHEJ pathway failed to create InDel mutations. Alternatively, it is also possible that the InDel mutations introduced were very small (e.g. single nucleotide

mutations) and harder to detect with simple PCRs. A surveyor assay used to detect single nucleotide mutations in the first litter of pups generated was attempted, but results were not conclusive. For this reason, subsequent attempts at creating a *Dexi* KO NOD mouse used the two sgRNA sequences described in Table 1 which target the beginning and end of *Dexi*'s exon 1. Ideally, the generation of two simultaneous DSBs would excise out *Dexi*'s protein-coding exon leaving the two non-homologous ends of the sequence before and after *Dexi*'s exon 1 to be joined by the NHEJ complex. Sequencing of the A1 mutation indeed revealed a complete excision of the targeted exon 1 sequence (Figures 3B). However, the extent of this mutation went beyond *Dexi*'s exon 1 with 544bp of the following intronic sequence also being deleted. A 3bp insertion was also observed in the sequence of the A1 mutation (Figure 4B). While further studies would be necessary to understand the precise occurrence of this mutation, it is likely that NHEJ-directed repair in the abundance of a homologous template made an error during repair that caused both a longer-than-expected deletion and a 3bp insertion[117-119].

The extensive 1330bp deletion in the A1 mutation allowed the genotyping PCR to clearly determine WT from mutated *Dexi* NOD mice. However, the primers used made it difficult to distinguish heterozygote from homozygote mutations in the mice (Figure 4E). This was likely due to the resulting smaller sequencing being more readily available for amplification by the primers. Designing a second PCR protocol with primers targeting a small region in the beginning of the CRISPR-targeted region made it possible to clearly detect a WT band in both NOD mice and NOD.*Dexi*$^{+/-}$ A1 mice and to consequently interbreed to obtain NOD.*Dexi*$^{-/-}$ A1 mice. Surprisingly, this second PCR protocol also

uncovered a second, much shorter, InDel mutation in the founder mice and F1 progeny (Figure 3C). The A2 mutation only lacked 185bp along the start of *Dexi*'s exon 1 — not including the protein-coding ORF — (Figure 4C) and likely resulted from a single 5' sgRNA-induced DSB. The founder's F1 progeny allele genotypes were puzzling as each of the mutant alleles segregated into 25% of the progeny each, instead of the expected 50%, with the resulting 50% progeny carrying only WT alleles. These data suggest that the gene editing event occurred at the two-cell stage of the founder's germ cells, with two separate editing events occurring in one allele of each of the cells (Figure 5) and making them chimeric in nature. Chimeric mice are an expected result when making KO mice via the microinjection of mutated embryonic stem cells into blastocysts[90]. However, while it is expected to obtain mosaic mice from pronuclear injections[90], little has been reported regarding the accidental emergence of chimeric mice when generating KO mice with CRISPR/Cas9 injection into the blastocysts of mice. This finding makes this surprising piece of data relevant for the future use of CRISPR/Cas9-mediated mouse genome engineering.

Overexpression of a FLAG-tagged mouse Dexi fusion protein in 293T cells made it possible to identify a reliable mouse anti-Dexi antibody and to create a successful IP-WB protocol for the detection of Dexi protein levels in mice (Figures 8). Characterization of the NOD.*Dexi*$^{-/-}$ A1 mice confirmed complete absence of *Dexi* transcript and protein in relevant organs (Figure 11). Moreover, expression of the other three genes in Ch16p13.13 remained consistent in most organs of both NOD and NOD.*Dexi*$^{-/-}$ A1 (Figure 12), making it ideal for solely studying *Dexi*'s role in autoimmune development. Of note, while NOD.*Dexi*$^{-/-}$ A2 mice mostly lacked *Dexi* transcript, some levels of

transcript were observed in the spleen (Figure 7A) making it a less reliable model. Nevertheless, these mutant mice were studied along with the NOD.*Dexi*$^{-/-}$ A1. NOD.*Dexi*$^{-/-}$ A2 mice mostly showed no differences in the expression of Ch16p13.13 genes, albeit transcript levels were not assayed as extensively.

NOD.*Dexi*$^{-/-}$ A1 & A2 mice developed normally and showed no observable phenotypical differences when compared to NOD. Further analysis of the cellular immune system by flow cytometry revealed a reduced amount of total splenocytes in NOD.*Dexi*$^{-/-}$ A1 (Figure 13E). While the frequency of T cells, B cells and myeloid cells did not appeared altered, there appears to be a reduction in the total amount of T_h cells in the spleen of NOD.*Dexi*$^{-/-}$ A1 & A2 mice (Figure 14E). Moreover, spleen weight but not size was also significantly reduced in both NOD.*Dexi*$^{-/-}$ A1 & A2 when compared to NOD (Figure 13C). Further functional studies falling outside the scope of the present dissertation are necessary to understand how the observed decrease in splenic T cells relates to *Dexi* function and immunity.

Ultimately, *Dexi* KO alone was not sufficient to significantly affect the frequency of CY-induced or spontaneous diabetes development in NOD mice (Figure 19). In order to study the joint contribution of *Dexi* and *Clec16a* in diabetes development, NOD.*Dexi*$^{-/-}$ mice were intercrossed with NOD.*Clec16a*^{KD} mice to generate the double deficient NOD.*Dexi*$^{-/-}$*Clec16a*^{KD} mice. This was possible due to the *Clec16a* KD being mediated by a lentiviral transgene that is located outside of the Ch16p13.13 region. NOD.*Dexi*$^{-/-}$ *Clec16a*^{KD} mice had a significant delay in spontaneous diabetes onset when compared to NOD mice which was similar to what was previously reported by our group in NOD.*Clec16a*^{KD} mice[66]. No significant changes in diabetes incidence were observed

when comparing NOD.*Dexi*$^{-/-}$*Clec16a*^{KD} mice to NOD.*Clec16a*^{KD} mice supporting a lack of *Dexi*'s participation alone or in combination with *Clec16a*^{KD} in the diabetes onset of NOD mice. Furthermore, *Dexi* deletion had no effects on the glucose tolerance or severity of lymphocyte infiltration into the islets of NOD mice, a process that precedes disease onset (Figure 20). Collectively, the data presented herein do not support a significant role for *Dexi* alone or in combination with *Clec16a* on the development of autoimmune diabetes in the NOD mouse model.

5.2 Addressing conflicting data in two recent reports on *Dexi*'s function.

Two recent articles have also addressed *Dexi*'s potential role in autoimmune diabetes. A peer-reviewed article by Dos Santos et al.[75] claims *DEXI* to be "the aetiological gene for T1D in Ch16p13.13…" owing to its ability to regulate type 1 IFN-STAT signaling and thus participate in virus-induced pancreatic β cell inflammation. With the goal of clarifying *Dexi*'s potential participation in T1D pathogenesis at the level of the β cells, this group treated a human and a rat β cell line as well as rat primary β cells with the synthetic viral dsRNA analogue polyinosinic:polycytidylic acid [Poly(I:C)] to mimic viral-induced β cell inflammation. They observed a significant increase in the expression of *DEXI* mRNA expression and protein after Poly(I:C) treatment for 24 hours (h) in all of the studied cells[75]. Unexpectedly, infection of the rat β cell line INS-1E with diabetogenic coxsackievirus B5 (CVB5) reduced *Dexi* expression instead[75]. Upon silencing of *Dexi* in rat primary cells and the INS-1E cell line using RNA interference (RNAi), a decrease in virus-induced apoptosis, STAT1 signaling, interferon-sensitive response element — a

gene element which regulates downstream pro-inflammatory genes — activation, pro-inflammatory cytokine transcription (i.e. *Cc15*, *Cxcl9*, *Cxcl1*), and Interferon-β (IFN-β; *Ifnb1*) expression and production was reported following 24h treatment with Poly(I:C)[75]. While data in this report strongly suggest a role for *DEXI* in T1D development and a localization for *Dexi* within chromatin allowing it to act as a transcription factor regulating IFN-β expression, it also possess a conundrum between previously published data on *DEXI* as well as with the data herein.

Previously reported *DEXI* eQTLs correlate T1D protection alleles with increased *DEXI* expression[3,41,77,83]. In this context, overexpression of *DEXI* would be consistent with a reduction in events promoting diabetes or autoimmune development, which was not observed in NOD.*Dexi*$^{-/-}$ mice. However, the data presented in the report by Dos Santos et al.[75] portray that overexpression of *DEXI* results in the opposite effect with an increase of virus-induced β cell apoptosis and islet inflammation, events that precede diabetes development. Furthermore, while *DEXI* is indeed expressed at a higher level in the pancreas than in immune cells and organs (Figure 1 & [75]), changes in *DEXI* expression have been associated with multiple immune diseases suggesting an immune-related function[3,41,61,77-82]. While the function reported by Dos Santos et al.[75] is immune in nature, model immune cells were not considered or used as controls when studying immune-related pathways. Claims in this report are thus restricted to pancreatic β cells and fail to explain the association of *DEXI* with other immune-related diseases.

To replicate the experiments reported in Dos Santos et al.[75], bone marrow-derived Mφs (BM-DM) — commonly used for the study of type 1 IFN signaling — from NOD and NOD.*Dexi*$^{-/-}$ A1 mice were cultured and transfected with Poly(I:C) for 24 hours. NOD BM-DMs showed no significant changes in *Dexi* expression upon Poly(I:C) treatment (Figure 27A). Moreover, Poly(I:C) treatment equally increased *Ifnb1* transcript levels (Figure 27B) and *Viperin* transcript levels (Figure 27C). *Viperin* (or *Rsad2*) is downstream in the IFN-β-induced type 1 IFN signaling pathway, its expression is upregulated following STAT1 nuclear translocation and it is an effector protein that can regulate viral replication[120]. Data collected from the BM-DMs of NOD and NOD.*Dexi*$^{-/-}$ A1 mice strongly suggest *Dexi* does not participate in virus-induced type 1 IFN signaling, a pathway reported to be conserved between tissues and cell types[121,122].

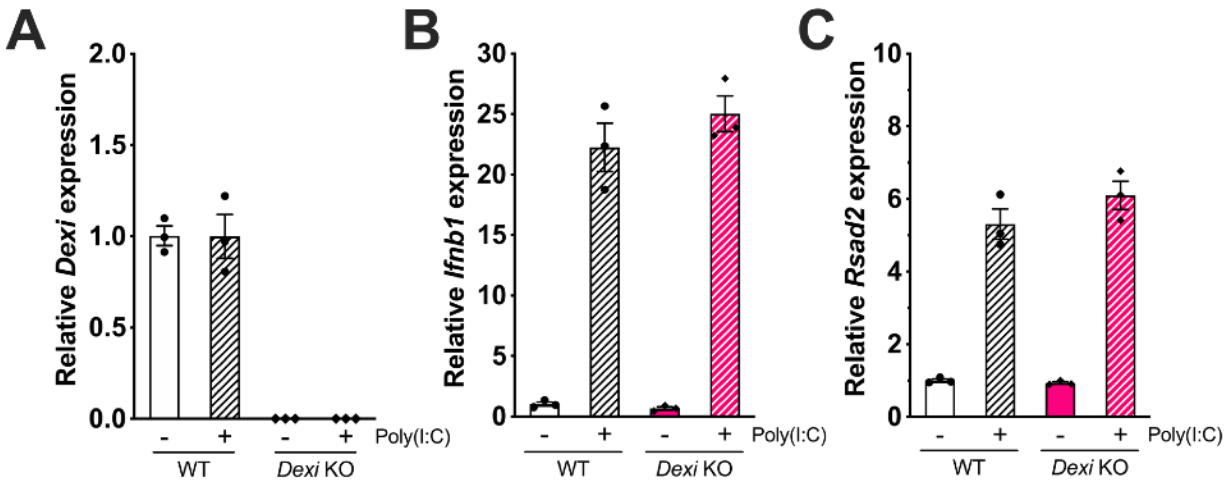

Figure 27. <u>BM-DMs from NOD.*Dexi*$^{-/-}$ mice do not have an impaired production of IFN-β following treatment with Poly(I:C).</u> **A** Quantification of *Dexi* mRNA expression by qPCR in BM-DMs from NOD and NOD.*Dexi*$^{-/-}$ A1 mice following transfection and 24h treatment with Poly(I:C). **B** IFN-β and **C** IFN-β-induced *Rsad* (*Viperin*) expression in Poly(I:C)-treated BM-DMs from NOD and NOD.*Dexi*$^{-/-}$ A1 mice. Data show individual values, mean ± SEM and are representative of at least two similar experiments. *Dexi* expression in samples from NOD.*Dexi*$^{-/-}$ A1 mice was not detected.

While the data in this dissertation has a strong foundation to challenge the report

by Dos Santos et al.[75], it is important to further discuss the data in these studies as well as to address several caveats. Even though the type 1 IFN response is conserved within cell types[121,122] and species[123], this signaling pathway can be regulated by different environmental factors that can be tissue-specific[121,122]. Taking this into consideration, it is possible that the differences observed herein stem from the use of a different cell type (macrophages instead of β cells) and/or the use of a different species (mouse vs rat and human) in testing the virus-induced type 1 IFN response. Steady state *Ifnb1* transcript levels were measured in the islets of NOD and NOD.*Dexi*$^{-/-}$ A1 mice but expression was not detected. Testing the IFN-β transcript levels upon transient overexpression of *Dexi* in NIT-1 cells and in primary islets from NOD.*Dexi*$^{-/-}$ A1 treated with Poly(I:C) would be a simple way to corroborate if the differences observed are in fact stemming from the use of a different cell type. Treatment of NOD mice with Poly(I:C)[124] and CVB[125-127] has been reported to accelerate diabetes, albeit effects of treatment with the latter are quite controversial[126,128,129] and seem well defined in rats as opposed to mice[87,129,130]. Measuring diabetes incidence as well as the type 1 IFN response in NOD and NOD.*Dexi*$^{-/-}$ A1 mice treated with Poly(I:C) would thus be necessary to conclusively refute the data presented by Dos Santos et al.[75]

Another important difference to discuss is the experimental systems used to diminish *DEXI*/*Dexi* expression. Dos Santos et al.[75] relied on RNAi, which uses small-interfering RNA (siRNA) to partially interrupt *DEXI*/*Dexi* mRNA transcription rather than complete deletion of a portion of the genomic *Dexi* sequence as reported herein. It has been reported that the use of siRNA for gene silencing can result in the stimulation of an

inflammatory response and in the release of pro-inflammatory cytokines including type 1 IFNs via TLR-signaling[131,132]. Additionally, off-target effects due to sequence similarity are also often reported when using RNAi for gene silencing[131,132]. While the data presented by Dos Santos et al.[75] contains appropriate controls to minimize the likelihood of the observed phenotypes resulting from off-target effects, a possibility exists that the observed phenotype effect is due to off-target effects of the *DEXI*/*Dexi*-targeting siRNA sequences themselves containing immune-stimulatory motifs[131,132] which can be harder to circumvent[131]. Due to the lack of sequence specification for each siRNA used in the study by Dos Santos et al.[75], it is challenging to analyze any sequence-related off-target effects. Of note, the Dos Santos et al.[75] report lacks data on the expression of the three other genes in Ch16p13.13 — specifically *SOCS1* — upon *DEXI* silencing. Ergo, the different phenotype observed upon *DEXI* silencing could stem from off-target effects on *SOCS1*, which can modulate STAT-signaling[29-31] and virus-induced pancreatic inflammation[133]. An off-target silencing of *TYK2/Tyk2*, or even altered function of TYK2 via SOCS1, would also be consistent with the reduction in viral-induced apoptosis, IFN-β and *Stat1*[134] seen in the study by Dos Santos et al.[75,134]

Dexi function in the inflammatory response should not be completely excluded, however, considering that this gene is in a LDB with genes that modulate inflammation directly or indirectly. Stressing NOD.*Dexi*$^{-/-}$ A1 mice *in vivo* and mouse-derived primary cells *in vitro* with known model antigens commonly used to model other types of inflammation would be a useful tool to rule out a function for *Dexi* in inflammatory responses. Moreover, using NOD.*Dexi*$^{-/-}$ A1 mice to study the effects of *Dexi* KO in other NOD-derived autoimmune mouse models could still uncover a role for *Dexi* in

autoimmunity.

A pre-print article also reported a function for *Dexi* in autoimmune diabetes using the NOD mouse model. Similar to the work reported in this dissertation, Davison et al.[9] used CRISPR/Cas9 to disrupt *Dexi* expression in the NOD mouse and assess its role in autoimmune development. In their case, both *Dexi* mutated NOD mice had a higher incidence of diabetes, an increased concentration of serum IgM and IgA, gut microbiome differences, and changes in microbial-metabolism-associated molecular metabolites when compared to NOD mice. Due to the contradicting results reported herein, it is necessary to discuss key differences between both of these studies and to offer a rationale for these.

In the report by Davison et al.[9], the generation of *Dexi*-deficient NOD mice via CRISPR/Cas9 was carried out in a similar manner to that reported here, with the only differences being that a single sgRNA sequence targeting the start of *Dexi*'s protein-coding ORF was injected with the Cas9 protein and not Cas9 RNA. While injecting Cas9 protein or RNA should not have major effects on the generation of these mice, using only one sgRNA sequence did result in significantly different mutations with shorter portions of *Dexi* genomic DNA deleted when compared to those observed in the NOD.*Dexi*$^{-/-}$ A1 and A2 mice (Figure 3). Davison et al.[9] describe a 1bp insertion (INS1BP) and a 12bp deletion (DEL12BP) both located within the protein-coding ORF of *Dexi*.

Albeit smaller, both the INS1BP and DEL12BP mutations should have resulted in loss-of-function, as explained in the report[9]. As they expected, the 1bp insertion —

which contained a frame-shift in the coding sequence and produced a nonsense transcript — had the strongest phenotype with 100% of these female mice being spontaneously diabetic by 200 days of age. To a lesser extent DEL12BP NOD females also had significantly higher incidence of spontaneous diabetes, with about 90% diabetic by 200 days of age. Interestingly, the phenotype reported in both INS1BP and DEL12BP mice was not observed in males. While the female NOD mice used in the study by Davison et al.[9] had a higher incidence of spontaneous diabetes (~75%) when compared to the NOD mice used in the current study (~50%), it is important to note that their NOD colony was bred from the WT progeny obtained during heterozygous crosses, as opposed to out-breeding mutant NOD mice with pure WT NOD mice. Using this strategy could have introduced and/or perpetuated any off-target effects that led to the phenotypical differences observed.

Several environmental factors have been described to influence diabetes incidence in different NOD colonies, including diet and gut microbiome composition[84,135-138]. As reported by Davison et al.[9], both INS1BP and DEL12BP mice had different fecal microbiomes when compared to their NOD colony. Since the composition of the microbiome in the gut of NOD.*Dexi*$^{-/-}$ A1 and A2 mice was not assessed, the possibility exists that a difference in their gut microbiome composition is reversing the effects of *Dexi* deficiency observed in Davison et al.[9] However, due to the phenotype described in Davison et al.[9] being related to changes in gut microbiome, i.e. an absence of gut microbial metabolites, it is also likely that the phenotype they observed is related to other unforeseen environmental factors and not the *Dexi* mutations per se, especially since it is not indicated whether NOD and mutated mice

were housed separately.

However, the most important and relevant distinction between the study by Davison et al.[9] and the present study with NOD.*Dexi*$^{-/-}$ A1 mice is that although significant alterations were made in the genomic sequence of *Dexi* in both cases, only the data presented here was able to provide clear and definitive evidence of the complete absence of *Dexi* mRNA and Dexi protein. Ultimately, the lack of definitive *Dexi* KO validation in the study by Davison et al.[9] is sufficient to question the validity of their phenotypic findings and strengthen the validity of the findings reported in the current work.

5.3 Conclusion & Final Remarks

Overall, the work presented in this dissertation provides conclusive data that complete *Dexi* ablation was achieved following CRISPR/Cas9 in the NOD mouse. Moreover, *Dexi* KO alone was not sufficient to play a role in the development of CY-induced or spontaneous diabetes. *Dexi* KO in NOD was also unable to reverse the effects of *Clec16a* KD previously reported in our lab, suggesting that interactions between *Dexi* and *Clec16a* do not modulate diabetes risk. Furthermore, while NOD.*Dexi*$^{-/-}$ A1 mice had a significantly decreased amount of total splenocytes, specifically T_h cells, and lighter-weighing spleens, the composition of immune cellularity was not significantly changed in the LNs, spleens and thymi of these mice. Additionally, β cell function was not impaired in NOD.*Dexi*$^{-/-}$ A1 mice as evidenced by a normal response to glucose injection following fasting in glucose tolerance tests. NOD.*Dexi*$^{-/-}$ A1 mice also had similar levels of insulitis when compared to NOD. Contrary to previously

published data on *Dexi* function[75], *Dexi* KO BM-DMs did not have an impaired type 1 IFN response to Poly(I:C). Due to the conservation of the type 1 IFN response[121-123], it is thus likely that Dexi does not function in the virus-induced pancreatic inflammation which is hypothesized to precede diabetes.

As suggested by Dexi's localization within the chromatin[75] of cells, SNPs within intron 19 of *CLEC16A* could still be affecting the *DEXI* expression via chromosomal interactions. However, the data presented here suggest that these changes in expression likely have no effect in T1D risk. However, it remains unclear if this change in expression plays a role in the development of other autoimmune diseases. Moreover, since *Dexi* KO had no effects on the previously reported delay in diabetes onset of NOD.*Clec16a*^{KD} mice[66] it is likely that *CLEC16A* is the more relevant gene among Ch16p13.13's T1D-associated variations.

The role of Dexi still remains a mystery and further studies will be necessary to characterize its function. Since *Dexi* expression among the immune cellular compartments is highest in splenic CD11b^{+}CD11c^{+}DCs, which are a type of professional APC[72,139], it would be interesting to assess the efficiency of antigen presentation in the APCs of NOD.*Dexi*$^{-/-}$ A1 mice using various model antigens. Additionally, while *Dexi* does not play a role in T1D, it remains a question whether its function does play a role in other autoimmune diseases associated with Ch16p13.13. In order to conclusively say that *Dexi* plays no role in autoimmunity, effects of *Dexi* KO in mouse models for MS, RA, and/or psoriatic arthritis would have to be tested. For example, the autoimmune demyelination seen in MS can be experimentally modeled in mice with autoimmune encephalomyelitis (EAE). EAE is commonly induced by immunization of NOD mice with

myelin oligodendrocyte glycoprotein ($MOG_{[35-55]}$) an encephalitogenic peptide which models the relapsing-remitting to secondary-progressive transition observed in 50% of MS patients[140]. Studying the effects of *Dexi* KO on EAE following immunization of NOD and NOD.*Dexi*$^{-/-}$ A1 mice with $MOG_{[35-55]}$ could thus offer insights on whether *Dexi* plays a role in MS or not. Ultimately, the generation of the NOD.*Dexi*$^{-/-}$ mice in this study has provided an essential tool to advance the understanding of Dexi's function and its relationship to immunoregulatory diseases. The generation of NOD.*Dexi*$^{-/-}$*Clec16a*^{KD} mice has also provided the unique opportunity to study *Dexi*'s role in the previously reported delay in diabetes onset among NOD.*Clec16a*^{KD} mice[66], as well as the joint contribution of two out of the four Ch16p13.13 genes (*Clec16a* & *Dexi*) to diabetes onset.

Moreover, since *Dexi* is conserved between species[3] and it is within reason to assume that its function is similar in mouse and human, the findings herein suggest that *DEXI* alone does not have a significant role in human T1D. Although disease-associated SNPs modify the expression of *DEXI* in some tissues[3,61,77-82], this is not sufficient to ascertain that DEXI function impacts T1D or perhaps even autoimmunity. With the available data regarding the genes within Ch16p13.13, it is more likely that *CLEC16A* is causal for the association of Ch16p13.13's SNPs with T1D[44,63,66-71]. Importantly, this study is evidence that eQTL data analyses without functional studies are not enough to establish the causality of an associated gene's function with a disease.

Appendix I

Experimental Procedures

Mice

NOD.*Dexi*$^{-/-}$ mice were generated by CRISPR-Cas9 genome editing in nonobese diabetic (NOD/ShiLtJ) mice (Jackson Laboratory) as described below. NOD mice purchased from Jackson Laboratory were bred and maintained in house (Joslin Diabetes Center). PCR genotyping of digested ear clippings was performed using two distinct primer pairs and corresponding PCR protocols to distinguish homozygote and heterozygote mice, with primers A1 amplifying a large region that spans the Dexi coding region, and primers A2 that amplify smaller region near the start the coding region (Table 1). NOD.*Dexi*$^{-/-}$ mouse lines where backcrossed onto the NOD background for ~10 generations to maintain NOD background purity and reduce the selection of any potential off-target mutations. NOD.*Dexi*$^{-/-}$ mice were intercrossed with NOD.*Clec16a*^{KD} mice, which were previously generated in our lab[66], to generate NOD.*Dexi*$^{-/-}$*Clec16a*^{KD} mice. Further propagation of each line was performed by homozygous intercrosses. Doxycycline-inducible NOD.*Cd5*^{KD} mice were previously generated in our lab using lentiviral transgenesis[93] and supplemented with 50mg/mL of doxycycline in drinking water starting at 3 weeks of age. Mice were cared for and maintained as approved by the Institutional Animal Care and Use Committee (IACUC) at the Joslin Diabetes Center (Protocol #2014-01).

Genome editing

To increase the chances of obtaining a complete deletion of *Dexi*'s protein-coding genomic sequence, two sgRNAs with corresponding PAM sequences (Table 1) were designed and selected using a published algorithm by Xu et al.[92]. The first sgRNA:

mDexiKO-g1 contained a sequence homologous to the beginning of *Dexi*'s unique coding exon while a second sgRNA — mDexiKO-g2 — included a homologous sequence present near the end of *Dexi*'s exon 1, flanking the whole exon (Figure 3A). Design of sgRNAs and methodology for generation of transgenic mice was performed as described in Yang et al.[90]; all sequences are listed in Table 1. To generate the selected sgRNAs and prepare them for injections, complementary single-stranded oligonucleotide (ssDNA) sequences for each of the guides were first annealed to each other. This process allowed the generation of two separate double-stranded (dsDNA) nucleotide sequences. Each of these dsDNA sequences were then cloned into the pX330 vector (Addgene) and plasmid incorporation was verified via Sanger-Sequencing. Using PCR amplification and the Megashortscript T7 kit (Life Technologies), both dsDNA were transcribed into RNA. Each of the generated gsRNAs, as well as the Cas9 mRNA (Trilink Technologies) were purified using the Megaclear clean-up kit (Life Technologies) prior to microinjection. Both sgRNAs and Cas9 mRNA were injected into into the pronucleus of NOD zygotes, to generate DSBs at either end of the protein-coding exon. Injected NOD zygotes were then re-implanted into pseudo-pregnant Swiss-Webster mice.

Quantitative PCR analyses

RNA was isolated from whole organs using mechanical disruption, from single cell suspensions of mechanically-disrupted organs or from islets isolated via collagenase P digestion of Pancreas using the NucleoSpin® RNA Plus Kit (Macherey-Nagel) or the RNeasy Micro Kit (Qiagen). RNA from cultured BM-DM was also isolated using the

RNeasy Micro Kit (Qiagen), by adding RLT Buffer Plus + β-Mercaptoethanol directly to the culture dish to collect cell lysates. cDNA was synthesized using the SuperScript™ III First-Strand Synthesis System Kit (Invitrogen) or the AzuraQuant™ cDNA Synthesis Kit (Azura Genomics). Quantitative RT-PCRs were performed using the Power SYBR™ Green PCR Master Mix (Applied Biosystems) or the AzuraQuant™ Green Fast qPCR Mix HiRox (Azura Genomics). Primers used are described in Table 1.

FLAG-DEXI Fusion Protein Expression & Puromycin Treatment

The genomic sequence for the generation of a FLAG-Dexi recombinant fusion protein was purchased as a gBlock (IDT) and ~58ng were ligated with 100ng of pMSCV-puro (Addgene) plasmid (Figure 10) which also provides ampicillin resistance. Cloning was performed by transforming ligation product using heat-shock into NovaBlue Singles™ competent bacteria (Novagen). Ampicillin-resistant clones were selected at random and vector DNA was isolated using the NucleoSpin® Plasmid Kit (Macherey-Nagel). Sequence incorporation for mutant clones was tested prior to DNA isolation via PCR amplification, and by Sanger sequencing following DNA isolation; primers used are described in Table 1. Verified pMSCV-puro-FLAG-DEXI vector DNA was transformed into competent bacteria to produce greater amounts of the plasmid. Plasmid DNA from a higher concentration of bacteria was isolated using the NucleoBond® Xtra Maxi Plus Kit (Macherey-Nagel). NIT-1 or HEK293T cells were transiently transfected with 300ng of pMSCV-puro-FLAG-DEXI plasmid DNA and the FuGENE® 6 Transfection Reagent (Promega) in serum-free media and cultured at 37°C for 48 hours. Cells were then treated with 0.5µg/mL of puromycin and cultured at 37°C for another 48 hours.

Protein Isolation & Immunoprecipitation

Organs were harvested, chopped and mechanically disruptex in 1X Cell Lysis Buffer (Cell Signaling Technology) supplemented with protease inhibitors (cOmplete™, Mini, EDTA-free Protease Inhibitor Cocktail, Roche) and 1mM PMSF (Cell Signaling Technology) to obtain whole protein lysates. Half of the whole protein lysate was used further for immunoprecipitation, and the remaining was used to quantify total protein with the Pierce™ BCA Protein Assay Kit (Thermo Scientific). Whole protein lysates were nutated at 4°C with a 1:50 dilution of DEXI Antibody (NOVUS) overnight and subsequently with Protein A Agarose Beads (Cell Signaling Technology) for 3-4 hours or with ANTI-FLAG® M2 Affinity Gel (Millipore-Sigma) beads for 3 hours.

For CD5 experiments, supplemented cell lysis buffer was added directly into cell culture plate wells and mechanical disruption consisted of mixing by pipetting or with a plate shaker. Cellular fractionation lysates were obtained using the Cell Fractionation Kit (Cell Signaling Technology).

Western Blotting

All samples were mixed with 4X Laemmli buffer (Bio-Rad) supplemented with 2-Mercaptoethanol (Millipore-Sigma) at a 3:1 (sample:buffer) ratio, and subsequently incubated at 65°C for 5 minutes prior to loading onto a 15% SDS-PAGE gel for size separation. A lower temperature was used to avoid denaturing DEXI, due to its small size, but not for CD5 samples which were incubated at 95°C. Proteins were transferred onto a nitrocellulose membrane (Bio-Rad) and detected using rabbit anti-DEXI (NOVUS), rabbit anti-DEXI (abcam), rabbit anti-FLAG (Millipore-Sigma), rabbit anti-

STAT3 (Cell Signaling Technology), rabbit anti-STAT3 (Cell Signaling Technology), rabbit anti-phospho-STAT3-Ser727 (Cell Signaling Technology), rabbit anti-phospho-STAT3-Tyr705 (Cell Signaling Technology), rabbit anti-MEK1/2 (Cell Signaling Technology), rabbit anti-Histone H3 XP® (Cell Signaling Technology) and rabbit β-Actin (Cell Signaling Technology) antibodies followed by HRP-conjugated anti-rabbit antibody (Cell Signaling Technology) and autoradiography. Western blot band intensity was measured in scanned autoradiography blots using the ImageJ/Fiji software.

Lymphocyte Isolation

Spleens, thymi, and mesenteric, inguinal, cervical, axillary, braquial and pancreatic LNs were harvested and mechanically disrupted with two frosted slides and filtered to create single cell suspensions. Blood for genotyping was collected from the tail vein and via cardiac puncture for circulating lymphocyte analysis. This was followed by treatment with ACK Lysing Buffer (Gibco) for red blood cell lysis. Single cell suspensions were counted using a hematocytometer and trypan blue solution (Gibco). Pan T cells or naîve T_h cells were purified by magnetic-activated cell sorting using the mouse Pan T Cell Isolation Kit II (Myltenyi Biotec) or Naive $CD4^+$ T Cell Isolation Kit (Myltenyi Biotec) accordingly. Cells were plated into 24-well plates at ~$5x10^6$/well in complete RPMI which consists of Advanced Roswell Park Memorial Institute (RPMI) 1640 media (Gibco) supplemented with 10% fetal bovine serum (Gibco), 1% penicillin and streptomycin (Gibco), 1% L-glutamine (Gibco), 1M HEPES (Gibco), and 6.05μM 2-Mercaptoethanol (Gibco). Cells were incubated at 37°C for the period indicated.

In vitro T cell stimulation

Purified T cells were stimulated *in vitro* by plating cells into pre-coated wells with 5μg/mL of purified anti-CD3ε (Biolegend) and/or anti-CD5 (Biolegend) antibodies. For CKII inhibition experiments, cells were treated with 80nM of TBB diluted into complete RPMI upon plating.

T_h17/22 differentiation

Purified naîve T_h cells were differentiation *in vitro* by plating cells into pre-coated wells with 2μg/mL of purified anti-CD3ε (Biolegend) antibody and cytokine supplemented complete RPMI. For T_h0-polarization, media was supplemented with 2μg/mL of purified anti-CD28 (Biolegend) antibody. For T_h17-polarization, media was supplemented with 2μg/mL of purified anti-CD28 (Biolegend) antibody, 5μg/mL of purified anti-IFN-γ (Biolegend) and anti-IL-4 (Biolegend) antibodies, 50ng/mL of recombinant IL-6 (Biolegend), 10ng/mL of recombinant IL-1β (Biolegend), and 1ng/mL of recombinant TGF-β1 (Biolegend). For T_h22-polarization, media was supplemented with 2μg/mL of purified anti-CD28 (Biolegend) antibody, 5μg/mL of purified anti-IFN-γ (Biolegend) and anti-IL-4 (Biolegend) antibodies, 50ng/mL of recombinant IL-6 (Biolegend), and 50ng/mL of recombinant IL-23 (Biolegend). Cells were incubated at 37°C for ~48 hours.

Flow Cytometry

Cell surface staining of single cell suspensions was performed in PBS supplemented with 2% fetal bovine serum (Gibco) and 2.5mM EDTA. Cell suspensions were incubated

with CD16/32 Fc-receptor blocking antibody prior to labeling with fluorescence-conjugated antibodies. The Zombie Green™ Fixable Viability Kit (Biolegend) or eBioscience™ Propidium Iodide (ThermoFisher Scientific) were used for dead cell exclusions. Intracellular staining was required for proper staining with FoxP3, this was performed using the eBioscience™ Foxp3/Transcription Factor Staining Buffer Set (ThermoFisher Scientific). Conjugated antibodies were purchased from Biolegend or ThermoFisher Scientific and included the following: CD25-PerCP-Cy5.5, CD8α-APC, CD8α-Pacific Blue, CD4-Brilliant Violet 605, CD3-APC, TCR-β-APC-eFlour 780, CD69-PECy7, FoxP3-PE, CD44-PECy7, CD62L-APC, IgG2A-PE, B220-APC, CD19-Pacific Blue, IgM-PE-Cy7, IgD-PE, CD11c-Brilliant Violet 711, F4/80-Brilliant Violet 421, Gr-1-Brilliant Violet 510, CD11b-PE-Cy7 and I-Ak-PE (which cross-reacts I-Ag7). Flow cytometry measurements were collected using a BD™ LSR II flow cytometer (BD Biosciences) or a MACSQuant® Analyzer (Myltenyi Biotec). Data analysis was performed using the FlowJo software (BD Biosciences).

Diabetes measurements

Spontaneous diabetes onset was assessed weekly by measuring glycosuria using Diastix (Bayer). Female mice were considered diabetic if they had at least two consecutive readings of >250mg/dL within a period of 1-3 weeks of the initial positive, at which point they were euthanized. Similarly, CY-accelerated diabetes onset was assessed thrice-weekly in mice, 10 days after an intraperitoneal injection with 250mg/kg of cyclophosphamide (Millipore-Sigma) by measuring glycosuria. In this case mice were considered diabetic if they had at least two consecutive readings of >250mg/dL within a

period of 1-3 days of initial positive, at which point they were euthanized. Upon three weeks of the initial injection (21 days), mice were supplemented with a second intraperitoneal injection of 250mg/kg of cyclophosphamide. Age-matched, contemporary cohorts of mice were used for both diabetes studies described.

Glucose Tolerance Test

Glucose Tolerance Test was performed as described in Rozman et al.[141] Blood glucose levels of mice fasted overnight were determined using a Contour blood glucose monitor (Bayer). Blood samples were collected from the tail vain 15 minutes before, at the moment of intraperitoneal injection with 2g of glucose/kg of body weight, and 15 minutes, 30 minutes, 60 minutes, 90 minutes, and 120 minutes following glucose injection.

Insulitis

Fresh pancreata was harvested and fixed in 10% paraformaldehyde in PBS overnight at 4°C. Samples were then further processed, sectioned, mounted and stained with Hematoxylin & Eosin by the Dana-Farber/Harvard Cancer Center Rodent Histopathology Core. Insulitis was scored blindly by counting the amount of islets that fell under the following three categories: no infiltration, moderate infiltration (i.e. peri-infiltration, less than half of the islet infiltrated), severe infiltration (i.e. more than half-infiltration, complete infiltration) as shown in representative image. A total of 3 slides per mouse were counted using a light microscope. Representative images were captured with the MicroPublisher 6™ microscope camera (Q Imaging), using the Ocular software (Teledyne Photometrics).

Differentiation of Bone Marrow Derived Macrophages

Femur and tibia were harvested from each mouse and cleaned with sterilized dissection scissors. Bone marrows were flushed with sterile PBS using a syringe and filtered into single cell suspensions. Cell suspensions were then plated in macrophage differentiation media[142] at $1x10^6$ cells per untreated 10cm culture dish and supplemented with 5mL of macrophage differentiation media[142] on day 3 of differentiation as indicated in Evavold et al.[142] On day 7 of differentiation, cells were harvested using cold sterile 2mM EDTA-containing PBS and re-suspended in complete media supplemented with 30% L-929 M-CSF conditioned media[142]. The L-929 M-CSF conditioned media was collected and generously provided by Charlie Evavold from Jonathan Kagan's laboratory.

Poly(I:C) Treatment

Polyinosinic–polycytidylic acid sodium salt [Poly(I:C)] (Millipore-Sigma) was resuspended in ultrapure non-pyrogen containing water (Invitrogen) and used for treatment at a final concentration of 0.5µg. $2.5x10^6$ BM-DMs were plated into 6-well plates and transfected with PolyI:C using FuGENE® 6 Transfection Reagent (Promega) and incubated at 37°C for 24 hours.

Statistical Analyses

Data were analyzed using the Prism software GraphPad. Quantitative PCR data were compared using a two-sided unpaired t-test as indicated in figure legends. Insulitis was compared using Fisher's exact test. Diabetes frequencies were compared by Mantel–

Cox log-rank test. $P<0.05$ was considered statistically significant. Sufficient sample size was estimated without the use of a power calculation. No samples were excluded from the analysis. Randomizations was not used for animal experiments and data analysis was not blinded, with the exception of the histological scoring of insulitis.

Appendix II

Published Manuscript

Genes & Immunity
https://doi.org/10.1038/s41435-019-0083-y

BRIEF COMMUNICATION

The type 1 diabetes candidate gene *Dexi* does not affect disease risk in the nonobese diabetic mouse model

Janice M. Nieves-Bonilla[1,2] · Badr Kiaf[2] · Cornelia Schuster[2] · Stephan Kissler[2]

Received: 5 March 2019 / Revised: 25 July 2019 / Accepted: 2 August 2019

Abstract

Genome-wide association studies have implicated more than 50 genomic regions in type 1 diabetes (T1D). A T1D region at chromosome 16p13.13 includes the candidate genes *CLEC16A* and *DEXI*. Conclusive evidence as to which gene is causal for the disease association of this region is missing. We previously reported that *Clec16a* deficiency modified immune reactivity and protected against autoimmunity in the nonobese diabetic (NOD) mouse model for T1D. However, the diabetes-associated SNPs at 16p13.13 were described to also impact on *DEXI* expression and others have argued that *DEXI* is the causal gene in this disease locus. To help resolve whether *DEXI* affects disease, we generated *Dexi* knockout (KO) NOD mice. We found that *Dexi* deficiency had no effect on the frequency of diabetes. To test for possible interactions between *Dexi* and *Clec16a*, we intercrossed *Dexi* KO and *Clec16a* knockdown (KD) NOD mice. *Dexi* KO did not modify the disease protection afforded by *Clec16a* KD. We conclude that *Dexi* plays no role in autoimmune diabetes in the NOD model. Our data provide strongly suggestive evidence that *CLEC16A*, not *DEXI*, is causal for the T1D association of variants in the 16p13.13 region.

Introduction

The risk of type 1 diabetes (T1D) is modulated by more than 50 genomic regions [1]. Most of these regions include several genes and exactly how disease-associated genetic variants affect islet autoimmunity is largely unresolved. The region at chromosome 16p13.13 contains many T1D-associated single-nucleotide polymorphisms (SNPs), the most significant of which are located in introns 8, 10, and 19-22 of *CLEC16A* [2]. Owing to the location of these SNPs, *CLEC16A* had initially been suggested as the causal gene for the disease association of 16p13.13 [3, 4]. Gene expression analyses subsequently provided evidence that disease SNPs affect *CLEC16A* expression [5, 6]. Notably, a significant effect was attributed to rs12708716 that is associated with both T1D and multiple sclerosis, and this SNP was described to modify *CLEC16A* expression in human thymus [5]. We previously reported that *Clec16a* deficiency in thymic epithelial cells modified T-cell selection, impacted immune function, and was protective against autoimmune diabetes [7]. Despite functional data that support *CLEC16A* as the causal gene for the association of the 16p13.13 locus, it was argued that *DEXI* is instead a more likely candidate, because disease-associated SNPs also modify *DEXI* expression [2, 8, 9]. A recent publication suggested that *DEXI* participates in the type I interferon pathway and modulates β-cell inflammation [10]. However, whether this gene has any role in autoimmunity remains unresolved. In our earlier report, we described that *Clec16a* knockdown (KD) was strongly protective against diabetes in the nonobese diabetic (NOD) mouse model for T1D [7]. In the present study, we tested whether *Dexi* deficiency alone or in combination with *Clec16a* KD would modify disease risk in NOD mice. To this end, we generated *Dexi* knockout (KO) NOD mice by CRISPR-Cas9 genome editing. We found that *Dexi* KO had no effect on the frequency of diabetes in this model, and that it also did not affect the strong protective effect of *Clec16a* KD. Our data provides strongly suggestive functional evidence that *CLEC16A* and not *DEXI* is causal for the association of the 16p13.13 region.

✉ Stephan Kissler
stephan.kissler@joslin.harvard.edu

[1] Graduate Program in Biological and Biomedical Sciences, Division of Medical Sciences, Harvard Medical School, Boston, MA, USA

[2] Section for Immunobiology, Joslin Diabetes Center, Harvard Medical School, Boston, MA, USA

Published online: 22 August 2019

Materials and methods

Mice

NOD *Dexi* KO mice were generated by CRISPR-Cas9 genome editing in NOD (NOD/ShiLtJ) mice (Jackson Laboratory). PCR genotyping was performed using two distinct primer pairs to distinguish homozygote and heterozygote mice, with primers A1 amplifying a large region that spans the *Dexi* coding region and primers A2 that amplify smaller region near the start the coding region (Table 1). Mice were cared for and maintained as approved by the Joslin Institutional Animal Care and Use Committee (IACUC) (Protocol #2014-01).

Genome editing

Two guide RNAs (gRNAs; Table 1) were selected to flank exon 1 *Dexi*, using a published algorithm (http://crispr.dfci.harvard.edu/SSC/) [11], and were synthesized as described in ref. [12] using the pX330 vector (Addgene). gRNAs were generated with the Megashortscript T7 kit (Life Technologies) and purified using the Megaclear clean-up kit (Life Technologies) prior to microinjection into the pronucleus of NOD zygotes together with Cas9 mRNA (Trilink Technologies).

Quantitative PCR analyses

RNA was isolated using the NucleoSpin® RNA Plus Kit (Macherey-Nagel). cDNA was synthesized using the SuperScript™ III First-Strand Synthesis System Kit (Invitrogen) or the AzuraQuant™ cDNA Synthesis Kit (Azura Genomics). Quantitative reverse-transcription PCRs were performed using the Power SYBR™ Green PCR Master Mix (Applied Biosystems) or the AzuraQuant™ Green Fast qPCR Mix HiRox (Azura Genomics). Primers used are described in Table 1.

Protein isolation and immunoprecipitation

Organs were prepared using TissueLyserII (Qiagen) in 1X Cell Lysis Buffer (Cell Signaling Technology) supplemented with protease inhibitors (cOmplete™, Mini, EDTA-free Protease Inhibitor Cocktail, Roche) and 1 mM phenylmethylsulfonyl fluoride (Cell Signaling Technology). Protein content was quantified using a Pierce™ BCA Protein Assay Kit (Thermo Scientific). Protein lysates were incubated with DEXI Antibody (NOVUS) overnight then with Protein A Agarose Beads (Cell Signaling Technology) for 3–4 h.

Western blotting

Samples mixed with 4× Laemmli buffer (Bio-Rad) supplemented with 2-Mercaptoethanol (Sigma-Aldrich) at a 3:1 (sample:buffer) ratio were incubated at 65 °C for 5 min before loading onto a 15% SDS-PAGE gel, followed by a transfer onto a nitrocellulose membrane (Bio-Rad). Protein were detected using Rabbit DEXI (NOVUS) and rabbit β-Actin (Cell Signaling Technology) antibodies followed by horseradish peroxidase-conjugated anti-rabbit antibody (Cell Signaling Technology).

Glucose tolerance test

Blood glucose concentration of mice fasted overnight was determined using a Contour blood glucose monitor (Bayer) before and after intraperitoneal injection of glucose (2 g/kg body weight).

Insulitis

Pancreata were fixed in 10% paraformaldehyde in phosphate-buffered saline (PBS) overnight at 4 °C, processed, sectioned, mounted, and stained with hematoxylin and eosin. Insulitis was scored blindly as having no, moderate, or severe infiltration as shown in representative images.

Differentiation of bone marrow-derived macrophages

Bone marrow from the femur and tibia was differentiated in high glucose (4 g/L) Dulbecco's modified Eagle medium (DMEM) containing sodium pyruvate and L-glutamine, supplemented with 10% fetal bovine serum, 1% penicillin and streptomycin, 1% L-glutamine, and 1% sodium pyruvate with 30% L-929 M-CSF conditioned media (kind gift from Charles Evavold, Harvard Medical School) for 7 days, then collected using cold 2 mM EDTA-containing PBS and resuspended in DMEM supplemented with 5% L-929 M-CSF conditioned media.

Poly I:C treatment

Polyinosinic–polycytidylic acid sodium salt (Poly I:C) (Millipore Sigma) was resuspended in ultrapure non-pyrogen containing water and used for treatment at a final concentration of 0.5 µg. Bone marrow- derived macrophages (BM-DMs; 2.5×10^6/well) were transfected with Poly I:C using FuGENE® 6 Transfection Reagent (Promega). Gene expression was measure after 24 h.

Table 1 gRNA, PCR, and qPCR primer sequences

Name	Sequence
mDexiKO-g1-Forward	5′-CACCGATGGGCAGTGAGCCTGCGG-3′
mDexiKO-g1-Reverse	5′-AAACCCGCAGGCTCACTGCCCATC-3′
mDexiKO-g2-Forward	5′-CACCGGGATGGGACCCCAGGAAG-3′
mDexiKO-g2-Reverse	5′-AAACCTTCCTGGGGTCCCATCCC-3′
T7_mDexiKO_g1-Forward (in vitro transcription)	5′-TTAATACGACTCACTATAGGATGGGCAGTGAGCCTGCGG-3′
T7_mDexiKO_g2-Forward (in vitro transcription)	5′-TTAATACGACTCACTATAGGGGGATGGGACCCCAGGAAG-3′
T7_mDexiKO-Reverse (in vitro transcription)	5′-AAAAGCACCGACTCGGTGCC-3′
mDexiKO_genoA1-Forward	5′-ACAAAGGTGGTCTGTAAACCG-3′
mDexiKO_genoA1-Reverse	5′-TGGCAATGTTGGCAATCAGG-3′
mDexiKO_genoA2-Forward	5′-CTTTTCCACCCGGCATCATT-3′
mDexiKO_genoA2-Reverse	5′-TTGACACCCCGAGATGCT-3
mActb-Forward	5′-GGCTGTATTCCCCTCCATCG-3′
mActb-Reverse	5′-CCAGTTGGTAACAATGCCATGT-3′
mDexi-Forward	5′-CTGCTGCCCTCTATGTTCTACG-3′
mDexi-Reverse	5′-GCCAGGGTCTGAAAGTACGC-3′
mClec16a-Forward	5′-CCTGATTTGGGGCGATCAAAA-3′
mClec16a-Reverse	5′-CATAACGGCCTGATTTCTGCC-3′
mSOCS1-Forward	5′-CTGCGGCTTCTATTGGGGAC-3′
mSOCS1-Reverse	5′-AAAAGGCAGTCGAAGGTCTCG-3′
mCIITA-Forward	5′-TGCGTGTGATGGATGTCCAG-3′
mCIITA-Reverse	5′-CCAAAGGGGATAGTGGGTGTC-3′

Diabetes measurements

Glycosuria was measured using Diastix (Bayer). Mice were considered diabetic with two consecutive readings of >250 mg/dL. Mice were checked weekly and thrice weekly for spontaneous and cyclophosphamide (CY)-accelerated (250 mg/kg at day 0 and 21, Sigma-Aldrich) diabetes, respectively.

Statistics

Data were analyzed using the Prism software (GraphPad). Quantitative PCR (qPCR) data were compared using a two-sided unpaired *t*-test. Insulitis was compared using Fisher's exact test. Diabetes frequencies were compared by Mantel–Cox log-rank test. Age of onset was compared by Mann–Whitney test. All data were obtained from age- and sex-matched contemporary mice. $P < 0.05$ was considered statistically significant. Sufficient sample size was estimated without the use of a power calculation. No samples were excluded from the analysis. No randomization was used for animal experiments. Data analysis was not blinded, except for histological scoring of insulitis.

Results and discussion

To investigate the role of *Dexi* in autoimmune diabetes, we deleted this gene in the NOD mouse model for T1D using CRISPR-Cas9 genome editing. We microinjected gRNAs and Cas9 mRNA into NOD zygotes, to generate double-stranded DNA breaks at either end of exon 1 that encompasses the entire protein-coding sequence (Fig. 1a). Among the seven pups born following microinjection, we identified one mutant mouse. Unexpectedly, this founder carried two separate mutant alleles in addition to the wild-type (WT) sequence at the targeted region of *Dexi*. Upon breeding, the mutant alleles each segregated into ~25% of the progeny, with the remaining pups carrying only WT alleles (Fig. 1b). These data indicate that the original founder was chimeric, with the gene-editing event occurring at the two-cell stage, giving rise to two mutant alleles that we termed Allele #1 and #2. DNA sequencing established that Allele #1 comprised a near-complete deletion of the exon 1 (Fig. 1a). In contrast, the deletion in Allele #2 was very short and preceded the start codon (not shown), likely resulting from a single, double-stranded DNA break caused by the gRNA 5′ of the coding region. We proceeded to verify that Allele #1 caused the loss of *Dexi* expression. After intercrossing

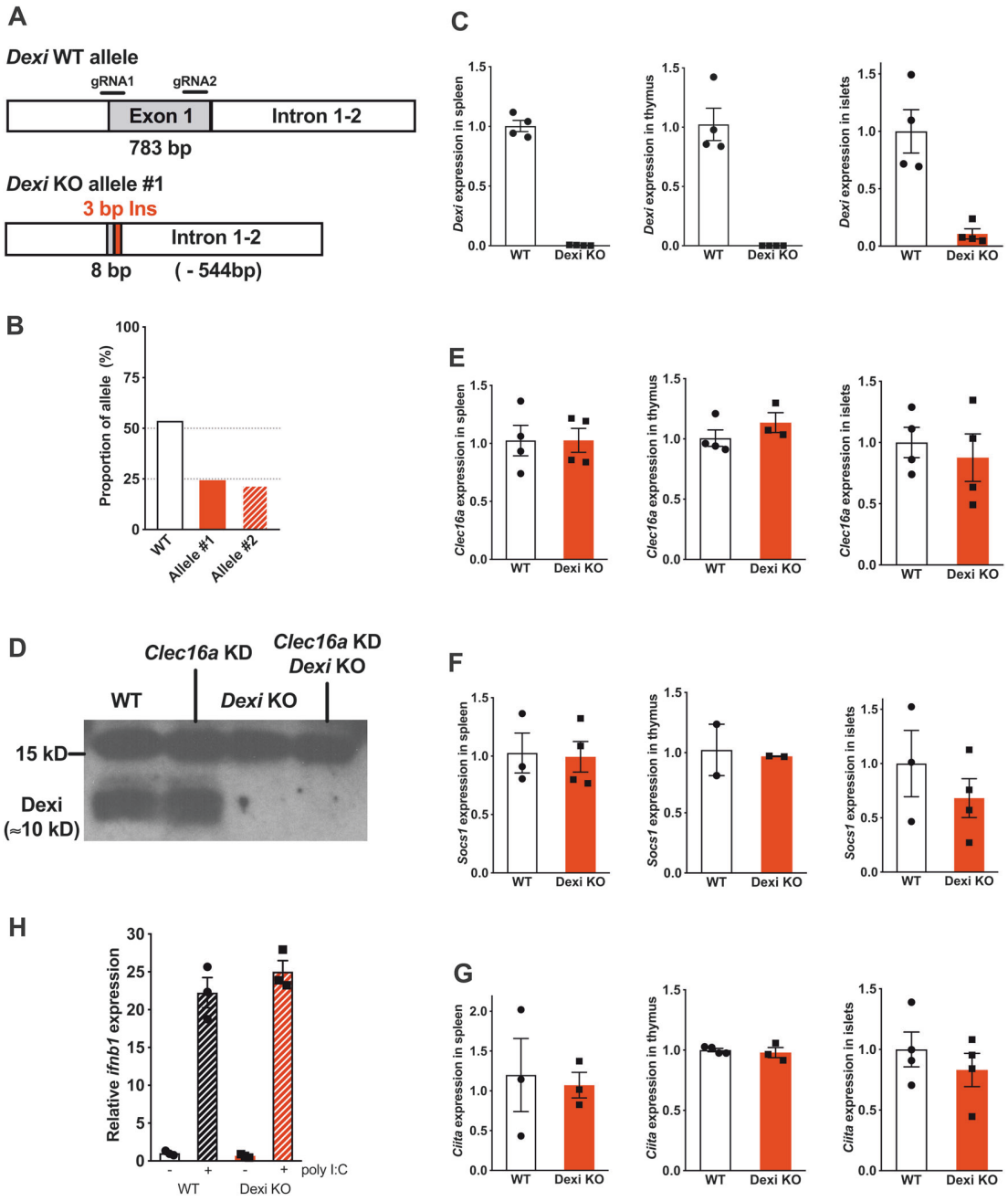

Fig. 1 Generation of *Dexi* KO NOD mice. **a** Schematic representation of the region targeted by CRISPR-Cas9 genome editing in the *Dexi* genomic (top) region and of the mutant allele #1 (bottom). Only the first 8 bp of exon 1 remain, followed by a 3 bp insertion and a 544 bp deletion at the start of intron 1–2. **b** Inheritance pattern of the two mutant *Dexi* alleles (#1 and #2) present in the founder male NOD mouse. The proportion of wild-type and mutant alleles inherited from the founder in the F1 progeny (total 41 mice, of which 10 carried allele #1 and 9 carried allele #2) is shown. **c** Quantification of *Dexi* mRNA in the spleen, thymus, and pancreatic islets of WT and *Dexi* KO mice by quantitative PCR. $n = 4$ mice per group, data show individual values and mean ± SEM and are representative of at least three similar experiments. $^{***}P < 0.001$ (two-tailed *t*-test). **d** Detection of Dexi protein by western blotting following immune-precipitation with anti-Dexi antibody. Data are shown for WT, Clec16a KD, Dexi KO, and Clec16a KD/Dexi KO mice, and are representative for two similar experiments. **e**–**g** Quantification of *Clec16a* (**e**), *Socs1* (**f**), and *Ciita* (**g**) mRNA by quantitative PCR in the spleen, thymus, and pancreatic islets. $n = 2$-4 mice per group. Data show individual values, mean ± SEM and are representative of at least two similar experiments. **h** Interferon-β expression in bone marrow-derived macrophages from WT and *Dexi* KO mice stimulated with poly I:C. Data show individual values, mean ± SEM and are representative of two similar experiments

Allele #1 mutant mice, we measured *Dexi* levels in homozygous mutants by qPCR (Fig. 1c) and western blotting (Fig. 1d). The results of these analyses confirmed that *Dexi* mRNA and protein were absent in *Dexi* KO mice.

DEXI is a candidate gene for a region that includes three additional candidates, *CIITA*, *CLEC16A*, and *SOCS1*[2]. As this chromosomal region is conserved between mouse and human, all three genes are also in close proximity to *Dexi* in the mouse genome. We established that *Dexi* deletion had no effect on *Ciita*, *Clec16a*, or *Socs1* expression (Fig. 1e–g). Of interest, it was reported that *Dexi* modulates type-I interferon expression in response to poly I:C, a synthetic viral double-stranded RNA [10]. Unexpectedly, *Dexi* deletion had no effect on this pathway in our model. We found that *Dexi* KO and WT cells had comparably robust interferon responses to poly I:C stimulation (Fig. 1h).

Having established that *Dexi* KO mice had the expected loss of *Dexi* expression without affecting the expression of nearby genes, we tested the frequency of autoimmune diabetes in both male and female mice. We reported previously that *Clec16a* KD was protective in the NOD model [7]. In addition to exploring a role for *Dexi* in diabetes susceptibility, we tested for a possible interaction between *Clec16a* and *Dexi* by intercrossing *Dexi* KO mice with *Clec16a* KD animals, to generate a cohort of double-deficient NOD mice. The *Clec16a* KD is mediated by a lentiviral transgene that is not located within proximity of the *Dexi/Clec16a* region and can be combined with the *Dexi* mutant allele by breeding.

We first tested the diabetes susceptibility of male cohorts using the CY-accelerated model. As reported earlier, *Clec16a* KD protected NOD mice against CY-induced diabetes (Fig. 2a). In contrast, *Dexi* KO did not affect the frequency of diabetes on its own and also had no independent effect when combined with *Clec16a* KD. *Dexi* KO also did not change the day of disease onset (median: day 29 for both WT and *Dexi* KO groups, $P = 0.42$, Mann–Whitney test).

We proceeded to measure the frequency of spontaneous diabetes in female cohorts. Again, *Dexi* KO neither

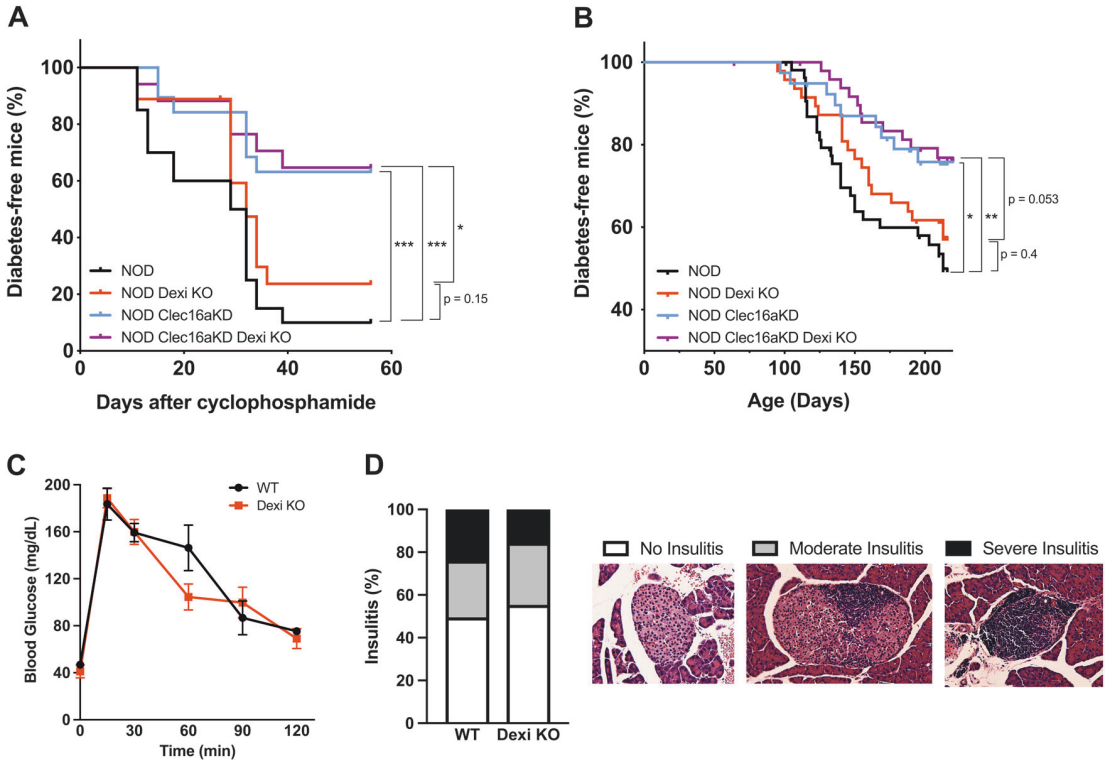

Fig. 2 *Dexi* KO does not modify the frequency of diabetes in NOD mice. **a** Cyclophosphamide-accelerated diabetes was measured in groups of WT ($n = 20$), *Dexi* KO ($n = 18$), *Clec16a* KD ($n = 19$), and *Clec16a* KD/*Dexi* KO ($n = 17$) male NOD mice injected with cyclophosphamide at age 9–10 weeks. **b** Spontaneous diabetes was measured in groups of WT ($n = 54$), *Dexi* KO ($n = 47$), *Clec16a* KD ($n = 39$), and *Clec16a* KD/*Dexi* KO ($n = 50$) female NOD mice. Differences between groups were measured using the Log-rank test. *$P < 0.05$, **$P < 0.01$, ***$P < 0.001$. **c** WT and Dexi KO mice (9 weeks old) were injected with glucose intraperitoneally to test their glucose tolerance. Data show mean ± SEM values from six mice per group. **d** Histological analysis was performed on 10-week-old WT and *Dexi* KO mice to quantify the degree of insulitis. Data show the proportion of WT islets ($n = 402$) and *Dexi* KO islets ($n = 354$) with no infiltration, moderate or severe insulitis from three mice per group. Fisher's exact test $P = 0.1$ comparing the proportion of infiltrated islets in WT and *Dexi* KO mice

increased nor decreased disease risk either alone or in combination with *Clec16a* KD (Fig. 2b). Again, *Dexi* KO had no significant effect on the age at diabetes onset (WT vs. *Dexi* KO: $P = 0.4$, Mann–Whitney test). Of note, *Dexi* deficiency also had no effect on glucose tolerance in pre-diabetic mice (Fig. 2c) and did not affect the severity of islet infiltration that precedes disease onset (Fig. 2d). Collectively, our data indicate that *Dexi* plays no significant role in autoimmune diabetes in the NOD model.

The ongoing debate over which gene is causal for the T1D association of the 16p13.13 region stems from the ambiguous effect of disease-associated SNPs on gene expression [2, 5, 6, 8, 9] and limited functional data for *DEXI* [10]. Of note, our experiments with *Dexi* KO cells did not replicate the previously reported effects of *Dexi* inhibition on the type I interferon signaling pathway [10]. The difference between our results and those of Dos Santos et al. [10] may stem from our use of a different cell type (macrophages vs. β-cells) or species (mouse vs. rat and human) in these experiments, even though the interferon response is known to be conserved [13].

Here we provide data implicating *Clec16a* but not *Dexi* in autoimmune diabetes. Both genes are conserved between species and it is reasonable to assume that the function of *Dexi*, similar to that of *Clec16a* [7, 14], is similar in mouse and human. Therefore, the finding that *Dexi* KO had no effect on the risk of diabetes in NOD mice is strongly suggestive that this gene plays no role in human T1D. Of note, unpublished data by Davison et al. [15] suggest that *Dexi* mutation increased disease in female NOD mice, although surprisingly not in males. However, the mutant strains used in this study carry incompletely characterized mutations that were not conclusively shown to eliminate *Dexi* expression [15], unlike our model in which the coding sequence for *Dexi* is completely deleted, leading to the absence of both *Dexi* mRNA and protein. Even though disease-associated SNPs may well modify the expression of *Dexi* in some tissues [8], this does not imply that *Dexi* function impacts autoimmunity. Genetic association data, even when combined with expression quantitative trait loci (eQTL) analyses are insufficient to establish causality. Instead, functional studies are needed to provide convincing support for a gene's effect on disease. Data from our experimental model that combines both *Clec16a* and *Dexi* deficiency strongly suggest that *CLEC16A*, not *DEXI*, is causal for the effects of 16p13.13 in T1D.

Acknowledgements We thank John Stockton for embryo microinjections, and also thank Charles Evavold for advice on BM-DM experiments and providing conditioned media. JMNB was supported by a predoctoral training fellowship from NIDDK (T32DK007260). This research was funded in part by a grant from NIDDK (R56DK109954-01) to SK and supported by core facilities funded by the NIDDK Diabetes Research Center award P30DK036836 to the Joslin Diabetes Center.

Author contributions JMNB performed experiments, analyzed data, and wrote the manuscript. BK performed experiments. CS helped with experimental design and data interpretation. SK supervised the study, analyzed data, and wrote the manuscript. SK is the guarantor of this work and, as such, had full access to all the data in the study and takes responsibility for the integrity of the data and the accuracy of the data analysis.

Compliance with ethical standards

Conflict of interest The authors declare that they have no conflict of interest.

References

1. Onengut-Gumuscu S, Chen WM, Burren O, Cooper NJ, Quinlan AR, Mychaleckyj JC, et al. Fine mapping of type 1 diabetes susceptibility loci and evidence for colocalization of causal variants with lymphoid gene enhancers. Nat Genet. 2015;47:381–6.
2. Tomlinson MJ 4th, Pitsillides A, Pickin R, Mika M, Keene KL, Hou X, et al. Fine mapping and functional studies of risk variants for type 1 diabetes at chromosome 16p13.13. Diabetes. 2014;63:4360–8.
3. WellCome Trust Case Control Consortium Genome-wide association study of 14,000 cases of seven common diseases and 3,000 shared controls. Nature. 2007;447:661–78.
4. Hakonarson H, Grant SF, Bradfield JP, Marchand L, Kim CE, Glessner JT, et al. A genome-wide association study identifies KIAA0350 as a type 1 diabetes gene. Nature. 2007;448:591–4.
5. Mero IL, Ban M, Lorentzen ÅR, Smestad C, Celius EG, Sæther H, et al. Exploring the CLEC16A gene reveals a MS-associated variant with correlation to the relative expression of CLEC16A isoforms in thymus. Genes Immun. 2011;12:191–8.
6. Leikfoss IS, Keshari PK, Gustavsen MW, Bjolgerud A, Brorson IS, Celius EG, et al. Multiple sclerosis risk allele in CLEC16A acts as an expression quantitative trait locus for CLEC16A and SOCS1 in CD4+ T cells. PLoS ONE. 2015;10:e0132957.
7. Schuster C, Gerold KD, Schober K, Probst L, Boerner K, Kim MJ, et al. The autoimmunity-associated gene CLEC16A modulates thymic epithelial cell autophagy and alters T cell selection. Immunity. 2015;42:942–52.
8. Davison LJ, Wallace C, Cooper JD, Cope NF, Wilson NK, Smyth DJ, et al. Long-range DNA looping and gene expression analyses identify DEXI as an autoimmune disease candidate gene. Hum Mol Genet. 2012;21:322–33.
9. Leikfoss IS, Mero IL, Dahle MK, Lie BA, Harbo HF, Spurkland A, et al. Multiple sclerosis-associated single-nucleotide polymorphisms in CLEC16A correlate with reduced SOCS1 and DEXI expression in the thymus. Genes Immun. 2013;14:62–66.
10. Dos Santos RS, Marroqui L, Velayos T, Olazagoitia-Garmendia A, Jauregi-Miguel A, Castellanos-Rubio A, et al. DEXI, a candidate gene for type 1 diabetes, modulates rat and human pancreatic beta cell inflammation via regulation of the type I IFN/STAT signalling pathway. Diabetologia. 2019;62:459–72.
11. Xu H, Xiao T, Chen CH, Li W, Meyer CA, Wu Q, et al. Sequence determinants of improved CRISPR sgRNA design. Genome Res. 2015;25:1147–57.

12. Yang H, Wang H, Jaenisch R. Generating genetically modified mice using CRISPR/Cas-mediated genome engineering. Nat Protoc. 2014;9:1956–68.
13. Langevin C, Aleksejeva E, Passoni G, Palha N, Levraud JP, Boudinot P. The antiviral innate immune response in fish: evolution and conservation of the IFN system. J Mol Biol. 2013;425:4904–20.
14. Soleimanpour SA, Gupta A, Bakay M, Ferrari AM, Groff DN, Fadista J, et al. The diabetes susceptibility gene Clec16a regulates mitophagy. Cell. 2014;157:1577–90.
15. Davison LJ, Wallace MD, Preece C, Hughes K, Todd JA, Davies B, et al. Dexi disruption depletes gut microbial metabolites and accelerates autoimmune diabetes. bioRxiv 393421; https://doi.org/10.1101/393421.

References

1. Burgueño-Bucio E, Mier-Aguilar CA, Soldevila G. The multiple faces of CD5. Journal of Leukocyte Biology 2019;105:891-904.

2. Schuster C, Jonas F, Zhao F, Kissler S. Peripherally induced regulatory T cells contribute to the control of autoimmune diabetes in the NOD mouse model. European Journal of Immunology 2018;48:1211-6.

3. Davison LJ, Wallace C, Cooper JD, et al. Long-range DNA looping and gene expression analyses identify DEXI as an autoimmune disease candidate gene. Human Molecular Genetics 2011;21:322-33.

4. Amatya N, Garg AV, Gaffen SL. IL-17 Signaling: The Yin and the Yang. Trends in Immunology 2017;38:310-22.

5. Erben U, Loddenkemper C, Doerfel K, et al. A guide to histomorphological evaluation of intestinal inflammation in mouse models. Int J Clin Exp Pathol 2014;7:4557-76.

6. Sestero CM, McGuire DJ, De Sarno P, et al. CD5-Dependent CK2 Activation Pathway Regulates Threshold for T Cell Anergy. The Journal of Immunology 2012;189:2918-30.

7. McGuire DJ, Rowse AL, Li H, et al. CD5 enhances Th17-cell differentiation by regulating IFN-γ response and RORγt localization. European Journal of Immunology 2014;44:1137-42.

8. Zhang C, Xin H, Zhang W, et al. CD5 Binds to Interleukin-6 and Induces a Feed-Forward Loop with the Transcription Factor STAT3 in B Cells to Promote Cancer. Immunity 2016;44:913-23.

9. Davison L, Wallace M, Preece C, et al. Dexi disruption depletes gut microbial metabolites and accelerates autoimmune diabetes. bioRxiv 2018.

10. Maahs DM, West NA, Lawrence JM, Mayer-Davis EJ. Epidemiology of Type 1 Diabetes. Endocrinology and Metabolism Clinics of North America 2010;39:481-97.

11. Wang Z, Xie Z, Lu Q, Chang C, Zhou Z. Beyond Genetics: What Causes Type 1 Diabetes. Clinical Reviews in Allergy & Immunology 2017;52:273-86.

12. Martinov T, Fife BT. Type 1 diabetes pathogenesis and the role of inhibitory receptors in islet tolerance. Annals of the New York Academy of Sciences 2020;1461:73-103.

13. Hisanaga-Oishi Y, Nishiwaki-Ueda Y, Nojima K, Ueda H. Analysis of the expression of candidate genes for type 1 diabetes susceptibility in T cells. Endocr J 2014;61:577-88.

14. Onengut-Gumuscu S, Chen W-M, Burren O, et al. Fine mapping of type 1 diabetes susceptibility loci and evidence for colocalization of causal variants with lymphoid gene enhancers. Nature Genetics 2015;47:381-6.

15. Todd JA, Walker NM, Cooper JD, et al. Robust associations of four new chromosome regions from genome-wide analyses of type 1 diabetes. Nature Genetics 2007;39:857-64.

16. Martínez A, Perdigones N, Cénit MC, et al. Chromosomal region 16p13: further evidence of increased predisposition to immune diseases. Annals of the Rheumatic Diseases 2010;69:309-11.

17. Hakonarson H, Grant SFA, Bradfield JP, et al. A genome-wide association study identifies KIAA0350 as a type 1 diabetes gene. Nature 2007;448:591-4.

18. Gingerich MA, Sidarala V, Soleimanpour SA. Clarifying the function of genes at the chromosome 16p13 locus in type 1 diabetes: CLEC16A and DEXI. Genes and Immunity 2019;360:1-4.

19. Singer D, Devaiah B. CIITA and Its Dual Roles in MHC Gene Transcription. Frontiers in Immunology 2013;4.

20. Zuvich RL, Bush WS, McCauley JL, et al. Interrogating the complex role of chromosome 16p13.13 in multiple sclerosis susceptibility: independent genetic signals in the CIITA–CLEC16A–SOCS1 gene complex. Human Molecular Genetics 2011;20:3517-24.

21. Gyllenberg A, Asad S, Piehl F, et al. Age-dependent variation of genotypes in MHC II transactivator gene (CIITA) in controls and association to type 1 diabetes. Genes and Immunity 2012;13:632-40.

22. Hong M, Ye BD, Yang S-K, et al. Immunochip Meta-Analysis of Inflammatory Bowel Disease Identifies Three Novel Loci and Four Novel Associations in Previously Reported Loci. Journal of Crohn's and Colitis 2018;12:730-41.

23. Skinningsrud B, Husebye ES, Pearce SH, et al. Polymorphisms in CLEC16A and CIITA at 16p13 Are Associated with Primary Adrenal Insufficiency. The Journal of Clinical Endocrinology & Metabolism 2008;93:3310-7.

24. Liu H, Irwanto A, Fu Xaa, et al. Discovery of six new susceptibility loci and analysis of pleiotropic effects in leprosy. Nature Genetics 2015;47:1-8.

25. Dubois PCA, Trynka G, Franke L, et al. Multiple common variants for celiac disease influencing immune gene expression. Nature Genetics 2010;42:1-10.

26. Ryan RJH, Drier Y, Whitton H, et al. Detection of Enhancer-Associated Rearrangements Reveals Mechanisms of Oncogene Dysregulation in B-cell Lymphoma. Cancer Discovery 2015;5:1058-71.

27. Cui Q, Feng Q-S, Mo H-Y, et al. An extended genome-wide association study identifies novel susceptibility loci for nasopharyngeal carcinoma. Human Molecular Genetics 2016;25:3626-34.

28. Carey BS, Poulton KV, Poles A. Factors affecting HLA expression: A review. International Journal of Immunogenetics 2019;46:307-20.

29. Sharma J, Larkin J. Therapeutic Implication of SOCS1 Modulation in the Treatment of Autoimmunity and Cancer. Frontiers in Pharmacology 2019;10.

30. Yoshimura A, Ito M, Chikuma S, Akanuma T, Nakatsukasa H. Negative Regulation of Cytokine Signaling in Immunity. Cold Spring Harbor Perspectives in Biology 2018;10:a028571-16.

31. Wang H, Wang J, Xia Y. Defective Suppressor of Cytokine Signaling 1 Signaling Contributes to the Pathogenesis of Systemic Lupus Erythematosus. Frontiers in Immunology 2017;8:215-13.

32. Butterbach K, Beckmann L, de Sanjosé S, et al. Association of JAK-STAT pathway related genes with lymphoma risk: results of a European case-control study (EpiLymph). British Journal of Haematology 2011;153:318-33.

33. Ellinghaus D, Ellinghaus E, Nair Rajan P, et al. Combined Analysis of Genome-wide Association Studies for Crohn Disease and Psoriasis Identifies Seven Shared Susceptibility Loci. The American Journal of Human Genetics 2012;90:636-47.

34. Leikfoss IS, Keshari PK, Gustavsen MW, et al. Multiple Sclerosis Risk Allele in CLEC16A Acts as an Expression Quantitative Trait Locus for CLEC16A and SOCS1 in CD4+ T Cells. PLOS ONE 2015;10:e0132957-12.

35. Disanto G, Kjetil Sandve G, Ricigliano VAG, et al. DNase hypersensitive sites and association with multiple sclerosis. Human Molecular Genetics 2013;23:942-8.

36. Lopez de Lapuente A, Pinto-Medel MJ, Astobiza I, et al. Cell-specific effects in different immune subsets associated with SOCS1genotypes in multiple sclerosis. Multiple Sclerosis Journal 2015;21:1498-512.

37. Dong M, Li J, Tang R, et al. Multiple Genetic Variants Associated with Primary Biliary Cirrhosis in a Han Chinese Population. Clinical Reviews in Allergy & Immunology 2015;48:316-21.

38. Hirschfield GM, Xie G, Lu E, et al. Association of primary biliary cirrhosis with variants in the CLEC16A, SOCS1, SPIB and SIAE immunomodulatory genes. Genes and Immunity 2019:1-8.

39. Mostecki J, Cassel SL, Klimecki WT, et al. A SOCS-1 promoter variant is associated with total serum IgE levels. Journal of immunology (Baltimore, Md : 1950) 2011;187:2794-802.

40. Zhao M, Wang J, Liao W, et al. Increased 5-hydroxymethylcytosine in CD4+ T cells in systemic lupus erythematosus. Journal of Autoimmunity 2016;69:64-73.

41. Tomlinson MJ, Pitsillides A, Pickin R, et al. Fine Mapping and Functional Studies of Risk Variants for Type 1 Diabetes at Chromosome 16p13.13. Diabetes 2014;63:4360-8.

42. Burton PR, Clayton DG, Duncanson A, et al. Genome-wide association study of 14,000 cases of seven common diseases and 3,000 shared controls. Nature 2007;447:661-78.

43. Mero I-L, Ban M, Lorentzen ÅR, et al. Exploring the CLEC16A gene reveals a MS-associated variant with correlation to the relative expression of CLEC16A isoforms in thymus. Genes and Immunity 2011;12:191-8.

44. Soleimanpour SA, Gupta A, Bakay M, et al. The Diabetes Susceptibility Gene Clec16a Regulates Mitophagy. Cell 2014;157:1577-90.

45. Barrett JC, Clayton DG, Concannon P, et al. Genome-wide association study and meta-analysis find that over 40 loci affect risk of type 1 diabetes. Nature Genetics 2009;41:703-7.

46. Wu X, Zhu X, Wang X, et al. Intron polymorphism in the KIAA0350gene is reproducibly associated with susceptibility to type 1 diabetes (T1D) in the Han Chinese population. Clinical Endocrinology 2009;71:46-9.

47. Gomez-Lopera N, Alfaro JM, Leal SM, Pineda-Trujillo N. Type 1 diabetes loci display a variety of native American and African ancestries in diseased individuals from Northwest Colombia. World Journal of Diabetes 2019;10:534-45.

48. Onuma H, Kawamura R, Tabara Y, et al. Variants in the BACH2and CLEC16Agene might be associated with susceptibility to insulin−triggered type 1 diabetes. Journal of Diabetes Investigation 2019;10:1447-53.

49. Reddy MVPL, Wang H, Liu S, et al. Association between type 1 diabetes and GWAS SNPs in the southeast US Caucasian population. Genes & Immunity 2011;12:208-12.

50. Howson JMM, Rosinger S, Smyth DJ, Boehm BO, , Todd JA. Genetic Analysis of Adult-Onset Autoimmune Diabetes. Diabetes 2011;60:2645-53.

51. Elboudwarej E, Cole M, Briggs FBS, et al. Hypomethylation within gene promoter regions and type 1 diabetes in discordant monozygotic twins. Journal of Autoimmunity 2016;68:23-9.

52. Bakay M, Pandey R, Grant SFA, Hakonarson H. The Genetic Contribution to Type 1 Diabetes. Current Diabetes Reports 2019;19:55-14.

53. Cooper JD, Smyth DJ, Smiles AM, et al. Meta-analysis of genome-wide association study data identifies additional type 1 diabetes risk loci. Nature Genetics 2008;40:1399-401.

54. Leikfoss IS, Mero I-L, Dahle MK, et al. Multiple sclerosis-associated single-nucleotide polymorphisms in CLEC16A correlate with reduced SOCS1 and DEXI expression in the thymus. Genes and Immunity 2012;14:62-6.

55. Rubio JP, Stankovich J, Field J, et al. Replication of KIAA0350, IL2RA, RPL5 and CD58 as multiple sclerosis susceptibility genes in Australians. Genes and Immunity 2008;9:624-30.

56. Nischwitz S, Cepok S, Kroner A, et al. More CLEC16A gene variants associated with multiple sclerosis. Acta Neurologica Scandinavica 2010;123:400-6.

57. Fransen NL, Crusius JBA, Smolders J, et al. Post−mortem multiple sclerosis lesion pathology is influenced by single nucleotide polymorphisms. Brain Pathology 2019;30:106-19.

58. Kiselev I, Bashinskaya V, Baulina N, et al. Genetic differences between primary progressive and relapsing-remitting multiple sclerosis_ The impact of immune-related genes variability. Multiple Sclerosis and Related Disorders 2019;29:130-6.

59. Tam R, Lee A, Yang W, Lau C, Chan V. Systemic Lupus Erythematosus Patients Exhibit Reduced Expression of CLEC16A Isoforms in Peripheral Leukocytes. International Journal of Molecular Sciences 2015;16:14428-40.

60. Márquez A, Varadé J, Robledo G, et al. Specific association of a CLEC16A/KIAA0350 polymorphism with NOD2/CARD15− Crohn's disease patients. European Journal of Human Genetics 2009;17:1304-8.

61. Bronson PG, Chang D, Bhangale T, et al. Common variants at PVT1, ATG13–AMBRA1, AHI1 and CLEC16A are associated with selective IgA deficiency. Nature Genetics 2016;48:1425-9.

62. Muhali F-S, Cai T-t, Zhu J-l, et al. Polymorphisms of CLEC16A Region and Autoimmune Thyroid Diseases. G3: Genes|Genomes|Genetics 2014;4:973-7.

63. Li J, rgensen SFJo, Maggadottir SM, et al. Association of CLEC16A with human common variable immunodeficiency disorder and role in murine B cells. Nature Communications 2019:1-7.

64. Skinningsrud B, Lie BA, Husebye ES, et al. A CLEC16A variant confers risk for juvenile idiopathic arthritis and anti-cyclic citrullinated peptide antibody negative rheumatoid arthritis. Annals of the Rheumatic Diseases 2010;69:1471-4.

65. Jagielska D, Redler S, Brockschmidt FF, et al. Follow-Up Study of the First Genome-Wide Association Scan in Alopecia Areata: IL13 and KIAA0350 as Susceptibility Loci Supported with Genome-Wide Significance. Journal of Investigative Dermatology 2012;132:2192-7.

66. Schuster C, Gerold KD, Schober K, et al. The Autoimmunity-Associated Gene CLEC16A Modulates Thymic Epithelial Cell Autophagy and Alters T Cell Selection. Immunity 2015;42:942-52.

67. van Luijn MM, Kreft KL, Jongsma ML, et al. Multiple sclerosis-associated CLEC16A controls HLA class II expression via late endosome biogenesis. Brain 2015;138:1531-47.

68. Pearson G, Chai B, Vozheiko T, et al. Clec16a, Nrdp1, and USP8 Form a Ubiquitin-Dependent Tripartite Complex That Regulates β-Cell Mitophagy. Diabetes 2018;67:265-77.

69. Tam RCY, Li MWM, Gao YP, et al. Human CLEC16A regulates autophagy through modulating mTOR activity. Experimental Cell Research 2017;352:304-12.

70. Pandey R, Bakay M, Hain HS, et al. CLEC16A regulates splenocyte and NK cell function in part through MEK signaling. PLOS ONE 2018;13:e0203952-18.

71. Pandey R, Bakay M, Hain HS, et al. The Autoimmune Disorder Susceptibility Gene CLEC16A Restrains NK Cell Function in YTS NK Cell Line and Clec16a Knockout Mice. Frontiers in Immunology 2019;10:661-18.

72. Heng TSP, Painter MW, Elpek K, et al. The Immunological Genome Project: networks of gene expression in immune cells. Nature Immunology 2008;9:1091-4.

73. Soleimanpour SA, Ferrari AM, Raum JC, et al. Diabetes Susceptibility Genes Pdx1and Clec16aFunction in a Pathway Regulating Mitophagy in β-Cells. Diabetes 2015;64:3475-84.

74. Edgar AJ, Birks EJ, Yacoub MH, Polak JM. Cloning of dexamethasone-induced transcript: a novel glucocorticoid-induced gene that is upregulated in emphysema. Am J Respir Cell Mol Biol 2001;25:119-24.

75. Dos Santos RS, Marroqui L, Velayos T, et al. DEXI, a candidate gene for type 1 diabetes, modulates rat and human pancreatic beta cell inflammation via regulation of the type I IFN/STAT signalling pathway. Diabetologia 2019;62:1-14.

76. Suzuki K. Identification of a potent epigenetic biomarker for resistance to camptothecin and poor outcome to irinotecan-based chemotherapy in colon cancer. International Journal of Oncology 2011:1-10.

77. Martin P, McGovern A, Orozco G, et al. Capture Hi-C reveals novel candidate genes and complex long-range interactions with related autoimmune risk loci. Nature Communications 2015;6:10069.

78. Almén MS, Jacobsson JA, Moschonis G, et al. Genome wide analysis reveals association of a FTO gene variant with epigenetic changes. Genomics 2012;99:132-7.

79. Wen H, Li Y, Malek SN, et al. New Fusion Transcripts Identified in Normal Karyotype Acute Myeloid Leukemia. PLOS ONE 2012;7:e51203-10.

80. Ferreira MAR, Matheson MC, Tang CS, et al. Genome-wide association analysis identifies 11 risk variants associated with the asthma with hay fever phenotype. Journal of Allergy and Clinical Immunology 2014;133:1564-71.

81. Li X, Hastie AT, Hawkins GA, et al. eQTL of bronchial epithelial cells and bronchial alveolar lavage deciphers GWAS-identified asthma genes. Allergy 2015;70:1309-18.

82. Kottyan LC, Maddox A, Braxton JR, et al. Genetic variants at the 16p13 locus confer risk for eosinophilic esophagitis. Genes and Immunity 2019;20:1-12.

83. Wallace C, Rotival M, Cooper JD, et al. Statistical colocalization of monocyte gene expression and genetic risk variants for type 1 diabetes. Human Molecular Genetics 2012;21:2815-24.

84. Pearson JA, Wong FS, Wen L. The importance of the Non Obese Diabetic (NOD) mouse model in autoimmune diabetes. Journal of Autoimmunity 2016;66:76-88.

85. You S, Chatenoud L. Autoimmune Diabetes: An Overview of Experimental Models and Novel Therapeutics. In: Cuturi MC, Anegon I, eds. Suppression and Regulation of Immune Responses: Methods and Protocols, Volume II. New York, NY: Springer New York; 2016:117-42.

86. Mullen Y. Development of the Nonobese Diabetic Mouse and Contribution of Animal Models for Understanding Type 1 Diabetes. Pancreas 2017;46:455-66.

87. Pharm SAM, PhD BG, PhD BEA-D, PhD ABN. Understanding Type 1 Diabetes: Etiology and Models. Canadian Journal of Diabetes 2013;37:269-76.

88. Lenzen S. Animal models of human type 1 diabetes for evaluating combination therapies and successful translation to the patient with type 1 diabetes. Diabetes/ Metabolism Research and Reviews 2017;33:e2915-5.

89. Ishino Y, Krupovic M, Forterre P. History of CRISPR-Cas from Encounter with a Mysterious Repeated Sequence to Genome Editing Technology. Journal of Bacteriology 2018;200:5429-17.

90. Yang H, Wang H, Jaenisch R. Generating genetically modified mice using CRISPR/Cas-mediated genome engineering. Nature Protocols 2014;9:1956-68.

91. Wyvekens N, Tsai SQ, Joung JK. Genome Editing in Human Cells Using CRISPR/Cas Nucleases. Current Protocols in Molecular Biology 2015;112:31.3.1-.3.18.

92. Xu H, Xiao T, Chen C-H, et al. Sequence determinants of improved CRISPR sgRNA design. Genome Research 2015;25:1147-57.

93. Kissler S, Stern P, Takahashi K, Hunter K, Peterson LB, Wicker LS. In vivo RNA interference demonstrates a role for Nramp1 in modifying susceptibility to type 1 diabetes. Nature Genetics 2006;38:479-83.

94. Hamaguchi K, Gaskins HR, Leiter EH. NIT-1, a pancreatic beta-cell line established from a transgenic NOD/Lt mouse. Diabetes 1991;40:842-9.

95. Freitas CMT, Hamblin GJ, Raymond CM, Weber KS. Naïve helper T cells with high CD5 expression have increased calcium signaling. PLOS ONE 2017;12:e0178799-16.

96. Ceuppens JL, Baroja ML. Monoclonal antibodies to the CD5 antigen can provide the necessary second signal for activation of isolated resting T cells by solid-phase-bound OKT3. The Journal of Immunology 1986;137:1816-21.

97. Verwilghen J, Vandenberghe P, Wallays G, et al. Simultaneous ligation of CD5 and CD28 on resting T lymphocytes induces T cell activation in the absence of T cell receptor/CD3 occupancy. The Journal of Immunology 1993;150:835-46.

98. Yashiro-Ohtani Y, Zhou X-Y, Toyo-oka K, et al. Non-CD28 Costimulatory Molecules Present in T Cell Rafts Induce T Cell Costimulation by Enhancing the Association of TCR with Rafts. The Journal of Immunology 2000;164:1251-9.

99. Zhou X-Y, Yashiro-Ohtani Y, Toyo-oka K, et al. CD5 Costimulation Up-Regulates the Signaling to Extracellular Signal-Regulated Kinase Activation in CD4⁺CD8⁺ Thymocytes and Supports Their Differentiation to the CD4 Lineage. The Journal of Immunology 2000;164:1260-8.

100. Azzam HS, DeJarnette JB, Huang K, et al. Fine Tuning of TCR Signaling by CD5. The Journal of Immunology 2001;166:5464-72.

101. Bhandoola A, Bosselut R, Yu Q, et al. CD5-mediated inhibition of TCR signaling during intrathymic selection and development does not require the CD5 extracellular domain. European Journal of Immunology 2002;32:1811-7.

102. Tarakhovsky A, Kanner S, Hombach J, et al. A role for CD5 in TCR-mediated signal transduction and thymocyte selection. Science 1995;269:535-7.

103. Tarakhovsky A, Müller W, Rajewsky K. Lymphocyte populations and immune responses in CD5-deficient mice. European Journal of Immunology 1994;24:1678-84.

104. Henderson JG, Hawiger D. Regulation of extrathymic Treg cell conversion by CD5. Oncotarget 2015;6.

105. Henderson Jacob G, Opejin A, Jones A, Gross C, Hawiger D. CD5 Instructs Extrathymic Regulatory T Cell Development in Response to Self and Tolerizing Antigens. Immunity 2015;42:471-83.

106. Soldevila G, Raman C, Lozano F. The immunomodulatory properties of the CD5 lymphocyte receptor in health and disease. Current Opinion in Immunology 2011;23:310-8.

107. Rozovski U, Harris DM, Li P, et al. Constitutive Phosphorylation of STAT3 by the CK2–BLNK–CD5 Complex. Molecular Cancer Research 2017;15:610-8.

108. Jang SW, Hwang SS, Kim HS, et al. Casein kinase 2 is a critical determinant of the balance of Th17 and Treg cell differentiation. Experimental & Molecular Medicine 2017;49:e375-e.

109. Muranski P, Restifo NP. Essentials of Th17 cell commitment and plasticity. Blood 2013;121:2402-14.

110. de Wit J, Souwer Y, van Beelen AJ, et al. CD5 costimulation induces stable Th17 development by promoting IL-23R expression and sustained STAT3 activation. Blood 2011;118:6107-14.

111. Souwer Y, de Wit J, Muller FJM, et al. Response: priming of human naive CD4+ T cells via CD5 costimulation requires IL-6 for optimal Th17 development. Blood 2012;119:4812-3.

112. Ayyoub M, Raffin C, Valmori D. Generation of Th17 from human naive CD4+ T cells preferentially occurs from FOXP3+ Tregs upon costimulation via CD28 or CD5. Blood 2012;119:4810-2.

113. Liu L, Okada S, Kong X-F, et al. Gain-of-function human STAT1 mutations impair IL-17 immunity and underlie chronic mucocutaneous candidiasis. Journal of Experimental Medicine 2011;208:1635-48.

114. Zheng Y, Qin H, Frank SJ, et al. A CK2-dependent mechanism for activation of the JAK-STAT signaling pathway. Blood 2011;118:156-66.

115. Stockinger B, Omenetti S. The dichotomous nature of T helper 17 cells. Nature Reviews Immunology 2017;17:535-44.

116. Eyerich K, Dimartino V, Cavani A. IL-17 and IL-22 in immunity: Driving protection and pathology. European Journal of Immunology 2017;47:607-14.

117. Brinkman EK, Chen T, de Haas M, Holland HA, Akhtar W, van Steensel B. Kinetics and Fidelity of the Repair of Cas9-Induced Double-Strand DNA Breaks. Molecular Cell 2018;70:801-13.e6.

118. Rodgers K, McVey M. Error-Prone Repair of DNA Double-Strand Breaks. Journal of Cellular Physiology 2015;231:15-24.

119. So A, Le Guen T, Lopez BS, Guirouilh-Barbat J. Genomic rearrangements induced by unscheduled DNA double strand breaks in somatic mammalian cells. The FEBS Journal 2017;284:2324-44.

120. Seo J-Y, Yaneva R, Cresswell P. Viperin: A Multifunctional, Interferon-Inducible Protein that Regulates Virus Replication. Cell Host & Microbe 2011;10:534-9.

121. Ivashkiv LB, Donlin LT. Regulation of type I interferon responses. Nature Reviews Immunology 2013;14:1-14.

122. Ng CS, Kato H, Fujita T. Fueling Type I Interferonopathies: Regulation and Function of Type I Interferon Antiviral Responses. J Interferon Cytokine Res 2019;39:383-92.

123. Langevin C, Aleksejeva E, Passoni G, Palha N, Levraud J-P, Boudinot P. The Antiviral Innate Immune Response in Fish: Evolution and Conservation of the IFN System. Journal of Molecular Biology 2013;425:4904-20.

124. Shimizu M, Yasuda H, Hara K, Takahashi K, Nagata M, Yokono K. The Dual Role of Scavenger Receptor Class A in Development of Diabetes in Autoimmune NOD Mice. PLOS ONE 2014;9:e109531-14.

125. Kanno T, Kim K, Kono K, Drescher KM, Chapman NM, Tracy S. Group B Coxsackievirus Diabetogenic Phenotype Correlates with Replication Efficiency. Journal of Virology 2006;80:5637-43.

126. King AJ. The use of animal models in diabetes research. Br J Pharmacol 2012;166:877-94.

127. McCall KD, Thuma JR, Courreges MC, et al. Toll-Like Receptor 3 Is Critical for Coxsackievirus B4-Induced Type 1 Diabetes in Female NOD Mice. Endocrinology 2015;156:453-61.

128. Tracy S, Drescher KM, Chapman NM, et al. Toward Testing the Hypothesis that Group B Coxsackieviruses (CVB) Trigger Insulin-Dependent Diabetes: Inoculating Nonobese Diabetic Mice with CVB Markedly Lowers Diabetes Incidence. Journal of Virology 2002;76:12097-111.

129. Tai N, Wong FS, Wen L. The role of the innate immune system in destruction of pancreatic beta cells in NOD mice and humans with type I diabetes. Journal of Autoimmunity 2016;71:26-34.

130. Qaisar N, Lin S, Ryan G, et al. A Critical Role for the Type I Interferon Receptor in Virus-Induced Autoimmune Diabetes in Rats. Diabetes 2016;66:145-57.

131. Jackson AL, Linsley PS. Recognizing and avoiding siRNA off- target effects for target identification and therapeutic application. Nature Reviews Drug Discovery 2009;9:1-11.

132. Meng Z, Lu M. RNA Interference-Induced Innate Immunity, Off-Target Effect, or Immune Adjuvant? Frontiers in Immunology 2017;8:110-7.

133. Stone VM, Hankaniemi MM, Svedin E, et al. A Coxsackievirus B vaccine protects against virus-induced diabetes in an experimental mouse model of type 1 diabetes. Diabetologia 2018;61:476-81.

134. Marroqui L, Dos Santos RS, Fløyel T, et al. TYK2, a Candidate Gene for Type 1 Diabetes, Modulates Apoptosis and the Innate Immune Response in Human Pancreatic β-Cells. Diabetes 2015;64:3808-17.

135. Hu C, Wong FS, Wen L. Type 1 diabetes and gut microbiota: Friend or foe? Pharmacological Research 2015;98:9-15.

136. Chia J, McRae J, Enjapoori A, Lefèvre C, Kukuljan S, Dwyer K. Dietary Cows' Milk Protein A1 Beta-Casein Increases the Incidence of T1D in NOD Mice. Nutrients 2018;10:1291-15.

137. Huang G, Xu J, Cai D, Chen S-Y, Nagy T, Guo TL. Exacerbation of Type 1 Diabetes in Perinatally Genistein Exposed Female Non-Obese Diabetic (NOD) Mouse Is Associated With Alterations of Gut Microbiota and Immune Homeostasis. Toxicological Sciences 2018;165:291-301.

138. Simon M-C, Reinbeck AL, Wessel C, et al. Distinct alterations of gut morphology and microbiota characterize accelerated diabetes onset in nonobese diabetic mice. Journal of Biological Chemistry 2020;295:969-80.

139. Li H, Zhang G-X, Chen Y, et al. CD11c⁺CD11b⁺ Dendritic Cells Play an Important Role in Intravenous Tolerance and the Suppression of Experimental Autoimmune Encephalomyelitis. The Journal of Immunology 2008;181:2483-93.

140. Ignatius Arokia Doss PM, Roy A-P, Wang A, Anderson AC, Rangachari M. The Non-Obese Diabetic Mouse Strain as a Model to Study CD8+ T Cell Function in Relapsing and Progressive Multiple Sclerosis. Frontiers in Immunology 2015;6:v3-8.

141. Rozman J, Rathkolb B, Neschen S, et al. Glucose tolerance tests for systematic screening of glucose homeostasis in mice. Curr Protoc Mouse Biol 2015;5:65-84.

142. Evavold CL, Ruan J, Tan Y, Xia S, Wu H, Kagan JC. The Pore-Forming Protein Gasdermin D Regulates Interleukin-1 Secretion from Living Macrophages. Immunity 2018;48:35-44.e6.